ACOUSTIC EMISSION DETECTION USING OPTICAL FIBRE SENSORS FOR AEROSPACE APPLICATIONS

RAJA PHANI PAPPU

Doctor of Philosophy

ASTON UNIVERSITY

March 2011

ASTON UNIVERSITY

ACOUSTIC EMISSION DETECTION USING OPTICAL FIBRE SENSORS FOR AEROSPACE APPLICATIONS

RAJA PHANI PAPPU

Doctor of Philosophy, March 2011

ABSTRACT

Structural Health Monitoring (SHM) ensures the structural health and safety of critical structures covering a wide range of application areas. This thesis presents novel, low-cost and good-performance fibre Bragg grating (FBG) based systems for detection of Acoustic Emission (AE) in aircraft structures, which is a part of SHM. Importantly a key aim, during the design of these systems, was to produce systems that were sufficiently small to install in an aircraft for lifetime monitoring.

Two important techniques for monitoring high frequency AE that were developed as a part of this research were, Quadrature recombination technique and Active tracking technique. Active tracking technique was used extensively and was further developed to overcome the limitations that were observed while testing it at several test facilities and with different optical fibre sensors. This system was able to eliminate any low frequency spectrum shift due to environmental perturbation and keeps the sensor always working at optimum operation point. This is highly desirable in harsh industrial and operationally active environments. Experimental work carried out in the laboratory has proved that such systems can be used for high frequency detection and have capability to detect up to 600 kHz. However, the range of frequency depends upon the requirement and design of the interrogation system as the system can be altered accordingly for different applications.

Several optical fibre configurations for wavelength detection were designed during the course of this work along with industrial partners. Fibre Bragg grating Fabry-Perot (FBG-FP) sensors have shown higher sensitivity and usability than the uniform FBGs to be used with such system. This was shown experimentally. The author is certain that further research will lead to development of a commercially marketable product and the use of active tracking systems can be extended in areas of healthcare, civil infrastructure monitoring etc. where it can be deployed.

Finally, the AE detection system has been developed to aerospace requirements and was tested at NDT & Testing Technology test facility based at Airbus, Filton, UK on A350 testing panels.

Keywords

Optical fibre sensing, Structural Health Monitoring, Acoustic emission detection

To my wife, parents, friends and the Almighty God

ACKNOWLEDGEMENTS

I am deeply indebted to a number of individuals who in one way or another contributed and extended their valuable support. First and foremost, I would like to thank Dr Kate Sugden who gave me the opportunity to pursue PhD under her supervision. She was the driving force behind me and has provided constant motivation and support throughout my tenure at Aston. I can proudly say that it was because of her encouragement and assistance I was able to finish my work and thesis.

A big thanks goes to Dr Wei Zhang who has provided his knowledge input and expert advice throughout my PhD. Without unstinted support and guidance of Wei, this PhD wouldn't have been possible. I would also like to thank Dr Ian Read who has always shared his experimental experience that has helped us to work further. I would also like to acknowledge Dr David Webb, head of the Photonics Research Group.

Many thanks, to Mr Bert Biggs and Mr Richard Reeves for their extensive technical support. Special thanks to Ms Yuen Chu and Ms Claire Pertford for their administrative support. Special thanks to all my PhD friends specially, Steve Grice and Graham Lee who have motivated me throughout.

Last but not the least I would like to express my gratitude to my wife Vibha(she is my lucky charm) and my close friends in Birmingham who have stood with me in all ups and downs of life in last few years.

TABLE OF CONTENTS

TABLE OF FIGURES

Chapter 1:

Chapter 2:

Chapter 3:

Chapter 4:

Chapter 5:

1 Introduction

The world has witnessed a revolutionary growth in the past 30 years in optical fibre technology. The need of long haul lossless and high-speed communication has made optical fibre a vital part of telecommunications and led to an outstanding research in optical fibre communication. Optical fibre is capable of carrying data, voice and video signals on the same channel in a cost effective, reliable and efficient way. Commercially service providers have been able to deliver 50Mbps or more data to residential premises through optical fibre, thus replacing the bulky traditional copper infrastructure. In parallel to this development, research in fibre optic sensing technology took an exponential rise. The severe fall in prices of optical components and systems, and integration of such sensors with sophisticated control systems has drawn considerable interest for development of this technology. Since being cost effective, surplus availability, ability to carry data signals it has been one of the main research interests. In general, the applications of optical fibre cover a wide range of areas such as telecommunications, instrumentation, material science, medicine etc.

1.1 *Introduction to Optical fibre Sensors*

Optical Fibre Sensors (OFS), shown in Fig. 1, can respond to different physical and chemical parameters such as strain, temperature, pressure, vibrations etc that modulate the light and can represent that information in form of different optical parameters such as wavelength, frequency, phase, intensity etc. which is demodulated on the receiver end [1]. The main consideration that needs to be taken while realising such system is to understand the relationship between the

measurand and demodulated signal and cost effectiveness of such systems in real-time [2].

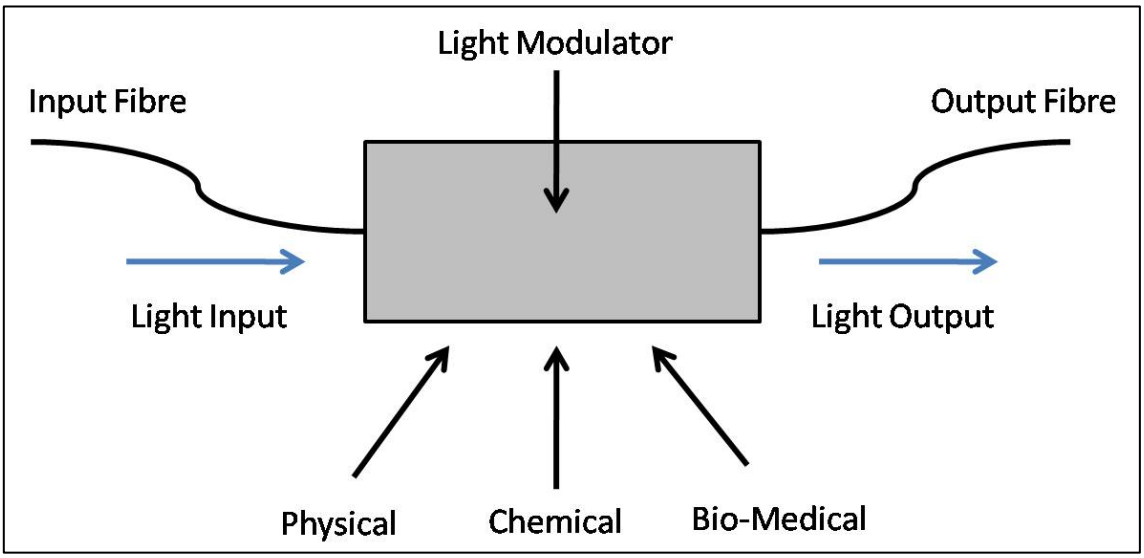

Figure 1.1 A basic fibre-optic sensors consist of an optical fibre and a light modulating arrangement

The Fibre Optic sensors are classified into two types according to their operation [1]:

1. Intrinsic Fibre Optic Sensor
2. Extrinsic Fibre Optic Sensor

Intrinsic sensors are all fibre sensors where the actual fibre is modified and modulation of the light takes place in the fibre. Extrinsic sensors use optical fibre to transmit modulated light from a non-fibre optical sensor or an electronic sensor to an optical transmitter. Modulation of light takes place in some medium that may be some dielectric or some other link.

The Intrinsic Optical fibre sensors have several advantages over the traditional transducers [1, 3]:

- Higher sensitivity – most of the optical fibre sensors offer high sensitivity in comparison with transducers.

- Compact size – It is very small compared to the existing transducers and can be easily embedded into structures.
- Reduced weight (Intrinsic fibre sensor) – The 1 metre length of optical fibre containing tens of sensors weighs less than 1 gram.
- Immunity to electromagnetic interference (EMI)
- wavelength-encoding multiplexing capability that allows tens of gratings on the same fibre
- Low cost
- Reliability
- Compatibility to optical communication and telemetry

Optical Fibre Sensors have inherent compatibility with the fibre-reinforced composite materials and can be embedded in many structural materials and this is one of the reasons for replacement of the traditional transducers. The development of structurally integrated fibre and use of fibre Bragg gratings for sensing applications became one of the major contributor in the evolution of smart structures, leading to improvements in both safety and economics in many engineering fields including roads, rails, tunnels, dams, ships, medical systems and aeronautical structures.

Most common sensing techniques that are used in such sensors are intensity-modulated [4] and phase modulated sensing. Intensity-modulated sensing can again be classified into two types: reflection type and transmission type. In transmission type sensing, light is launched from optical source into the fibre from one end and is collected at other end. In reflection type sensing, the light is launched into the optical fibre and a mirror reflects this light, which is at the end of fibre. This reflected light is modulated of there in case of any perturbation.

The measured parameter provides change in the light intensity, which is proportional or logarithmic, to the magnitude of perturbation, and a proper demodulation technique can evaluate the exact value of the measurand under observation.

Phase modulation uses interferometry principle where the light is split into two optical paths and is recombined at a distant end. One path is exposed to perturbation and that changes the effective path length that causes interference. Value of the external measurand can be determined by assessing the path length difference. These systems are widely accepted and can provide ultimate sensitivity to a range of weak physical fields. The accuracy can be an issue as the measurand under observation can be erroneous due to loss or fluctuation in the output signal. [1, 2]

1.2 *Introduction to Optical fibre Gratings*

The aforementioned disadvantages and the discovery of photosensitivity in optical fibre led to development of fibre Bragg Gratings (FBGs) and this has been reported in various research articles [5-7]. FBGs can perform primary functions, such as reflection and filtering with high efficiency and low loss [5]. The theory of optical Grating based fibre sensor is discussed in Chapter 3 in detail.

Hill et. al [8] demonstrated the formation of gratings in optical fibre while exposed to interference patterns of the laser. Since then it has been one of the most widely researched topics. A FBG is equivalent to mirrors that are inline and can reflect a defined range of wavelengths and allowing the transmission of remaining wavelengths. A FBG is written on a segment of optical fibre and consists of a periodic modulation of the refractive index along the core of the

fibre as shown in figure 2. There are different fabrication methods of FBGs wherein they are photo-induced in the core of fibre by exposing a pre-defined length of fibre to the UV laser radiation. There can be a variety of grating lengths and the reflectivity that can be achieved is approximately 100% [6].

Figure 1.2 Schematic diagram of in-fibre Bragg grating [6]

An FBG reflects light at a defined wavelength when the fibre illuminated by a broadband light source, which transmits light through the fibre core. According to Bragg's law the light from the broadband source will be reflected back along the fibre at a specific wavelength called the Bragg wavelength, λ_B. The Bragg wavelength is dependent upon the effective refractive index, η_{eff}, and the grating period, Λ, and is given by:

$$\boldsymbol{\lambda_B = 2\,\eta_{eff}\,\Lambda} \qquad \textbf{Equation 1.1}$$

Any variation in physical measurands will either change the value of the effective refractive index or grating period. Any change in these factors in turn changes the wavelength of the light which is reflected back. The measurand under monitoring can be assessed by estimating the shift in wavelength of reflected light with and without perturbation. The deformations of FBG can be determined on the basis of the spectral properties of the structure. FBG are therefore mostly strain sensors. They are also sensitive to temperature but need

to be temperature compensated when used as strain sensors. They need to be operated such that the physical measurand is to be converted to strain and thus can be measured by a FBG. [2]

Because they are compact, highly sensitive, passive and allow remote measurement of the measurand, FBGs are being used in place of traditional physical, chemical and electrical transducers. FBG sensors are deployed as transducers in numerous industries sensing measurands such as strain [9], structural damage [10, 11], vibration [12], pressure [13], temperature [14], fluid flow [15] and the detection of liquids and gases [16].

FBGs are becoming popular for structural health monitoring applications. To eliminate the risk of structural failure, continuous monitoring of structures is becoming increasingly desirable in the aerospace industry. FBGs that can measure a wide range of measurand and their inherent capability of multiplexing are becoming an attractive option. Structural health Monitoring (SHM) is a developing field that ensures the structural health and performance of safety critical structures and covers a wide range of applications from civil engineering to aerospace. In the aerospace industry, aircraft maintenance, reliability, safety and enhancement of performance are major concerns [17]. Failure of the structural integrity generates acoustic energy, emitted in form of ultrasonic waves and can be detected using various techniques to forecast the damage and failure probability of the structure.

1.3 *Thesis Overview*

This thesis presents practical FBG based solutions for structural health monitoring application in aeronautical industry. This work is a part of CONSTRUCT (Composite Wingbox Structural Health Monitoring Transducer

Technologies) program and was carried out in association with many industrial partners. This work focuses on designing and development of novel FBG based interrogation systems that could be used in the aircraft to monitor the health of composite structures and comparing them with the already existing transducer sensors with a view to replace them with optical sensors. Many interrogation techniques have been designed, analysed and tested during the course of this program. One of the systems was tested on a test rig at Airbus premises.

The readers (both academic and engineering) from various disciplines will find the techniques to be useful and would be interested in extending these designs for various applications and taking these techniques to the next level. The main aim of the research carried out was to match the capabilities of the existing piezo-electric technologies with optical fibre technology and improving them to be used in aircraft structures.

Chapter 2 provides a brief background of Structural Health Monitoring and its emergence in aeronautical industry. The reader will find it useful to understand the basics of Acoustic emission (AE) and various other approaches of structural monitoring that exist. It also provides a summary about CONSTRUCT details and requirements that were considered during the development of the interrogation systems. It gives a brief overview about the existing design of sensors and the new design requirements both for the electrical transducers and the optical sensors.

Chapter 3 gives the required theoretical background required to understand the further work. It also gives a brief summary of the work that has been carried out in optical fibre sensing. The first few sections tell the reader about the history and development of FBGs. Later, the fabrication techniques are discussed in

detail. The sensitivity of FBG to physical measurands follows providing the reader an overview of the sensing capabilities of the FBG and compensation techniques are also discussed. Then the chapter focuses on the development of the FBG Fabry-Perot interferometer devices and their behaviour under various physical measurands, their sensitivity and fabrication technique. Further in experimental chapters the reader will see the application of FBG and FBG-Fabry-Perot.

Chapter 4 describes the experimental work done to develop various sensing techniques. It concentrates on the development and execution of new concepts of wavelength interrogation. There are four major interrogation techniques discussed in this chapter which are, Interrogation system using matched pair gratings, fibre grating based laser, 3 by 3 coupler (Mach Zehnder Interferometer) and a two laser system. Matched Pair grating experiment uses identical FBGs wherein one is fixed and other is subjected to environmental perturbation. To cancel the effect of the low frequency perturbation, electronics were designed that make sure that the system is operating at its optimum performance. A novel Quadrature Recombination electronics has been designed and developed to be used in the 3 by 3 coupler experiment and to monitor high frequency acoustic emission another experiment using two lasers was proposed.

Chapter 5 discusses the development of a feedback system that can be used with different range of FBG devices. The electronics are based on the lines of the feedback electronics that are developed earlier but were modified for this experiment according to the requirements. The active feedback system is designed to eliminate the low frequency spectrum shifts caused by

environmental perturbations, ensuring the sensor always work at optimum operation point, detecting the Acoustic Emission events that occur. A reset mechanism is also designed and added to the feedback electronics which deals with any wavelength shift that is out of the tracking range of laser diode and make sure that the system is reset and locked again to its optimum operation point. It has been shown that the system proposed here can operate upto 600kHz.

Chapter 6 summarises the work carried out in this thesis and also discusses future work (a low frequency detection application that is being developed using the system that has been discussed in previous chapter).

1.4 *References*

[1] E. Udd, “An overview of Fibre Optic Sensors”, *Review of Scientific Instruments*, vol. 66, pp. 4015-4030, 1985.

[2] D. Donlagic, "Fibre optic sensors: An introduction and overview”, Maribor: University of Maribor.

[3] T. G. Giallorenzi, J. A. Bucaro, et al., “Optical Fiber Sensor Technology”, *IEEE Journal of Quantum Electronics*, Vol. QE-18, pp. 626-664, 1982.

[4] T. S. J. Lammerink and J. H. J. Fluitman, "Measuring method for optical fibre sensors", *Journal of Physics E: Scientific Instruments,* vol. 17, pp. 1127-1129, 1984.

[5] A. Othonos and K. Kalli, *Fibre Bragg Gratings: Fundamentals and Applications in Telecommunications and Sensing*. London: Artech House Publishers, 1999.

[6] Y. J. Rao, "In-fibre Bragg grating sensors", *Measurement Science and Technology,* vol. 8, pp. 355-375, 1997.

[7] K. O. Hill and G. Meltz, "Fibre Bragg grating technology: fundamentals and overview", *Journal of Lightwave Technology,* vol. 15, pp. 1263-1276, 1997.

[8] K. O. Hill, Y. Fujii, D. C. Johnson and B. S. Kawasaki, “Photosensitivity in optical fibre waveguides: application to reflection filter fabrication”, *Applied Physics Letters*, vol. 32, pp. 647-649, 1978.

[9] I. Read and P. D. Foote, “Sea and flight trials of optical fibre Bragg grating strain sensing systems”, *Smart Material Structures*, vol. 10, pp. 1085-1094, 2001.

[10] I. Read, P. D. Foote and S. Murray, “Optical fibre acoustic emission sensor for damage detection in carbon fibre composite structures”, *Measurements and Science Technology*, vol. 13, N5-N9, 2001.

[11] R. M. Measures, M. LeBlanc, K. Liu, S. Ferguson, T. Valis, D. Hogg, R. Turner and K. McEwen, "Fiber optic sensors for smart structures”, *Optics and Lasers in Engineering,* vol. 16, pp. 127-152, 1992.

[12] H. Y. Tam, S. Y. Liy, B. O. Guan, W. H. Chung, T. H. T. Chan and L. K. Cheng, “Fiber Bragg Grating Sensors for Structural and Railway Applications”, *Proc. of SPIE*, vol. 5634, pp. 85-97, 2005.

[13] T. Yamate, R. T. Ramos, R. J. Schroeder and E. Udd, “Thermally Insensitive Pressure Measurements up to 300 degree C using Fiber Bragg Gratings Written onto Side Hole Mode Fiber”, *14th Conference on Optical Fibre Sensing*, pp. 628-631, 2000.

[14] V. M. Murukeshan, P. Y. Chan, L. S. Ong and K. Seah, “Cure monitoring of smart composites using Fiber Bragg Grating based embedded sensors”, *Sensors and Actuators A,* vol. 79, pp. 153-161, 2000.

[15] S. Takashima, H. Asanuma and H. Niitsuma, “A water flowmeter using dual fiber Bragg grating sensors and cross-correlation technique”, Sensors and Actuators A, vol. 116, pp. 66-74, 2004.

[16] A. MacLean, C. Moran, W. Johnstone, B. Culshaw, D. Marsh, P. Parker, “Detection of hydrocarbon fuel spills using a distributed fibre optic sensor”, *Sensors and Actuators A: Physical,* vol. 109, pp. 60-67, 2003.

[17] D. C. Betz, G. Thursby, B. Culshaw and W. J. Staszewski, “Acousto-ultrasonic sensing using fiber Bragg gratings”, *Smart Material & Structure*, vol.12, pp. 122-128, 2003.

2 Structural Health Monitoring

2.1 Introduction

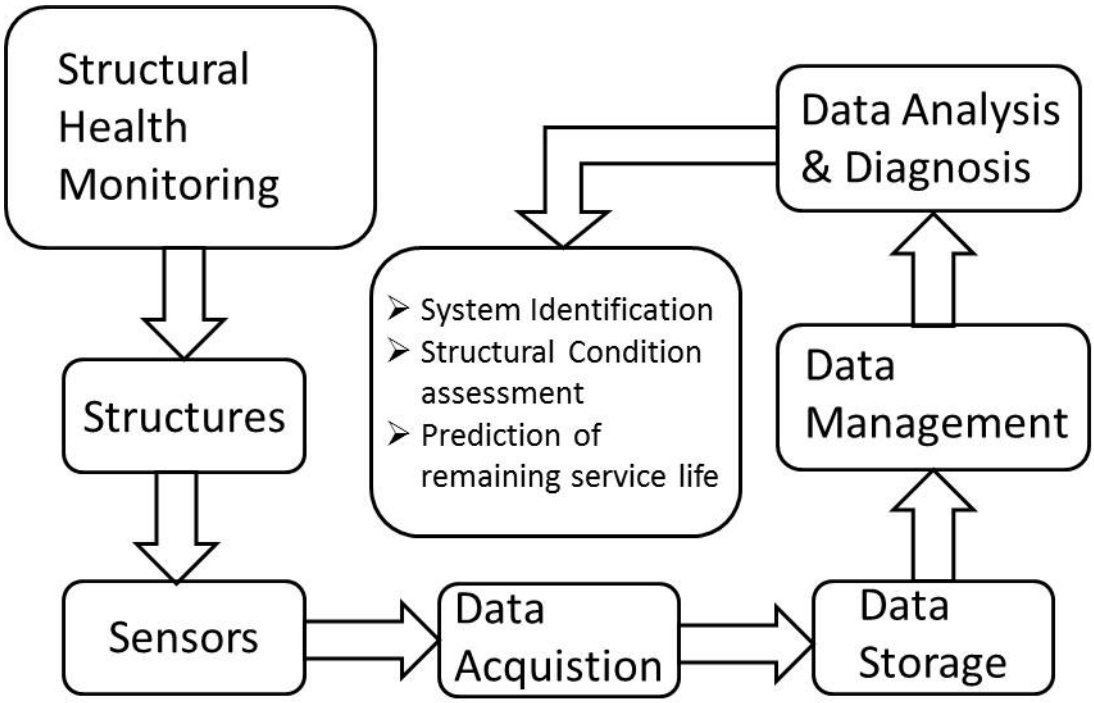

Figure 2.1 Process diagram of Structural Health Monitoring

Health and usage monitoring techniques are employed to ensure the structural integrity and maintain health of a structure in use. Any change in structural health, affect the structural performance and it becomes very important to take necessary maintenance action. However, this maintenance costs can be expensive as they can incur direct costs for design and implementation of repairs or the whole system has to be taken out of service temporarily for execution of repairs. Introduction of an effective damage detection system [2]:

i) allows an optimum use of the structure

ii) a minimized downtime

iii) avoidance of catastrophic failures

iv) improvement matrix for better manufacturing

v) reduced maintenance services and costs.

The process of implementation of a damage identification system covers a wide range of applications from civil engineering to aerospace and mechanical infrastructure and is referred to as structural health monitoring (SHM) [1-6]. Damage can be defined as material, structural or functional failure of a system. It need not be total loss of system or its functionality but it will not allow the system to function at its optimum performance. Damage of structure can be categorised in two groups:

i) Changes in geometric properties of a structural system, including changes to the boundary conditions i.e. displacements and/or forces on the boundary and system connectivity due to environmental perturbation, turbulence and accidents.

ii) Ageing of the structures due to excessive usage, fatigue and corrosion can also cause structural damage and adversely affect the overall system.

Damage detection in different engineering areas is carried out by using one of the following techniques or in combination [6]:

i) Structural health monitoring: SHM [4,5]

   SHM is an active damage detection technique used in aerospace, civil and mechanical structural systems. Many fibre optic systems using Fibre Bragg gratings, for monitoring of ultrasonic waves generated due to structural damage have also been developed for active monitoring of the structural health.

ii) Condition monitoring: CM [7]

   CM is similar to SHM, and is used for damage detection in rotating machinery such as steam and gas turbines and heavy machinery that are used in manufacturing and power generation.

iii) Non-destructive evaluation: NDE [8]

NDE is usually carried out off-line and is used for damage characterization, detection and as a severity check after the damage occurred and it has been located on the structure. NDE is also used as a monitoring tool for structures such as pressure vessels and rails. A large variety of extremely effective non-destructive evaluation (NDE) techniques are available for damage monitoring. SHM and NDE are often used synonymously in many areas of engineering.

iv) Statistical process control: SPC [9]

SPC is the application of statistical methods to the monitoring and control of a process to ensure that it operates at its optimum performance potential.

v) Damage prognosis: DP [10]

Once damage has been detected, DP is used to predict the remaining useful life of a system.

vi) Visual inspection

The first level of inspection can be done by visually monitoring the structure. Any damage on surface or near-surface of a structure can be detected by this method. This is very effective and commonly used method for aircraft structures.

This work mainly focuses on the SHM and its application in aircraft damage monitoring and inspection. Health of a structure is the ability to perform and maintain the structural integrity throughout the entire lifetime of the structure and monitoring is the process of forecasting and identification. In this context, it can be said that damage monitoring and detection is same as SHM.

SHM ensures the structural health and performance of safety critical structures. In the aerospace industry, aircraft maintenance, reliability, safety and enhancement of performance are major concerns [1]. Failure of the structural integrity generates acoustic energy, emitted in form of ultrasonic waves and can be detected using various techniques to estimate the damage and failure probability of the structure. SHM research is being conducted since last 50 years and it has attempted to classify damage in structures on a more extensive basis. However, in the last few years the SHM research has taken a new dimension and has been the topic of interest of many researchers.

SHM provides a diagnosis of the structure's constituent materials and different parts, and also of the whole assembly of these parts that constitute in formation of the structure as a whole. The state of structure should be maintained in domain that is specified in design unless it is altered because of usage, environmental perturbation or accidents. Time-dimension monitoring provides full record and database of the structure and a projection such as progression of damage, remaining structure life etc. with the help of usage monitoring. Usage monitoring is a valuable addition to SHM. Usage monitoring acquires operational loading data from a structure or system and provides information about evolution of damage, remaining life etc. Structural Health Monitoring involves the integration of various sensors, smart materials, data computation and transmission with powerful processing ability inside and outside the structures. SHM can give recommendations to amend the design of the structure and the overall administration of the structure. This is schematically presented in Figure 2.2. [2, 3]

Figure 2.2 Detailed organization of a typical Structural Health Monitoring system [2]

Figure 2.2, above shows detailed organization of a typical SHM system. The foremost part of the system corresponds to the structural integrity monitoring function and is defined by the following [2]:

i) The type of physical parameter, which is closely related to the damage, and is monitored by the sensor.

ii) The type of physical parameter that is used by the sensor to produce a signal proportional to the damage, which is sent to the data acquisition and storage sub-system.

Figure 2.3 shows the performance in terms of structural reliability and cost of maintenance comparison between the structures with SHM and structures that don't. It can be seen clearly how constant maintenance costs and reliability are brought down making it more economical, instead of increasing maintenance costs and decreasing reliability for classical structures without SHM. [2]

Figure 2.3 Performance analysis of a structure with and without SHM [2]

2.2 Types of NDE Testing

Among the various techniques available such as Eddy current testing, radiography, thermograph, Lamb wave technique and Acoustic emission testing offers a suitable and appropriate method for a fast and continuous inspection of structures. Various experiments [19-22] has been proposed and demonstrated for both techniques that demonstrate the success of these techniques. The detection techniques described in further chapters are based of Acoustic emission based sensing systems.

2.2.1 Lamb Wave Testing:

The principle of Lamb wave testing method is shown in figure 2.4. It consists of one transmitting piezoelectric transducer, which is used for exciting the

structure to produce stress waves and one receiver transducer, which is used to analyse the received signal that contains information about the structural integrity between the two transducers. The entire structure under test can be probed, as the lamb waves travels through the structure thickness and any change in the propagating signal from the exciting transducer can be detected and the damage can be measured. Based on these measurements, data can be retrieved and health of structure and extent of damage can be estimated. This method can also be used for continuous monitoring of the structure [11].

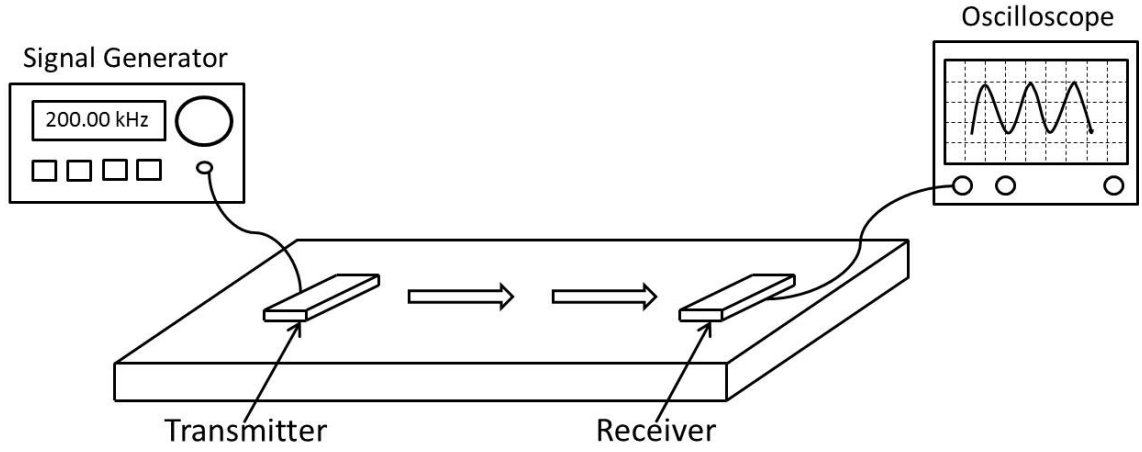

Figure 2.4 Basic Lamb wave testing setup

2.2.2 Acoustic Emission Testing:

Basic set up for Acoustic emission testing is shown in the figure 2.5. It is different to Lamb wave testing as it uses passive sensors to determine the integrity of a structure by monitoring the stress waves generated by the damage. This technique can detect the exact location and source of damage.

This method has few drawbacks such as the noise generated in the structure that actually does not contribute towards the damage and the damping of acoustic signals generated due to damage in the structure [11].

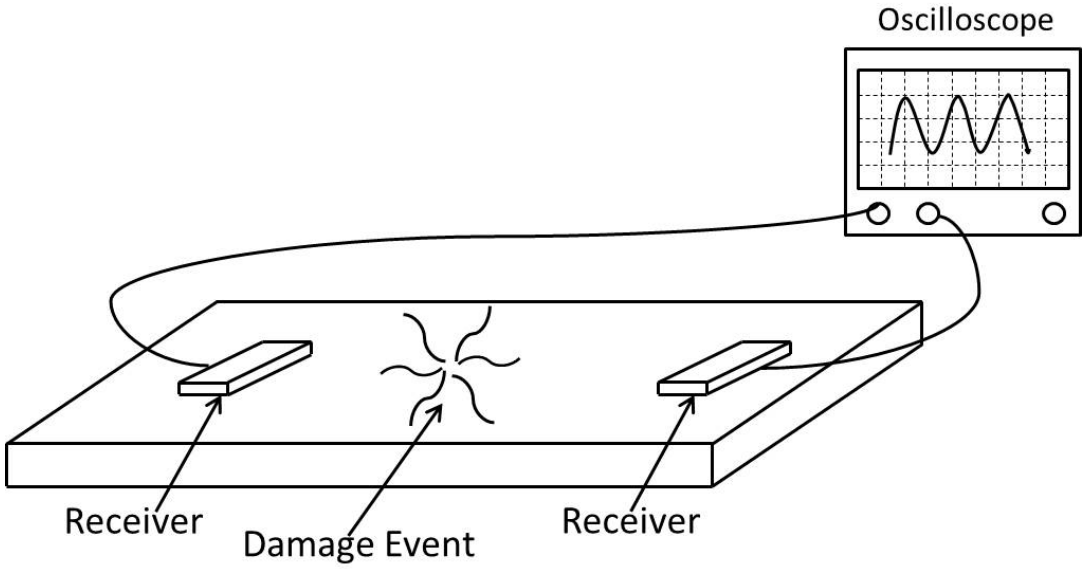

Figure 2.5 Basic Acoustic emission testing setup

2.3 Introduction to Acoustic Emission Testing

Recent years have seen a huge growth of interest in non-destructive testing (NDT) and non-destructive evaluation (NDE) techniques. These are the methods used to evaluate the properties of a material, component or system without causing damage or disturbing the actual structure. These methods depend upon the inherent properties of structures such as electromagnetic radiation, high frequency sound waves etc. Increasing safety standards and maintenance cycle of a structure is the main motivation behind NDT, but economic considerations are equally important, especially when the quality control of a material product is at issue. [12]

Acoustic emission (AE) is a method that uses high frequency sound waves, typically between 100 kHz and 1 MHz and generates transient elastic waves that is produced by quick redistribution of stress in a material.

Figure 2.6 show when there is a sudden emission of energy within a solid, which might be caused by the growth of a crack or fissure when a structure is subjected to external pressure, temperature etc., then some of the energy is dissipated in the form of elastic waves which propagate to the surface. An elastic wave describes a stress or strain wave, propagating through an elastic medium, typically a solid. The proportion of energy that is emitted as elastic waves is determined by the initial condition of the source. Particularly, it is necessary to know how localised it is and how rapidly the energy is released. Energy, which is localised, and rapid gives rise to elastic waves in the ultrasonic frequency range and if the waves have sufficient amplitude they can be detected by microphones or transducers attached to the surface of the specimen. This whole process is known as acoustic emission detection and signals detected are called AE signals. [13]

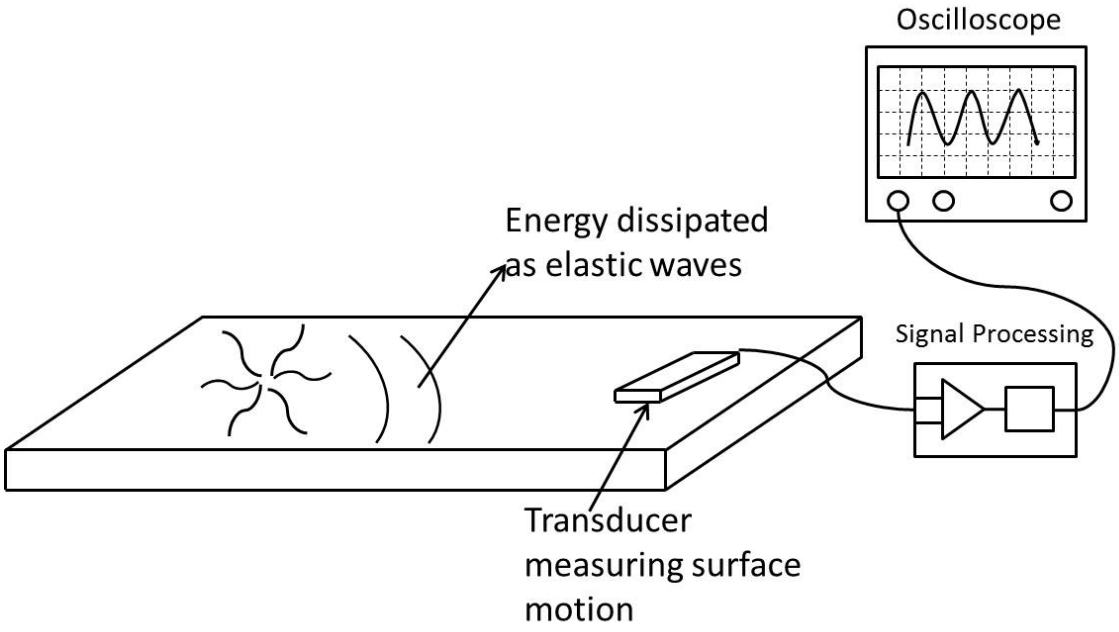

Figure 2.6 Sudden stress and strain generate energy in form of elastic waves

Over the years, the materials scientists have used the AE to understand the development of damage in composite materials that are used for structural applications, as it is related to the actual strength and life of a structure. Some examples of events that generate AE are given below [13]:

- Materials degradation - defect growth, crack advance, plastic deformation, inclusion or precipitate fracture, surface degradation including corrosion and disbonding of coatings.
- Reversible processes - crystallographic phase transformations, melting or solidification, thermoelastic effects, ferromagnetic and ferroelectric domain wall motion, friction between surfaces (e.g. crack face fretting, although not strictly reversible).
- Fabrication processes - welding noise (including defects), rolling, forging, machining, drilling, mixing, grinding, valve sequencing.
- Leak and flow - flow of single- and two-phase fluids and particles, leaks, gas evolution, boiling.

There are many different processes that generate AE signals and those signals that lie within the normal bandwidth for AE detection, i.e. above 20 kHz are considered. Many events that generate AE are short and transient that generates burst signals as shown in figure 2.7 and those that appear to be continuous signals as shown in figure 2.8 are actually the superposition of large numbers of overlapping transient events.

AE is different than other non-destructive testing (NDT) techniques. The main difference is related to the origin of the signal. AE monitors the energy that is emitted from the object instead of exciting the object under test.

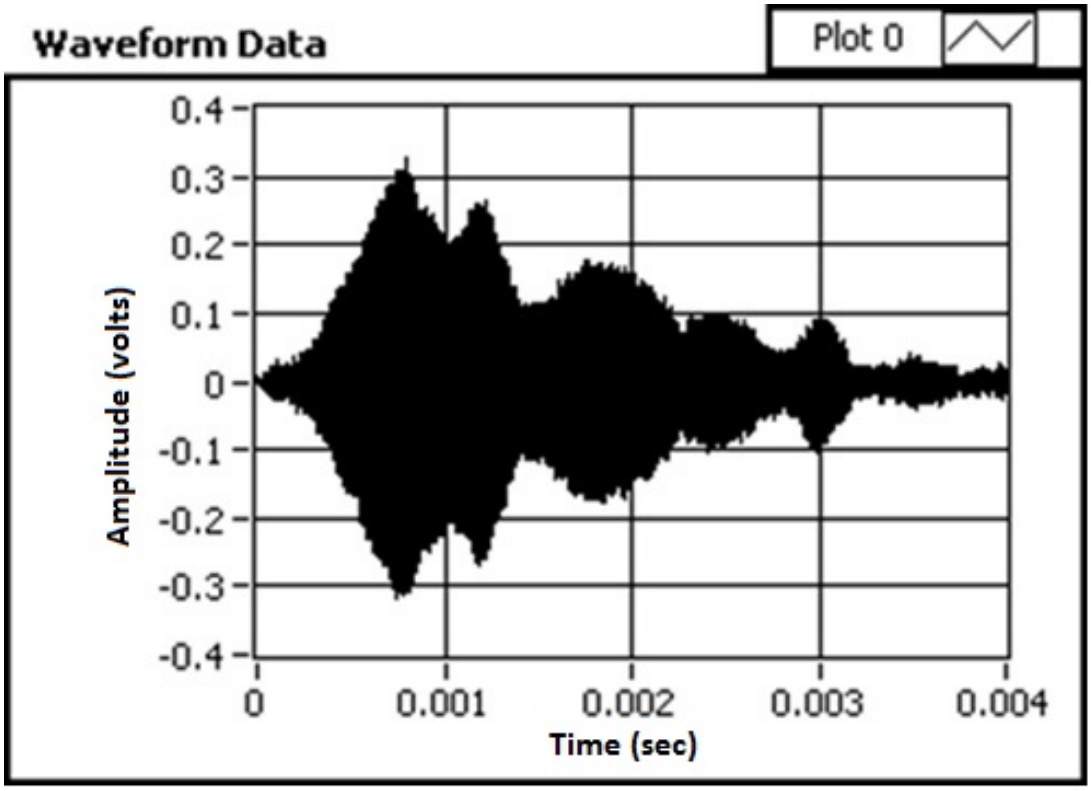

Figure 2.7 Example of a burst signal generated from the acoustic emission event

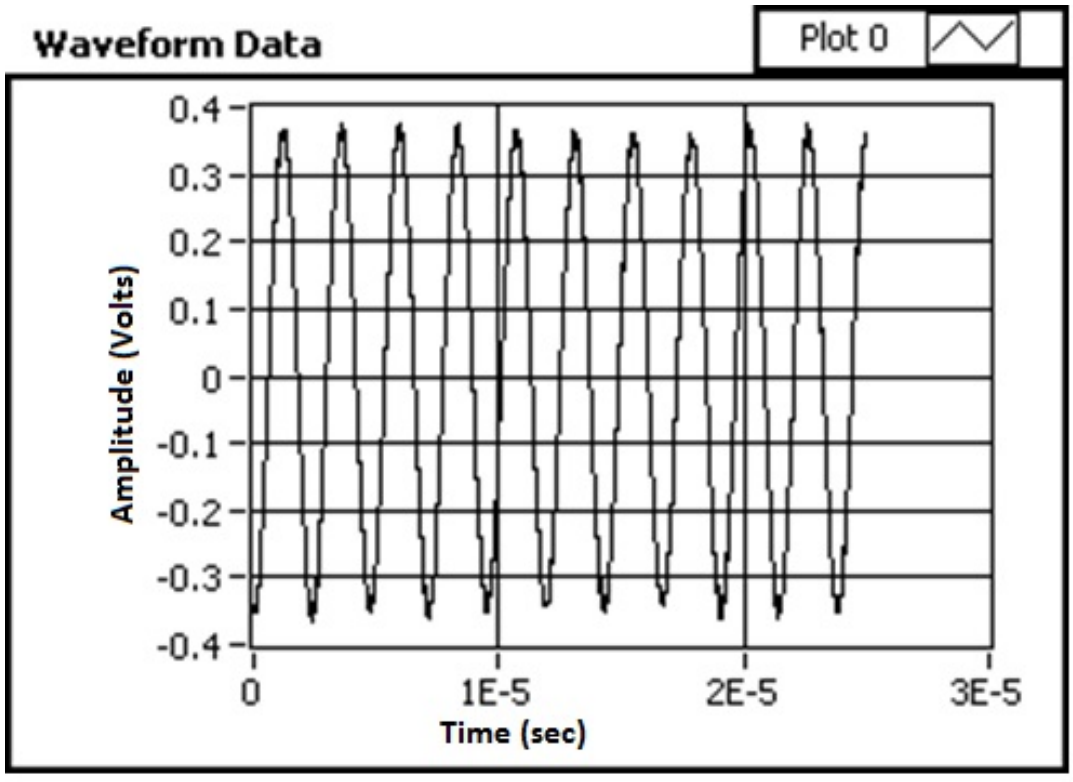

Figure 2.8 Example of a continuous signal generated from the acoustic emission event

These tests are often carried out on structures while they are in operation, as it provides sufficient loading for transmitting defects and triggering acoustic emissions. AE testing deals with active processes and changes that occur during operation in any material. This is particularly important as the active techniques can detect the crack growth and can very well differentiate between the developing and stagnant defects. However, sometimes it might happen that some damages might not be detected if the loading is not enough to cause an acoustic event. These tests make it possible to determine the strength or risk of failure of a component that is being used in the structure. Sometimes AE signals can carry noise and it is very important to detect the actual signal and reduce the noise so that accurate results can be obtained.

AE has several advantages and unique capabilities such as [12]:

- High Sensitivity
- Real-time capability
- Fast and complete volumetric inspection
- Location of the damaged region
- Sensitivity to process that generate stress waves

The analysis and detection of AE signals can provide important information that can help in locating the origin of the AE and can determine whether the material can be still used or needs to be discontinued. Because of its versatility it has been widely accepted and is being used in many applications in the aerospace industry, nuclear industry and in power industry etc. AE has also been applied to structural health monitoring in the aerospace industries and is discussed in detail further in the chapter.

The applications areas for acoustic emission can be classified into three categories [13]:

(i) Structural testing and surveillance: This category mainly includes the NDT applications for acoustic emission e.g. in petrochemical, nuclear, aerospace etc. and the main area of concern is structural integrity and safety.

(ii) Process monitoring and control: This category focuses on the monitoring of fabrication processes of different varieties of materials, including metals, non-metals, chemicals and food and main area of concern being the cost and safety

(iii) Materials characterisation and testing: This category deals with materials research and development.

2.4 Source of AE

An acoustic emission is generated in composite structures due to fracture, delamination or de-bonding. AE is generated mostly because of stress. When a material is subjected to stress a strain is also induced in the material. A material may deform forever (known as plastic deformation) or regain its original dimension when stress is removed (known as elastic deformation), depending on the nature and magnitude of the stress induced. Acoustic emission becomes detectable when the material experiences plastic deformation or when it is subjected to stress by loading the structure. In plastic deformation the atomic planes of the material slide because of dislocation and that generate energy in form on elastic waves that travel through the structure. The stress level at the crack is very high than the rest of the structure and AE is able to monitor both the crack development and the plastic deformation that might occur ahead of the crack development [14].

AE is also caused by two more sources. The first source is presence of particles that can emit energy at the centre of the crack. When strain is applied to these material they break very easily as these particles are more brittle than the rest of the structure, and thus generate AE signals. The second source is because of a developing crack that propagates in the structure and this occurs because of the movement of dislocations and small-scale cleavage produced by tri-axial stresses.

The amount of energy released during acoustic emission is directly proportional to the magnitude of the event and also depends on the severity and rapidness of the event. The amplitude of the emission is a measure of the speed of development of crack and the intensity of the energy released. The larger the crack growth, large will be the corresponding AE signal. As mentioned earlier, a small crack will generate a burst signal and large crack propagation will generate a continuous signal that is actually a packet of many burst signals is one envelope. A crack propagating slowly over a distance will generate smaller amplitude and a large crack covering the same distance will generate large amplitude [14].

Elastic waves generated during the acoustic events can be detected and converted to electrical signals using transducers. The aim of this research is to use cost effective and compact sensors for detection of acoustic waves. This study will give necessary recommendations about the origin of crack, longevity of a material and safety of that structure.

2.5 Noise

The sensors used to detect AE pick up unwanted signals and the sensitivity is thus compromised with the presence of the background noise. Sometimes, the

noise is larger than the actual signal and the required information can be missed. These signals can be due to frictional sources e.g. loose contacts, unshielded power sources, external unmonitored parameters, mechanical vibrations etc. and impact sources e.g. rain, flying objects, dust due to wind etc.

The effect of the background noise can be compensated using different methods depending on the application and the environment of test e.g. fabrication of special sensors, electronic filters to remove noise such as Low Pass and High Pass filtering etc. and by monitoring the changes in the spectral content of actual AE signals and background noise [14].

2.6 State of art - Sensors

Figure 2.9 Different piezo electric Acoustic emission sensors available in the market for AE testing [18]

A sensor is a very vital part of the AE system. An ideal sensor should be highly sensitive to the measurand, should be insensitive to the unmonitored external

properties and it should not affect the functionality of the measurand by allowing additional parameters to combine in the actual signal. There are several portable systems that are available in the market for Acoustic Emission Testing. Physical Acoustics Corporation design and manufactures low cost, high sensitive, resonant type sensors and there are many other companies who manufacture such sensors. An acoustic emission system basically consists of [14]:

- AE sensor
- Preamplifier
- Filters
- Amplifier
- Post processing equipment such as oscilloscope

An acoustic emission sensor picks up signal due to any dynamic motion that is caused because of an acoustic emission signal. AE sensors are basically transducers which have the ability to convert mechanical strain into electrical signal. These signals are than amplified and post processed.

A commercially available sensor's internal diagram is shown in figure 2.10. There is a transducer component in an AE sensor which is a piezoelectric crystal, and is generally made of lead zirconate titanate (PZT), the most common piezoelectric ceramic that is available today. Based on the operating frequency, sensitivity and environmental conditions these transducers are classified into two parts:

- Resonant
- Broadband

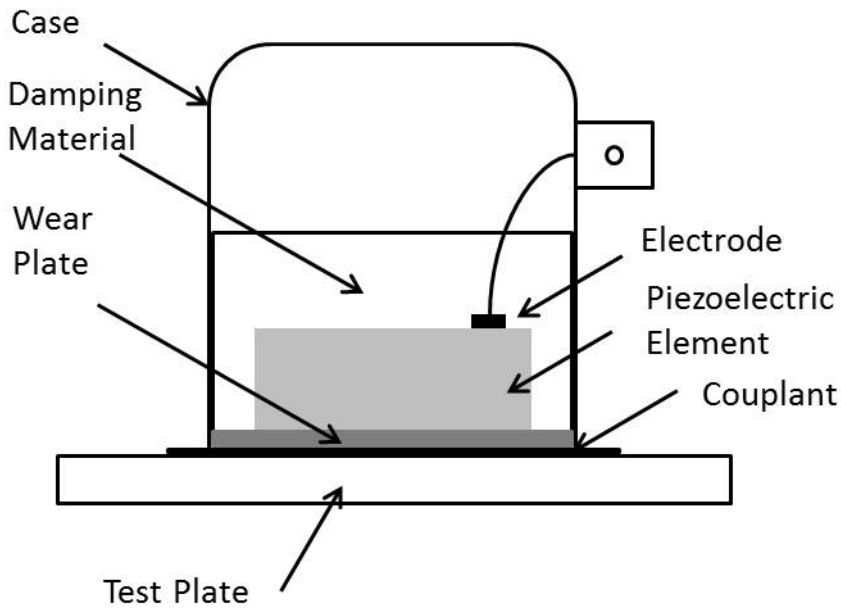

Figure 2.10 Internal diagram of a piezo electric based acoustic emission sensor

Several new sensing and actuating technologies have been reported in the recent past. Wilcox et al [19] proposed interdigital transducers, Blanquet et al [20] proposed phase array transducers, Egusa and Iwasawa [21] proposed piezoelectric paints and MEMS [22] was proposed by Khuri-Yakub et al. Chang proposed piezoceramic layers that can be embedded or bonded in structural components.

The acoustic emission system is designed such that the noise is removed and the actual signal is amplified and relayed for further processing. Multiple sensors can be multiplexed and connected to the AE system so that they can detect the source location. In such systems as shown in below figure 2.11 the sensors and preamplifiers try to remove the unwanted signal. The first stage consists of the sensor, which picks up any signal from the structure converts it to electrical voltage and sends it to preamplifiers, which amplifies the voltage to provide gain. Modern transducers are equipped with integrated preamplifiers

which make the system compact. These signals from preamplifier are sent to a bandpass filter for elimination of low frequencies (background noise) and high frequencies (these filters can be designed according to application requirement and for desired frequency range). After this signal processing the signal is sent for analysis and further to data storage. Post processing is done based on the noise conditions by providing filtering or amplification [14].

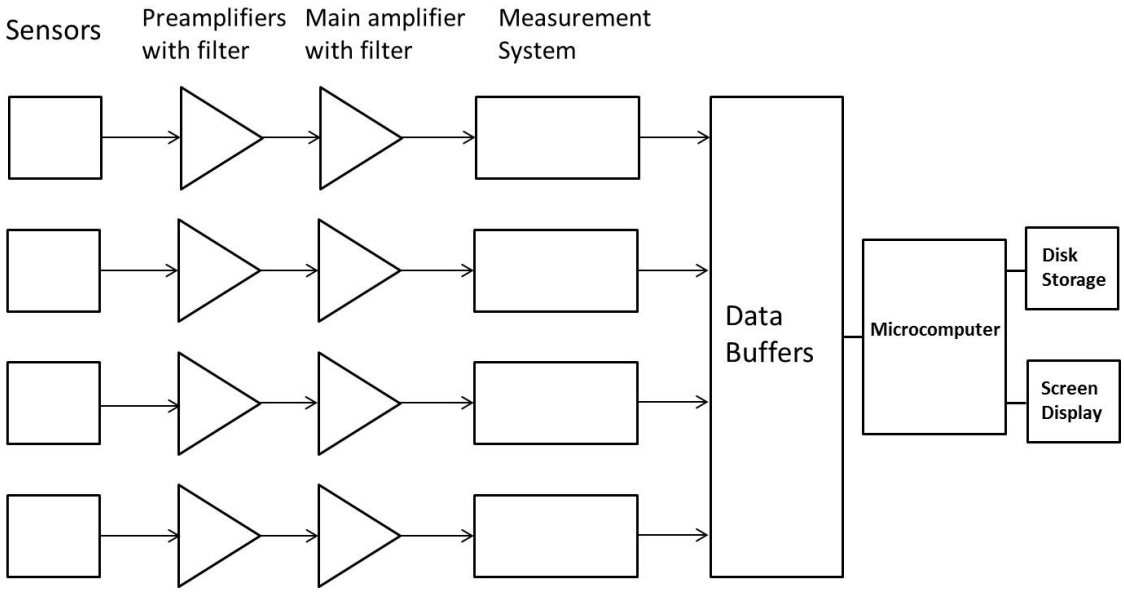

Figure 2.11 Schematic Diagram of a Basic Four-channel Acoustic Emission Testing System

When the signal is relayed to measurement system/circuit it is compared with a threshold voltage that is pre-programmed. The operation and design of measurement system may vary from system to system. The measurement circuit tries to compare the data it has stored with the random data that is coming from the acoustic event and generates a signal that is proportional to that event. If the event is continuous/ burst the data is compared and is stored in the microcomputer and the measurement circuit is reset.

2.7 About the Project

Composite Wingbox Structural Health Monitoring Transducer Technologies (CONSTRUCT) is a GBP 1.7 million project jointly funded by Department of Trade and Industry and industrial partners which include Airbus, BAE Systems, Insensys, Deutsch, Ultra Controls, Ultra Electronics and Aston University (ourselves). The main area of focus in this project was develop a sensing system for damage detection in aircraft based on acoustic emission detection and load monitoring based on fibre optic strain sensing which can match the capabilities of the existing transducer technologies. Optical fibre sensing using fibre Bragg gratings sensors has many advantages over the existing technologies, which include:

- Optical fibre is used for long distance communication and thus an ideal medium for low loss, long distance remote sensing.
- Many FBG sensors can be multiplexed onto a single fibre and electrically isolated from each other.
- Optical fibre is manufactured using abundantly available polymer and glass and also isolated to any electro-magnetic interferences.
- Optical transducers do not used electrical power and do not have any electrical risk that makes it ideal to be used in crucial areas such as oil and gas production.
- Since Optical fibre has a small diameter and very small it can be embedded into many composite materials as it provides close match to them and does not affect the overall structural strength.
- The optical fibre (standard telecommunications grade fibre) is not very expensive.

- FBGs are in-fibre devices and do not require any connections between transmission medium and the sensor.

The development of sensing systems was divided into two areas:

- Design and development of PZT type sensor and testing, work on which is jointly done by Ultra Electronics, Ultra Controls and Airbus.
- Design and development of Fibre Optic Sensor and testing, work on which is carried by BAE Systems, Insensys, Deutsch and Aston University. [15-17]

This project ran over a period of three years. BAE systems and Aston has worked jointly on the development of new fibre optic sensors with compatible detection systems that will be used instead of the existing resonant sensor or in conjunction with it, which is manufactured by Ultra Electronics. Thus, it widely expands the potential for structural health monitoring in both aerospace and other platforms.

2.7.1 Acoustic emission sensing for structural damage detection using fibre optic sensors

In CONSTRUCT, our main area of focus was development of a novel acoustic emission detection sensor based on a fibre optic concept. The aim of this development was to expand the structural health monitoring technology to high risk restricted areas such as fuel tanks. Additional to that the system should be compact, cost effective and the sensor able to do analysis during load monitoring and damage detection which will significantly reduce the complexity and reducing the number of sensors being currently used.

Airbus is currently using piezo-electric sensors for acoustic emission detection. Although, such systems are more robust and sensitive, and so does the optical fibre system and in addition to that they have some distinctive advantages over such technologies, which are already highlighted in previous chapter. Use of piezo- electric sensors in restricted areas as fuel tanks carries high risk but it can be overcome by using optical sensors. The major objective of the research was to match the capabilities of the existing technologies with optical fibre technology and enhancing them to be used in aircraft structures. The development of optical systems is covered in Chapter 4 and Chapter 5.

2.7.2 Design requirements of the project:

The sensor design in CONSTRUCT has the following requirements [15]:

- The sensor developed should be smaller in size and lighter than the previous design.
- It should be robust and rugged from the existing Ultra Electronics resonant sensor.
- It should be suitable for installation into aircraft structures.
- The EMC capability must be improved.
- The sensor and preamplifier must include additional lightning strike protection.

2.7.3 Existing Design

The sensor used now in the Airbus aircraft structures consists of a sensor head which has an integrated PZT actuator and a ceramic disk that forms the base of the sensor. This PZT actuator is directly connected to the preamplifier which conditions and amplifies the sensor output. This sensor also relays a pulse that

is communicated to the other sensors in the network/array to monitor sensor functionality and bond integrity.

Figure 2.12 RS sensor used by Airbus for AE detection. It consists of sensor head and a preamplifier stage.

2.7.4 Transducer vs. Optical Sensors

Although, the transducer based sensors are used widely in industry, researchers are trying to replace them by using more sophisticated and compact smart sensors that can be equally or more sensitive than the existing sensors and without damaging the integrity of structure. Optical Fibre sensors discussed in previous section are one of the choices that can perform same functions but has some advantages over traditional sensors. The size of optical sensor is much smaller than that of the WDI sensor (manufactured by PAC) and it can be embedded into the structure. Embedded sensors give more accurate sensing data as they are more close to the actual acoustic release area. However, it depends on the placement of the sensor, packaging and structure design.

The below table discuss few of the new sensor design requirements in comparison with the optical fibre sensors requirements [15, 16].

New design requirements	
Design requirements	**Comments on Optical fibre sensor**
The new sensor should be smaller and lighter than the previous design.	The fibre sensor will be smaller in size due to the size of optical fibre although the main concern will be how to package and deploy it on the structure.
It should be robust and rugged from the previous design.	Fibre Optic sensors are rugged and will be robust depending on the type of packaging deployed.
It should be suitable for installation into aircraft structures	Fibre optic sensors can be easily embedded in the structures or can be deployed as patches.
The EMC capability must be improved	Fibre optic sensors are immune to electromagnetic intereference.
The sensor and preamplifier must include additional lightning strike protection	N/A
The sensor and preamplifier should be powered from the 15V phantom power as did the previous design.	N/A

2.8 Overview of work in CONSTRUCT

The research carried at Aston and BAE focussed on the development of the optical fibre sensing systems and has also focussed on the following points [17]:

1. Development of optical sensors according to the aircraft and systems requirements. Optimising the detection range versus sensitivity of fibre optic sensors to meet damage detection requirements more accurately. At the beginning of the project the fibre optic devices were considered not to be as sensitive to acoustic pressures as their piezo-electric counterparts.
2. Design and fabrication of ruggedised fibre Bragg gratings and to develop an electro-optic interface between fibre sensors and the existing acoustic emission instrumentation.
3. Ruggedisation and adaptation to the specific needs of commercial aircraft structural health monitoring especially with respect to installation on pre-existing structures, connection and durability in fuel and high temperature environments.
4. The sensing system should be compatible with the already developed acoustic emission detection instruments BALRUE (signal detection, conditioning and data processing) developed by Ultra and Airbus. The aim of the project was to develop an interface that allows operation of the system with both optical and piezo-electrical sensors. The BALRUE system is a structural damage evaluation system based on acoustic emission detection. It was initially developed by Airbus, Ultra Electronics and Lloyd's Register EMEA. The system is in use since past 3 years. With the PZT-sensors and preamplifiers this system has been well

proven to locate structural damage in metallic aeronautical and off-shore structures.

5. Existing PZT sensors and preamplifiers will be ruggedised with the ultimate aim of them being used to locate structural damage on an Airbus, carbon fibre reinforced polymer (CFRP) Wingbox.

2.9 Chapter Conclusion

This chapter provides an overview of Structural Health monitoring. It introduces the reader to the concepts of Acoustic emission detection and discuss various damage monitoring techniques.

An overview of various AE sources was given and the presence of noise, which is a vital factor in the AE detection, is also discussed. The design of piezo sensors and a general comparison of existing sensors with fibre optic sensors was also discussed.

Overview of the aerospace structural health monitoring and project under which the work produced in this thesis was carried out, are introduced. The project requirements were outlined briefly and the use of optical fibre sensors inline with the new design requirements was also discussed.

2.10 References

[1] D. C. Betz, G. Thursby, B. Culshaw and W. J. Staszewski, "Acousto-ultrasonic sensing using Fibre Bragg gratings", *Smart Material & Structure,* vol. 12, pp. 122-128, 2003.

[2] D. Balageas, C.-P. Fritzen, et al., “Structural Health Monitoring”, Wiley-ISTE, 2006.

[3] C. Boller and M. Buderath, ”Fatigue in aerostructures - where structural health monitoring can contribute to a complex subject”, *Philosophical Transactions of the Royal Society A,* vol. 365, pp. 561–587, 2007.

[4] J. M. W. Brownjohn, ”Structural health monitoring of civil infrastructure”, *Philosophical Transactions of the Royal Society A,* vol. 365, pp. 589–622, 2007.

[5] C. R. Farrar, S. W. Doebling and D. A. Nix, ”Vibration-based structural damage identification”, *Philosophical Transactions of the Royal Society A*, vol. 359, pp. 131–149, 2001.

[6] C. R. Farrar and K. Worden, ”An introduction to structural health monitoring“, *Philosophical Transactions of the Royal Society A*, vol. 365, pp. 303–315, 2007.

[7] J. Courrech and R. Eshleman, “Condition monitoring of machinery”, Shock and Vibration Handbook, McGrawHill, pp. 16.1-16.25, 2002.

[8] R. Thompson and D.Thompson, “Ultrasonics in non-destructive evaluation”, *Proc. IEEE*, vol. 73, pp. 1716-1755, 1985.

[9] H. Sohn, J. J. Czarnecki and C. R. Farrar, ‘‘Structural Health Monitoring Using Statistical Process Control,’’ *Journal of Engineering Mechanics,* vol. 126, pp. 1356–1363, 2001.

[10] C. R. Farrar and N. A. J. Lieven, “Damage prognosis: the future of structural health monitoring”, *Philosophical Transactions of the Royal Society A* vol. 365, pp. 623–632, 2007.

[11] S. Grondel, C. Delebarre, J. Assaad, J-P. Dupuis and L. Reithler, ”Fatigue crack monitoring of riveted aluminium strap joints by Lamb wave analysis and

acoustic emission measurement techniques", *NDT&E International*, vol.35, pp.137–46, 2002.

[12] M. Hamstad, "A review: Acoustic emission, a tool for composite-materials studies", *Experimental Mechanics*, vol. 26, pp. 7-13, 1986.

[13] C. B. Scruby, "An introduction to acoustic emission", *Journal of Physics E: Scientific Instruments*, vol. 20, pp. 946-953, 1987.

[14] Web Address: http://www.ndt-ed.org: Accessed Dec 2010.

[15] A. G. Simpson, "CONSTRUCT: SHM system requirement and current capabilities", TES10121, 2007. – Restricted Access

[16] I. Read, "CONSTRUCT: Opto-Electronic Interface Configured", TES102366, 2008. – Restricted Access

[17] DTI requirements document. – Restricted Access

[18] Web Address: http://www.pacndt.com: Accessed Dec 2010.

[19] P. D. Wilcox, M. Castaings, R. Monkhouse, P. Cawley and M. J. S. Lowe, "An example of the use of interdigital PVDF transducers to generate and receive a high order Lamb wave mode in a pipe", *Rev.Prog. Quantitative NDE*, vol. 16, pp. 919-926, 1997.

[20] P. Blanquet, T. Demol and C. Delebarre, "Application of array transducers to health monitoring of aeronautic structures", Trends in NDE Science & Technology; *Proceedings of the 14th World Conference on Non-Destructive Testing, New Delhi*, vol. 4, pp. 2057-2060, 1996.

[21] S. Egusa and N. Iwasawa, "Poling characteristics of PZT/epoxy piezoelectric paints", *Ferroelectrics*., Vol. 145, pp. 45-60, 2011.

[22] B.T. Khuri-Yakub, F.L.Degertekin, X.-C Jin, S. Calmes, I. Ladabaum, S. Hansen and X.J. Zhang, "Silicon micromachined ultrasonic transducers", *Ultrasonics Symposium*, vol. 2, pp. 985-991, 1998.

3 Optical Fibre sensors

3.1 Chapter Overview

The main purpose of this chapter is to deliver the reader a brief introduction of the various trends in fibre Bragg grating field. This chapter discusses fibre Bragg gratings, their development, theory behind the gratings and their applications. It also provides necessary background about the Fabry-Perot sensors.

Further, it will discuss the fabrication techniques of gratings and their sensitivity to measurands such as temperature, strain, pressure etc. An introduction to the most common interrogation techniques that have been proposed by various researchers is also given.

3.2 Fibre Bragg Gratings

3.2.1 FBG Theory

The discovery of photosensitivity in optical fibres led to formation of fibre Bragg grating which is generally formed within the core of single mode silica fibre perpendicular to fibre's longitudinal axis [1]. The core refractive index is transformed periodically by exposing it to ultraviolet light and the fringes are formed that act as reflectors. Light reflected from these set of fringes over a certain length are in phase and reflect a certain wavelength. This structure acts as wavelength filter and the peak wavelength that is reflected from Bragg grating, λ_B, which is known as Bragg wavelength [2].

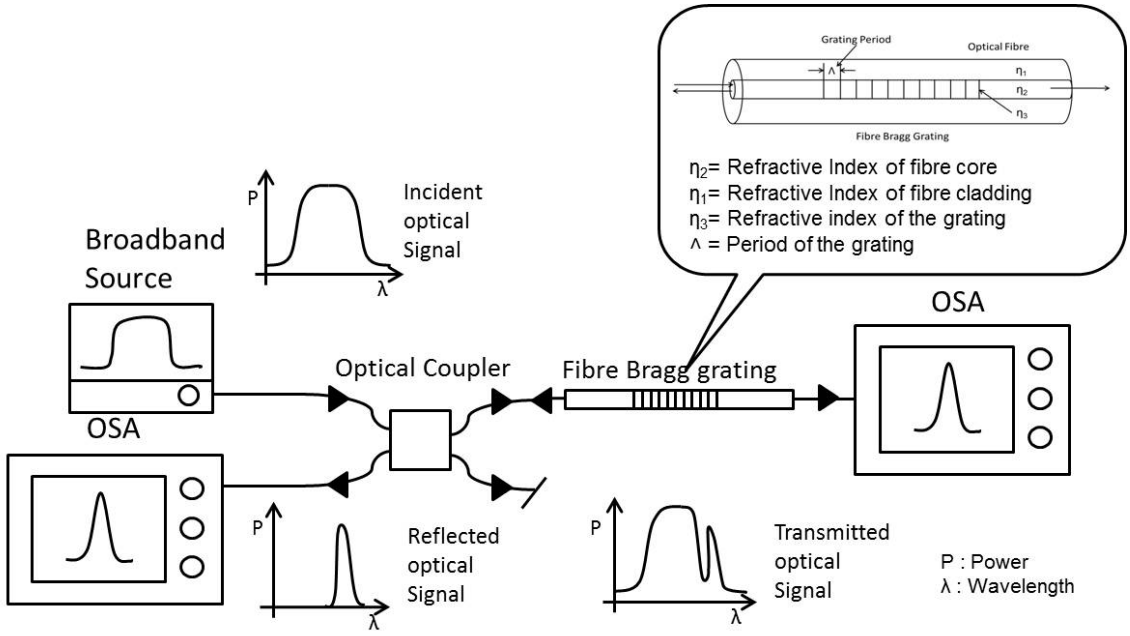

Figure 3.1 Response of fibre Bragg grating to incident broadband light.

The Bragg wavelength λ_B is given by:

$$\lambda_B = 2.n_{eff}.\Lambda \qquad \textbf{Equation 3.1}$$

where, n_{eff} is the effective refractive index of the fiber core and Λ is the period of the grating structure. The Bragg wavelength λ_B is reflected back and the remaining incident radiation is propagated with minimum attenuation and results in a transmitted signal that takes the form of the source but with the reflected component removed from it as shown in figure 3.1. FBG's can be described as the sinusoidal variation in refractive index of core fibre along its lengthwise axis *n(z)*.

$$n(z) = n_{core} + \Delta n \left[1 + V \cos\left(\frac{2.\pi.z}{\Lambda}\right)\right] \qquad \textbf{Equation 3.2}$$

where, n_{core} is the unexposed core refractive index, Δn is the amplitude of the induced refractive index change, Λ is the period of the modulation *V* is the UV fringe visibility. If V≠1, then Δn is the average index change.

Yariv [4] proposed coupled mode theory that evaluates reflection properties of Bragg grating. The reflectivity *R* of grating with constant modulation amplitude and grating length *L* is given as [2-3]:

$$R = \frac{\kappa^2 sinh^2(SL)}{\Delta\beta^2\ sinh^2(SL) + S^2 cosh^2(SL)}$$ **Equation 3.3**

$\kappa^2 > \Delta\beta^2$

$$R = \frac{\kappa^2 sin^2(QL)}{\Delta\beta^2 - cos^2(QL)}$$ **Equation 3.4**

$\kappa^2 < \Delta\beta^2$

where, $S = (\kappa^2 - \Delta\beta^2)^{1/2}$ and $Q = (\Delta\beta^2 - \kappa^2)^{1/2}$, κ is the coupling coefficient which is proportional to magnitude of index change.

$$\beta = 2.\pi.\frac{n_{eff}}{\lambda}$$ **Equation 3.5**

is the propagation constant and n_{eff} is the effective refractive index of core and λ is free space wavelength.

$$\Delta\beta = \beta - \frac{p\pi}{\Lambda}$$ **Equation 3.6**

is the differential Eigenmode propagation and *p* is an integer and Λ is grating period.

From equation 3.3 the maximum reflectivity R_{max} is achieved when $\Delta\beta = 0$ i.e. from equation 3.6 we get,

$$\beta - \frac{p\pi}{\Lambda} = 0 \Rightarrow \beta = \frac{p\pi}{\Lambda}$$

From equation 3.5 we get,

$$2.\pi.\frac{n_{eff}}{\lambda} = \frac{p\pi}{\Lambda}$$

$$p\lambda = 2n_{eff}\,\Lambda \equiv \lambda_B$$ **Equation 3.7**

which satisfies the Bragg conditions and λ_B is of order *p.*

When *Δβ*=0 than maximum reflectance is achieved and equation 3.3 becomes:

$$R = \frac{\kappa^2 sinh^2(\kappa L)}{\kappa^2 cosh^2(\kappa L)} => tanh^2(\kappa L)$$

$$R_{max} = tanh^2(\kappa L)$$ **Equation 3.8**

From above equation, it implies that the reflectivity of the Bragg gratings can be increased either by increasing the magnitude of the refractive index change or by inscribing long grating structures.

The full-width at half-maximum (FWHM) bandwidth of a grating [5] is difference between two wavelengths on either side of Bragg wavelength where reflectivity drops to half of its maximum. An increase in length of grating results in reduced FWHM bandwidth.

$$\Delta\lambda_{FWHM} = \lambda_B\, s \sqrt{\left(\frac{1}{2}\frac{\Delta n}{n}\right)^2 + \left(\frac{1}{N}\right)^2}$$ **Equation 3.9**

Where *s* ≈ 1 for strong gratings and *s* ≈ 0.5 for weaker gratings and *N* is the number of grating planes present in grating structure and *Δn/n* is the refractive index modulation [2,6].

3.2.2 Fabrication techniques:

The refractive index modulation of a fibre Bragg grating is achieved by exposing the core to intense UV interference fringe pattern that is generated by two main methods:

3.2.2.1 Two- beam holographic method

Meltz *et. al.* [7] first reported the fabrication of gratings by using two beam holographic method. In this approach gratings are written within the core of a photosensitive fibre by exposing the core to a coherent two-beam UV interference pattern as shown in figure 3.2 below. These were written for operation around 570nm range. The UV light is split into equal-intensity beams by a beam splitter. These beams are recombined to form an interference pattern on the core of the fibre.

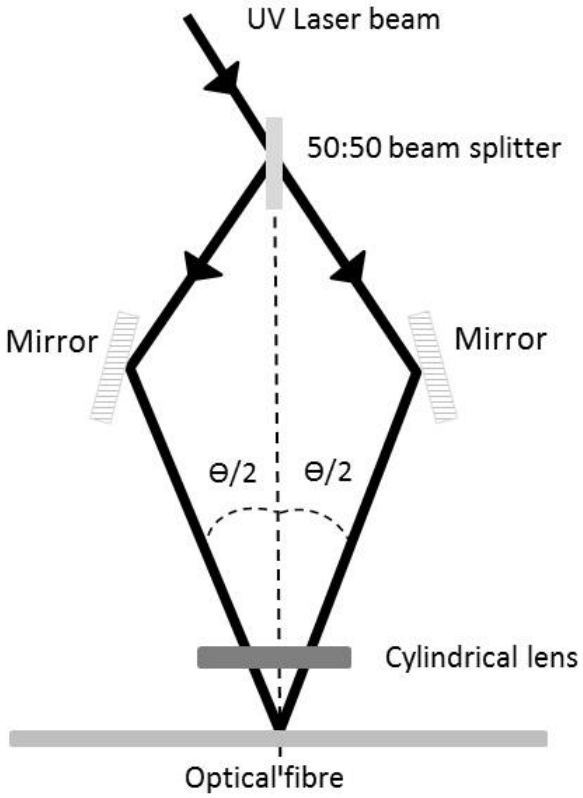

Figure 3.2 Two beam holographic technique for fibre Bragg grating fabrication

The intensity of the pattern is increased by using cylindrical lens. The grating period is observed to be a function of the incident laser wavelength and the angle of incidence of the beams and can be shown as:

$$\Lambda = \frac{\lambda_{UV}}{2.\sin(\frac{\theta}{2})}$$ **Equation 3.10**

By adjusting this angle gratings can be tailored for different Bragg wavelengths. The disadvantage of this technique is that it cannot write gratings with long exposure length that are longer in length than the interfering UV beams. This can be overcome by using some beam expanding lenses. This method can also result in undesirable chirped effect in grating structure due to beam shape producing uneven exposure.

Kashyap *et al* [8] at British Telecom Research Laboratories proposed and demonstrated the first FBG's that operate in the 1450nm - 1600nm region. This resulted in the increase in use of the fibre gratings in telecommunications and the research from then on has taken a new dimension.

3.2.2.2 Diffractive Phase mask technique

To overcome the limitation of two-beam holographic technique, phase mask technique for fabricating gratings was reported by Hill *et al* [9] and Anderson *et al* [10]. This is a simple technique and is functional even with low spatial and temporal coherence laser sources. Periodic patterns are etched on to the phase mask using photolithography that is made of a silica substrate.

A UV laser beam at normal incidence to the phase mask is diffracted and by placing the phase mask parallel and close in contact with fibre. Interference between the primary orders produces high-contrast intensity, periodic pattern on the fibre which inscribes a refractive index modulation into the core of photosensitive fibre.

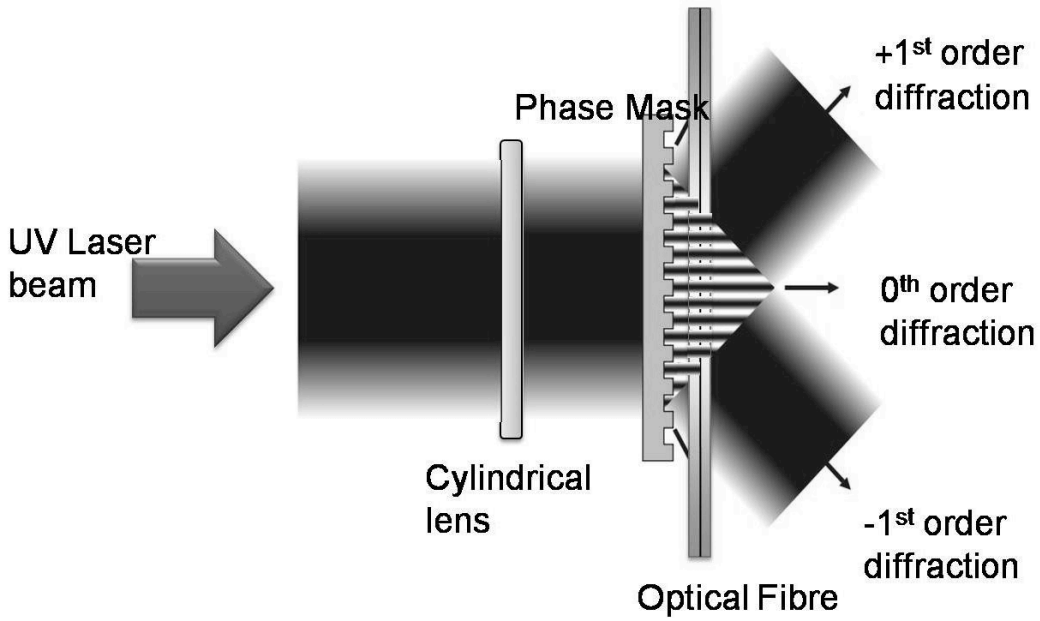

Figure 3.3 Phase mask technique for fibre Bragg grating fabrication

Unlike the two-beam holographic method, the period of the induced pattern (Λ) is dependent on the period of the mask corrugation (Λ_{PM}) in the phase mask technique and thus can be used to fabricate gratings of increased length [53].

$$\Lambda = \Lambda_{PM}/2 \qquad \textbf{Equation 3.11}$$

The UV induced index change is different in all fibres and for less photosensitive fibre the hydrogen loading method [11] is used to photosensitize them. After the hydrogenation the fibre jacket on the fibre is striped either by using a stripper or paint remover to allow UV inscription and is recoated after the exposure to increase the mechanical strength of fibre so that it can be used in practical devices. These UV exposed gratings are then annealed where in these gratings are kept under certain temperature to treat the gratings against subsequent degradation [6, 12, 13]. By using phase mask technique gratings ca be made with different profiles such as chirped, tilted, long period, phase shift. This method is best suited for mass production of gratings. Further to this,

Gaussian apodization [14, 15] is used to suppress the sidelobes while maintaining the reflectivity and narrow bandwidth and improves the filter response.

In both aforementioned inscription techniques, the protective fibre acrylate coating needs to be removed to reduce the effect of absorption of wavelengths that has been reported by Askins *et al* [16, 18] and to directly expose the core to UV light beam. The two main techniques commonly used are mechanical stripping using a fibre clad stripper or chemical stripping by using some coating removing paint. Although the coating removal process increases the risk of fibre breakage as it reduces mechanical strength of the fibre. The fibre is recoated after the inscription. Several techniques have been reported [17, 18] for inscription of low reflectivity sensors in line during the manufacturing stage and then applying the protective acrylate coating.

3.2.3 Physical measurand sensing

FBG sensors have been reported for measurement of temperature [19, 20], strain and ultrasound in smart structures [19 – 23] and pressure [24] etc. It can also measure dynamic magnetic fields, seismic vibrations, flow measurement etc. However, to study the Structural Health Monitoring in composite materials of aircraft structures measurement of strain and temperature is necessary. Since FBGs are less sensitive to vibration or heat and more reliable, they offer a significant advantage over traditional electronic gauges used for aerospace applications.

The peak reflected and transmitted wavelength changes with the change in any one parameter due to environmental or physical perturbation. This capability of

the fibre sensor makes it a suitable choice in aircraft structures monitoring, dam monitoring, military applications and telecommunications.

3.2.3.1 Temperature sensing

Due to change in temperature ΔT there is change in the effective refractive index of the fibre induced by the thermal expansion and thermo-optic effect of the fibre that cause shift in the Bragg wavelength λ_B and is given by [6]:

$$\lambda_T = \lambda_B (\alpha + \xi) \Delta T \qquad \textbf{Equation 3.12}$$

where, ξ is the fibre thermo-optic coefficient α is the thermal coefficient of linear expansion.

Wavelength (*nm*)	**Temperature sensitivity(pm $^{\circ}C^{-1}$)**
830	~6.8
1300	~10.0
1550	~13.0

Table 3.1 Wavelength shifts induced by temperature variations in FBGs operating in varying wavelength regions

Above table shows relationship between temperature and wavelength and shows the change in temperature for 1^0 C change at 830 nm, 1300nm and 1550nm [6].

3.2.3.2 Strain sensing

The wavelength change $\Delta\lambda_S$ for a longitudinal strain $\Delta\varepsilon$ that is applied to the fibre, is given by:

$$\Delta\lambda_s = \lambda_B (1 - \rho_\alpha) \Delta\varepsilon \qquad \textbf{Equation 3.13}$$

Where ρ_α is the photo-elastic coefficient and is given by:

$$\rho_\alpha = \frac{n^2}{2}[\rho_{12} - \nu (\rho_{11} - \rho_{12}) \qquad \textbf{Equation 3.14}$$

where ρ_{11} and ρ_{12} are components of fibre optic strain tensor and v is Poisson' ratio.

Wavelength (*nm*)	Strain sensitivity (pm $\mu\varepsilon^{-1}$)
830	~0.64
1300	~1.0
1550	~1.2

Table 3.2 Wavelength shifts induced by strain variations in FBGs operating in varying wavelength regions

For the single mode fibre, the wavelength–strain sensitivities of 800 *nm* and 1550 *nm* FBGs have been measured as ~0.64 pm $\mu\varepsilon^{-1}$ and ~1.15 pm $\mu\varepsilon^{-1}$ respectively [6, 25].

3.2.3.3 Pressure sensing

The wavelength change $\Delta\lambda_P$ due to change in external pressure ΔP is given by:

$$\frac{\Delta\lambda_P}{\lambda_B} = \frac{\Delta(n\Lambda)}{n\Lambda} = \left[\frac{1}{\Lambda}\frac{\partial\Lambda}{\partial P} + \frac{1}{n}\frac{\partial n}{\partial P}\right]\Delta P \qquad \textbf{Equation 3.15}$$

where Λ is the spatial period of the grating and n is the effective refractive index of the fibre core. In a single mode fibre the change in fibre diameter due to pressure is negligible. The change in physical length is given by:

$$\frac{\Delta L}{L} = \frac{(1-2v)P}{E} \qquad \textbf{Equation 3.16}$$

and refractive index is given by:

$$\frac{\Delta n}{n} = \frac{n^2 P}{2E}(1-2v)(2\rho_{12}+\rho_{11}) \qquad \textbf{Equation 3.17}$$

where E is the fibre Young's modulus and v is Poisson ratio of the fibre and $\rho_{11}$and ρ_{12} are components of the fibre-optic strain tensor. Assuming $\Delta L / L$ =

$\Delta\Lambda/\Lambda$, the normalised pitch-pressure and the index –pressure coefficients is given by:

$$\frac{1}{\Lambda}\frac{\partial\Lambda}{\partial P} = -\frac{(1-2v)}{E} \qquad \textbf{Equation 3.18}$$

And

$$\frac{1}{n}\frac{\partial n}{\partial P} = \frac{n^2}{2E}(1-2v)(2\rho_{12}+\rho_{11}) \qquad \textbf{Equation 3.19}$$

Substituting, equation (3.15) with equation (3.18) and equation (3.19) the wavelength–pressure sensitivity can be obtained as follows:

$$\Delta\lambda_P = \lambda_B\left[-\frac{(1-2v)}{E}+\frac{n^2}{2E}(1-2v)(2\rho_{12}+\rho_{11})\right]\Delta P \qquad \textbf{Equation 3.20}$$

$\Delta\lambda_P/\Delta P$ for a single mode FBG centred at a wavelength of 1550nm was measured as -3×10^{-3} nm MPa^{-1} over a pressure range of 70 MPa [26]. To monitor and control aircraft systems measurement of pressure in aerospace applications is very important, This covers monitoring of engine inlet pressure, cabin pressure, Engine Oil Pressure, De-icing, Fuel Level, Fuel Flow etc.

3.2.3.4 Strain and temperature sensing

Any change in strain and/or temperature, changes the grating period thus effectively changing the Bragg wavelength. As a result, this changes the reflected and transmitted wavelength. The strain directly affects the FBG as it expands or contracts the grating period and thus the refractive index is modified whereas, the temperature sensitivity of an FBG mainly occurs because of the change in induced refractive index. The wavelength shift in response to the strain and temperature is given by the following relationship:

$$\Delta\lambda_B = 2.n.\Lambda\left[\left\{1-\left(\frac{n^2}{2}\right).[\rho_{12}-v.(\rho_{11}+\rho_{12})]\right\}.\varepsilon+\left[\alpha+\frac{\left(\frac{dn}{dT}\right)}{n}\right].\Delta T\right]$$

Equation 3.21

Where $\Delta\lambda_B$ is the shift in Bragg wavelength for an applied strain ε or temperature change ΔT. Λ is the spatial period of the grating and *n* is the effective refractive index of the fibre core and *v* is Poisson ratio of the fibre and $\rho_{11}$and ρ_{12} are components of the fibre-optic strain tensor and α is coefficient of thermal expansion.

3.2.3.5 Compensation techniques to overcome dual sensitivity

Dual sensitivity is not desirable for many applications e.g. damage monitoring in aircrafts where the strain measurement is important to estimate the nature and location of damage. It needs to be very clear in such applications whether the change in Bragg wavelength is due to strain or temperature change thus, decoupling of two parameters become very important. Various solutions have been reported to overcome this dual sensitivity.

Most commonly used method is the use of two superimposed FBGs of different wavelength (850nm and 1300nm) [49]. Since, the wavelength change of the two superimposed gratings will be different even if each grating is subjected to the same amount of strain, it will yield values for temperature and strain coefficients which later on can be realised in a matrix and these pair of equations can be solved. Another solution is to use two FBGs written at same wavelength and spliced but have different diameters. Such gratings show same temperature response but different strain response to an applied stress [50]. Another way of differentiating between temperature and strain due to wavelength change is to use the responses of strain and temperature of FBG and a long period fibre grating, which are combined together [51]. Another method is to use a

combination of a Type I [54] grating with a Type IIA [55] grating which have different temperature coefficients [52] and thus can be used to determine the strain and temperature. Type I grating is a standard grating which can be inscribed in both hydrogenated or non-hydrogenated fibre using low-power UV radiation. A Type IIA grating is a regenerated grating written by partially erasing type I grating in hydrogen-free germanosilicate fibre.

3.3 Fabry Perot Interferometers

An ideal Fabry – Perot consists of two mirrors separated by distance d from each other and have a reflectivity R. A Fabry-Perot consists of two reflecting mirrors of same strength and reflectance *R* separated by a distance *L* on the same piece of fibre. In an ideal transmission stage the absorption can be assumed negligible and the transmission can be denoted as:

$$R = 1 - T$$ **Equation 3.22**

Theoretically, multiple waves reflected from the fibre end-faces interfere coherently. A Fabry-Perot interferometer is shown in figure 3.4 below.

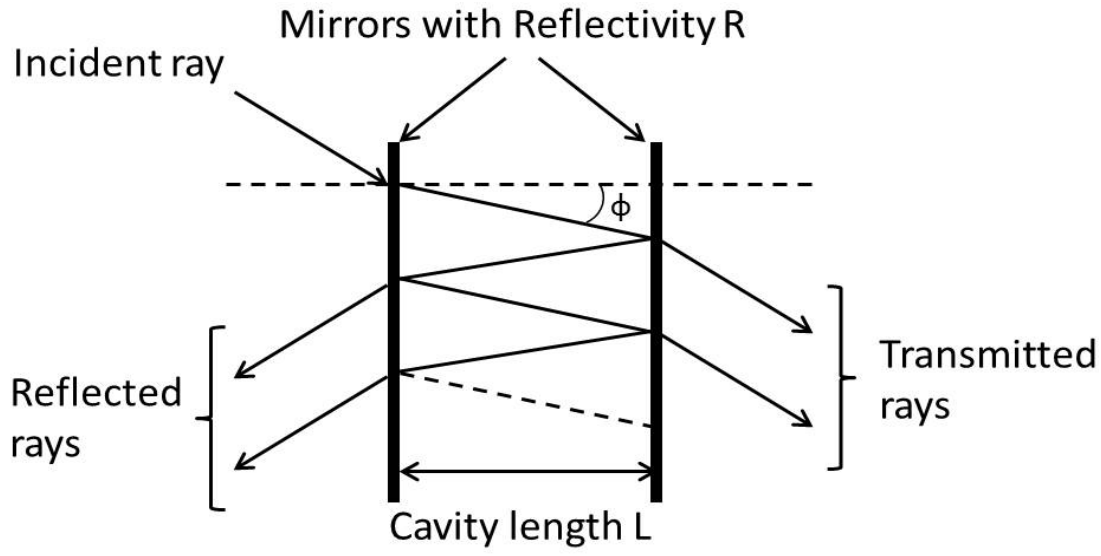

Figure 3.4 Arrangement of Fabry-Perot configuration

Like other interferometers this sensor also produces a change in output intensity which is dependent upon the phase shift of light in the sensing region [17]. The ratio of reflected power P_r and incident power P_i is given by [27]:

$$\frac{P_r}{P_i} = \frac{2R\ (1 - cos\phi)}{1 + R^2 - \ 2R\ cos\phi} \qquad \textbf{Equation 3.23}$$

where ϕ is the round trip static phase shift of the laser light inside the cavity, and is given by:

$$\phi = \frac{4.\pi.n.L}{\lambda} \qquad \textbf{Equation 3.24}$$

where L the length of the cavity, n its refractive index and λ the free space wavelength of the light. For a Fabry-Perot cavity with low reflective mirrors (R << I), equation (2.25) is simplified to:

$$\frac{\mathrm{P_r}}{\mathrm{P_i}} = 2\mathrm{R}\ (1 - \cos\phi) \qquad \textbf{Equation 3.25}$$

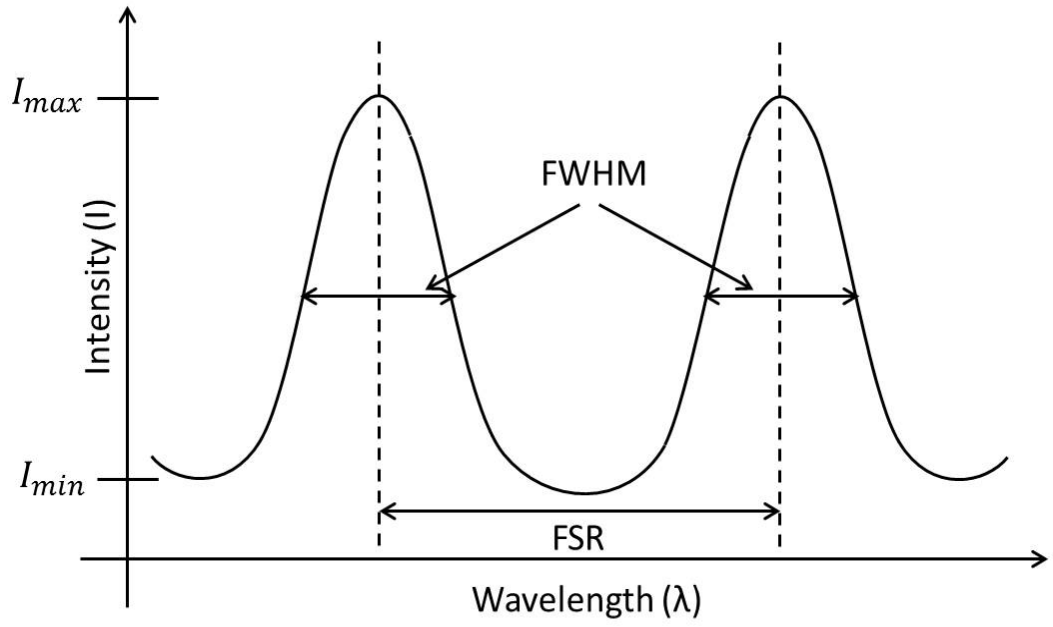

Figure 3.5 Transmission curve of a Fabry Perot interferometer

If the cavity length and wavelength change simultaneously, the phase shift can be expressed as [46]:

$$\Delta\phi = \frac{4.\pi.n}{\lambda}\,\Delta L - \frac{4.\pi.n.L}{\lambda^2}\,\Delta\lambda \qquad \textbf{Equation 3.26}$$

Free Spectral Range (FSR) of the Fabry-Perot (as shown in figure 3.5) depends on the distance L of the mirrors and is the measure of the separation of optical frequency or wavelength between adjacent reflected or transmitted peaks. In terms of optical frequency it can shown by:

$$\Delta\nu = \frac{c}{2.n.L} \qquad \textbf{Equation 3.27}$$

The value of FSR is the measure of the device sensitivity. The width of the resonant cavity mode is small for highly reflective mirrors, and is broad when reflectance is decreased.

The full width at half maximum $\Delta\upsilon$ (FWHM) is given by:

$$\Delta\upsilon = \frac{c}{2.n.L}.\frac{1-R}{\pi\sqrt{R}} \qquad \textbf{Equation 3.28}$$

and the Finesse (F) of the cavity which is the measure of the Fabry-Perot's resolution and depends on the reflectivity R of the mirrors is given by:

$$F = \frac{FSR}{\Delta\upsilon} \qquad \textbf{Equation 3.29}$$

From equation 3.27, 3.28 and 3.29

$$F = \frac{c}{2.n.L}.\frac{2.n.L}{c}.\frac{\pi\sqrt{R}}{(1-R)} \qquad \textbf{Equation 3.30}$$

We get:

$$F = \frac{\pi\sqrt{R}}{(1-R)}$$ **Equation 3.31**

The visibility, V of a Fabry-Perot determines how well the spectral features can be resolved and is given by:

$$V = \frac{I_{max} - I_{min}}{I_{max} + I_{min}}$$ **Equation 3.32**

Where $I_{max}$and I_{min} are the maximum and minimum transmissions.

3.3.1 Fibre Bragg grating Fabry- Perot Interferometers

Fibre Bragg gratings Fabry-Perot as acoustic sensors was demonstrated in several research papers. Alcoz *et al* [27], Lee *et al* [28] demonstrated fibre based Fabry –Perot sensors can be used for ultrasonic sound and temperature sensing in structures as they have high sensitive to strain and pressure. The pressure or strain on the sensor due to perturbation changes the refractive index of the core and also changes the optical path length that causes interference and there is a change in phase of light that is modulated by the pressure on the sensor. This can be detected by a proper demodulation system.

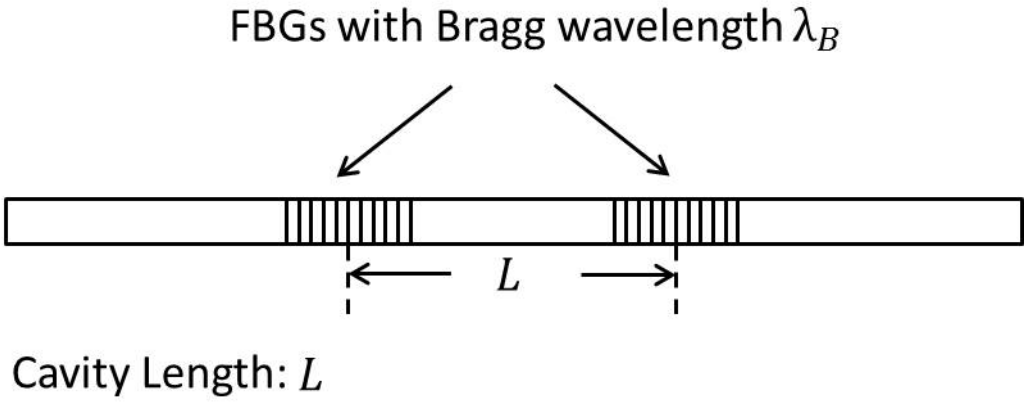

Figure 3.6 Fabry Perot Interferometer formed by two fibre Bragg gratings

A simple uniform Fabry-Perot sensor on a fibre optic can be formed by writing two gratings of equal strength separated by a distance Lmm sharing the same wavelength bandwidth. Each grating acts as a reflective mirror.

Legoubin et al. [47] reported one of the first optical fibre Fabry-Perot with a pair of Bragg gratings inscribed with a spacing of a few millimeters in a single mode fibre. Considering the FBGs to have identical reflectivity R, the peak reflectivity of the Fabry-Perot filter, R_{PF} can be given by [47]:

$$R_{PF} = 1 - T = \frac{4R}{(1+R)^2} \qquad \textbf{Equation 3.33}$$

same as conventional Fabry Perot response.

A chirped FBG Fabry Perot offers a large bandwidth in comparison to uniform FBG Fabry Perot [48]. Considering each grating to be lossless, and with no dispersion inside the Fabry-Perot cavity the FSR is given by:

$$\Delta\nu = \frac{c}{2.n.L} \qquad \textbf{Equation 3.34}$$

3.3.2 Sensing in Fibre optic Fabry-Perot sensor:

3.3.2.1 Temperature sensing

With change in temperature ΔT the optical phase shift of the Fibre Bragg grating Fabry-Perot sensor changes to $\Delta\phi$ and is given by[31]:

$$\Delta\phi = \frac{4.\pi.n.L}{\lambda}\left(\frac{1}{n}\frac{dn}{dT} + \frac{1}{L}\frac{dL}{dT}\right)\Delta T \qquad \textbf{Equation 3.35}$$

Hocker [30], at room temperature determined the values for:

$$\frac{1}{n}\frac{dn}{dT} = 7.0\ x\ 10^{-6}\ ^{\circ}\mathrm{C}^{-1}$$ **Equation 3.36**

and

$$\frac{1}{L}\frac{dL}{dT} = 5.0\ X\ 10^{-7}\ ^{\circ}\mathrm{C}^{-1}$$ **Equation 3.37**

From equation (3.36) and (3.37) it can be inferred that the effect of change of the refractive index is fourteen times larger than the effect of change of the length due to the temperature change.

3.3.2.2 Strain Sensing

The change in phase shift response $\Delta\phi$ of the FBG Fabry-Perot to the axial strain on the fibre can be given as [31]:

$$\Delta\phi = K\left(\frac{4.\pi.n}{\lambda}\right)\Delta L$$ **Equation 3.38**

where, *K* is a constant. *K* is determined as the strain-optic coefficient and is given by:

$$K = 1 - \left(\frac{n^2}{2}\right).[\rho_{12} - v.(\rho_{11} + \rho_{12})]$$ **Equation 3.39**

Where ρ_{11} and ρ_{12} are fibre optic strain tensor and *v* is Poisson's ratio. Hocker [30] determined the value for K =0.8 for silica optic fibre.

3.3.2.3 Ultrasound sensing

The phase of light in the sensing region of the FBG Fabry-Perot is modulated for a continuous ultrasound wave with a angular frequency ω_m in response to acoustic pressure change. The modulated phase can be shown as:

$$\phi = \phi_0 + \phi_m = \phi_0 + \beta sin\,\omega_m t$$ **Equation 3.40**

where ϕ_0 and ϕ_m are static and dynamic phase shift and β is amplitude of the induced phase shift. Modifying equation (3.25) and substituting ϕ with (3.40) we get,

$$\frac{P_r}{P_i} = 2R\left[1 - \left(1 - \frac{\beta^2}{4}\right)\cos\phi_0 + \beta\sin\phi_0\sin\omega_m t - \left(\frac{\beta^2}{4}\right)\cos\phi_0\, cos2\omega_m t + \cdots\right]$$

Equation 3.41

The modulating frequency can be determined by observing the spectral components of reflected optical power [31]. Ultrasound sensors are being used for Acoustic emission and NDT (Non Destructive Testing) and are explained in the next few chapters.

3.4 Fibre Bragg grating sensor interrogation techniques

To determine the value of different measurand using various interrogation schemes are proposed in many research articles [32-46]. They are mainly single grating sensing techniques but many of them can be extended to work with multiple sensors. The value of the measurand can be estimated by detecting the encoded optical signal and measuring it. The measurement of the encoded signal, resolution and speed however depends upon the type of interrogation system employed.

The simplest form of an interrogation system is shown in figure 3.7 and 3.8. These systems are economical and easy to setup but they are susceptible to the environmental perturbations and thus do provide the actual value of the measurand.

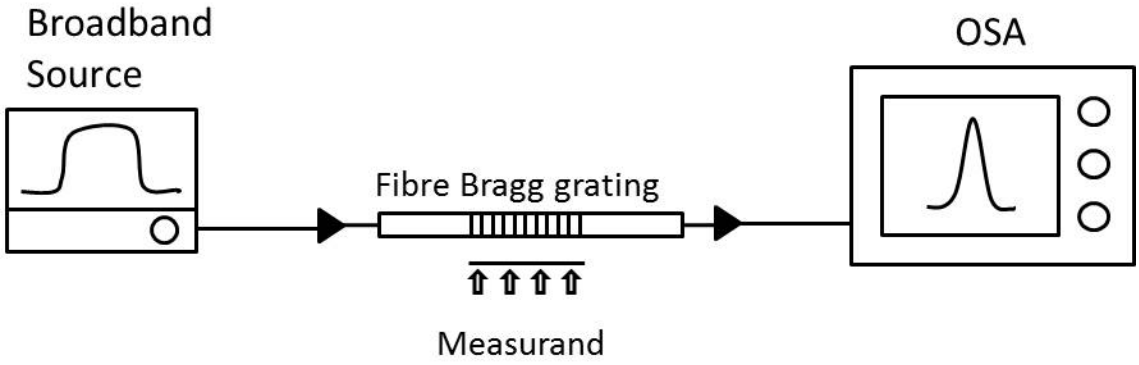

Figure 3.7 Transmission based interrogation system

The initial work on high frequency measurements was demonstrated by Webb et al.[32] and Fisher et al [33] in medical applications and frequencies upto 950kHz was detected. The experimental set up was similar to below figure 3.8.

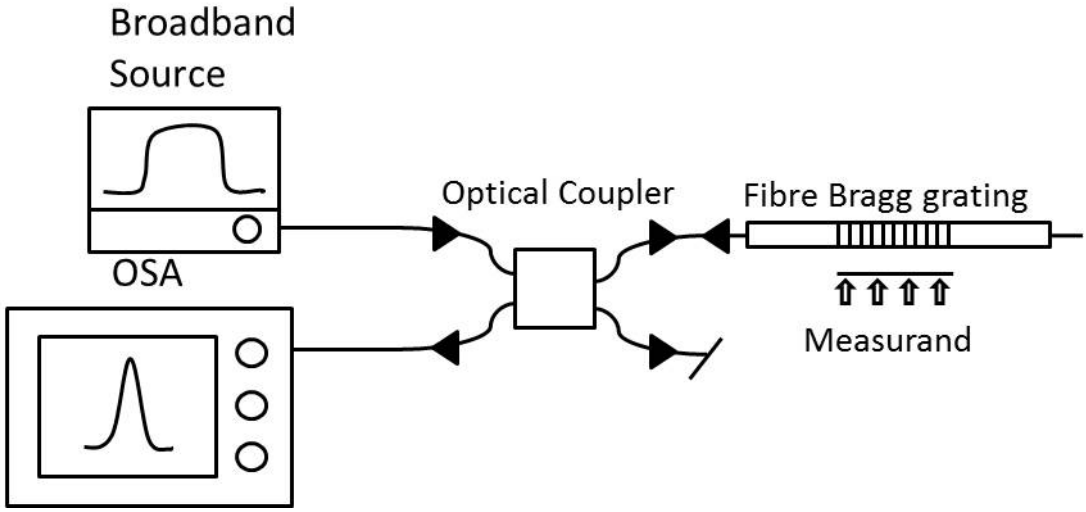

Figure 3.8 Reflection based interrogation system

It was also found that upper limit on the incident acoustic frequency is set by grating length and should be less than half the acoustic wavelength in fibre core [33].

Jackson and Ribeiro [35] proposed the work for the interrogation of a large number of fiber-optic grating sensors and demonstrated signal recovery by matching a sensing grating to its reference sensor and used the matched pair gratings set up as shown in below figure 3.9. The principle was to use

wavelength matched pair of gratings, one being a sensor and other is to track wavelength shifts from the sensor grating. Davis and Kersey [36] demonstrated an efficient and economical interrogation technique for the demodulation of FBG sensor arrays using matched grating array to optically filter and track wavelength shifts from the FBG sensors.

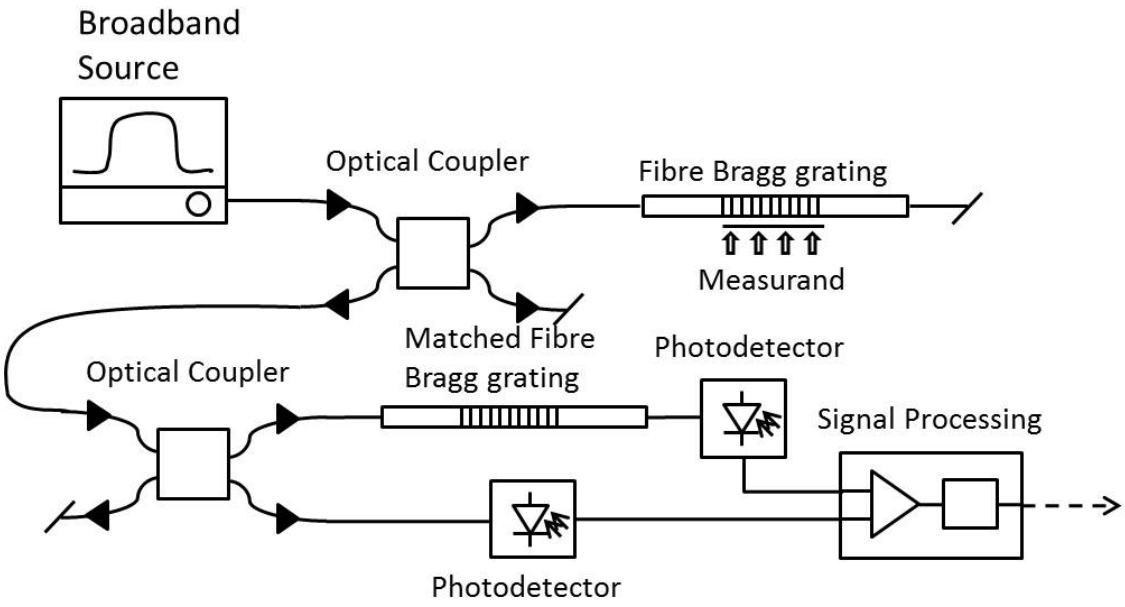

Figure 3.9 A matched fibre pair based interrogation system

Perez et al. [37] and Ribiero et al. [38] used the same method and were able to detect up to 1 MHz and they detected acoustic emissions generated by piezo-ceramic resonator, ultrasonic transducer and a pencil break test.

Kersey et al. [39-40] demonstrated a high-resolution technique for the detection of weak dynamic strain induced shifts using in-fibre interferometer as shown in figure 3.10. This consists of an unbalanced interferometer with fibre path length imbalance less than effective coherence length of sensor grating. This interferometer behaves as a spectral filter and the transfer function can be shown as:

$$I(\lambda) = A\{1 + k\cos[\psi(\lambda) + \phi]\}$$ **Equation 3.42**

Where, $\psi(\lambda) = 2\pi\eta d/\lambda$, A is proportional to the input intensity , d is the length imbalance between the fibre arms, η is the effective index of the mode, λ is the wavelength of the reflected light from the sensing grating and ϕ is a bias phase offset of the interferometer. Any change in sensing grating wavelength can be detected using such system.

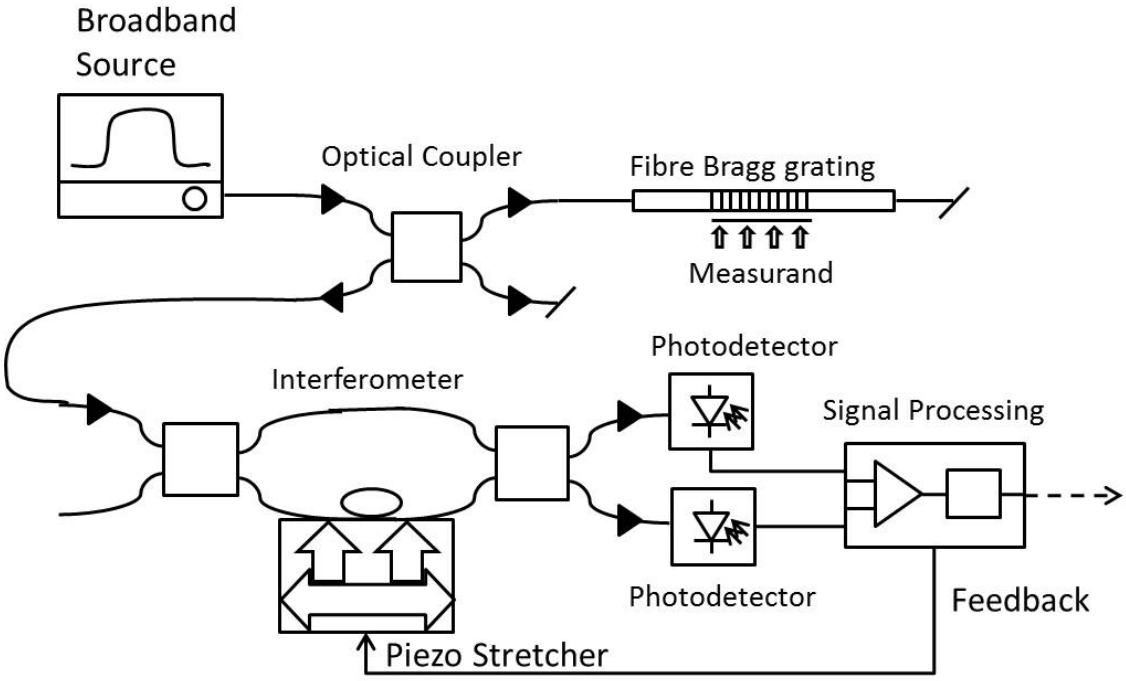

Figure 3.10 An interferometer based interrogation system

Betz et al. [41-43] were among the first few who used the FBGs to detect the ultrasonic lamb waves for damage monitoring of structures. This experiment used the setup as shown in figure 3.11 below. Analysis was carried out to study the impact of the ratio of the fibre grating length and the acoustic wavelength on the sensor signal. The work carried out provided numerical simulations to calculate the grating length to monitor lamb wave frequency and the maximum ultrasonic frequency that can be detected by a FBG sensor with a given grating length.

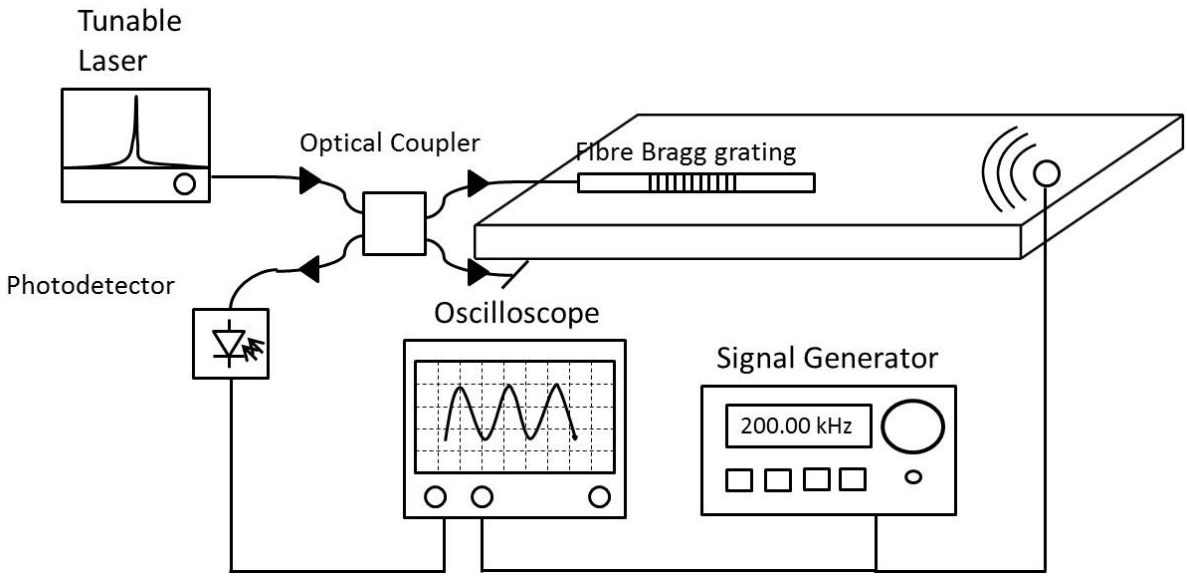

Figure 3.11 An acoustic emission detection system

Further work has been carried out to use multiplexed gratings to extend the system for structural health monitoring applications.

Bhatia et al. [44], Read et al. [45] and Dae-Hyun Kim [46] proposed the use of extrinsic Fabry–Perot interferometric (EFPI) sensor for applications in civil structures and for damage detection in carbon fibre composite structures which has parameters similar to a FBG based interferometer.

The EFPI sensor consists of a cavity made of two single-mode fibre ends in a capillary tube, as shown in figure 3.12. Theoretically, two light waves reflected from the fibre end-faces interfere with each other. Any change in phase of the interfered light is due to the change in the cavity length of the interferometer when a laser diode with a fixed wavelength is used.

Takahashi et al [34] reported the use of two FBGs written in series forming a Fabry-Perot cavity to measure acoustic emissions for use in the civil and marine industries.

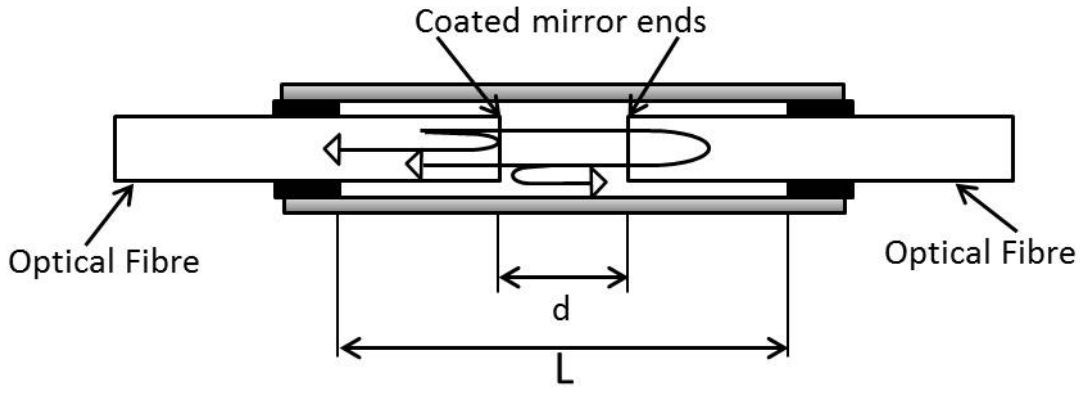

Figure 3.12 A typical EFPI sensor

3.5 Chapter conclusion

This chapter covered fibre Bragg grating technology's basics and its use in the recent technology. The reader will briefly understand the functionality of fibre Bragg grating and inscription techniques that are used to manufacture them such as holographic technique and phase mask technique.

Measurement of various measurands using FBG such as strain, temperature and pressure were also discussed. It also presented a brief overview of the Fabry-Perot fibre Bragg gratings and also discussed its sensitivity to aforementioned physical parameters.

This chapter also focussed on the common interrogation techniques and laid the foundation for experimental chapters that are discussed further.

3.6 References

[1] K. O. Hill, Y. Fujii, D. C. Johnson and B. S. Kawasaki, "Photosensitivity in optical fibre waveguides: application to reflection filter fabrication", *Applied Physics Letters,* vol. 32, pp. 647-649, 1978.

[2] I. Bennion, J. A. R. Williams, L. Zhang, K. Sugden and N. J. Doran, “UV-written in-fibre Bragg gratings”, *Optical and Quantum Electronics,* vol. 28, pp. 93-135, 1996.

[3] D. K. W. Lam and B. K. Garside, “Characterization of single-mode fibre filters”, *Applied Optics,* vol. 20, pp. 440-445, 1981.

[4] A. Yariv, "Coupled Mode Theory for guided wave optics”, *Journal of Quantum Electronics,* vol. QE-9, pp. 919-933, 1973.

[5] P. Russell, J. L. Archambault and L. Reekie, “Fibre gratings”, *Physics World*, vol. 6, pp. 41-46, 1993.

[6] Y. J. Rao, “In-fibre Bragg grating sensors”, *Measurement Science and Technology,* vol. 8, pp. 355-375, 1997.

[7] G. Meltz, W. W. Morey and W. H. Glenn, “Formation of Bragg gratings in optical fibers by a transverse holographic method”, *Optics Letters*, vol. 14, pp. 823-825, 1989.

[8] R. Kashyap, J. J. Armitage, R. Wyatt, S. T. Davey and D. L. Williams, “All-fibre narrowband reflection gratings at 1500nm”, *Electronic Letters*, vol. 26, pp. 730-732, 1990.

[9] K. O. Hill, B. Malo, F. Bilodeau, D. C. Johnson and J. Albert, “Bragg gratings fabricated in monomode photosensitive optical fiber by UV exposure through a phase mask”, *Applied Physics Letters*, vol. 62, pp. 1035-1037, 1993.

[10] D. Z. Anderson, V. Mizrahi, T. Erdogan, and A. E. White, “Production of in-fibre gratings using a diffractive optical element”, *Electronics Letters*, vol. 29, pp. 566-568, 1993.

[11] P. J. Lemaire, R. M. Atkins, V. Mizrahi and W. A. Reed, “High Pressure H2 loading as a technique for achieving ultrahigh UV photosensitivity and thermal sensitivity in GeO2 doped optical fibers”, *Electronic Letters*, vol. 29, pp. 1191-1193, 1993.

[12] A. Othonos and K. Kalli, Fibre Bragg Gratings: Fundamentals and Applications in Telecommunications and Sensing. London: Artech House Publishers, 1999.

[13] L. Zhang, W. Zhang and I. Bennion, “In-Fibre Grating Optic Sensors”, in *Fibre Optic Sensors* New York: Marcel Dekker Inc., 2002.

[14] S. J. Mihailov, F. Bilodeau, K. O. Hill, D. C. Johnson, J. Albert and A. S. Holmes, “Apodization technique for fiber grating fabrication with a halftone transmission amplitude mask”, *Applied Optics*, vol. 39, pp. 3670-3677, 2000.

[15] C. Yang and Y. Lai, “Improving the spectral sharpness of an apodized fibre grating”, *Journal of Optics A: Pure and Applied Optics*, vol. 2, pp. 422-425, 2000.

[16] C. G. Askins, M. A. Putnam, H. J. Patrick and E. J. Friebele, “Fibre strength unaffected by on-line writing of single-pulse Bragg gratings”, *Electronics Letters,* vol. 33, pp. 1333-1334, 1997.

[17] L. Dong, J.-L. Archambault, L. Reekie, P. S. J. Russell and D. N. Payne, “Single pulse Bragg gratings written during fibre drawing”, *Electronics Letters*, vol. 29, pp. 1577-1578, 1993.

[18] C. G. Askins, M. A. Putnam, G. M. Williams, and E. J. Friebele, “Stepped-wavelength optical-fiber Bragg grating arrays fabricated in line on a draw tower”, *Optics Letters*, vol. 19, pp. 147-149 1994.

[19] Y. J. Rao, “Recent progress in applications of in-fibre Bragg grating sensors”, Optics and Lasers in Engineering, vol. 31, pp. 297-324, 1999.

[20] B. Lee, “Review of the present status of optical fiber sensors”, Optical Fiber Technology, vol. 9, pp. 57-79, 2003.

[21] V. E. Saouma, D. Z. Anderson, K. Ostrander, B. Lee and V. Slowik, “Application of fiber Bragg grating in local and remote infrastructure health monitoring”, *Materials and Structures,* vol. 31, pp. 259-266, 1998.

[22] K.-T. Lau, “Fibre-optic sensors and smart composites for concrete applications”, Magazine of Concrete Research, vol. 55, pp. 19-34, 2003.

[23] K. Kageyama, H. Murayama, I. Ohsawa, M. Kanai, K. Nagata, Y. Machijima, and F. Matsumura, “Acoustic emission monitoring of a reinforced concrete structure by applying new fiber-optic sensors”, Smart Material & Structure, vol. 14, pp. S52-S59, 2005.

[24] S. C. Tjin, J. Hao, Y.-Z. Lam, Y. C. Ho, and B. K. Ng, “A Pressure Sensor Using Fiber Bragg Grating”, Fiber and Integrated Optics, vol. 20, pp. 59-69, 2001.

[25] Y. J. Rao, A. B. L. Ribeiro, D. A. Jackson, L. Zhang, and I. Bennion, “Combined spatial- and time-division-multiplexing scheme for fiber grating sensors with drift-compensated phase-sensitive detection”, *Optics Letters,* vol. 20, pp. 2149-2151, 1995.

[26] M. G. Xu, L. Reekie, Y. T. Chow, and J. P. Dakin, “Optical in-fibre grating high pressure sensor”, *Electronics Letters,* vol. 29, pp. 398-399, 1993.

[27] J. J. Alcoz, C. E. Lee and H. F. Taylor, “Embedded Fiber-optic Fabry-Perot Ultrasound Sensor”, *IEEE Transactions on Ultrasonics, Ferroelectrics and Frequency Control,* vol. 37, pp. 302-306, 1990.

[28] C. E. Lee, H. F. Taylor, A. M. Markus and E. Udd, “Optical-fiber Fabry-Perot embedded sensor”, *Optics Letters*, vol. 14, 1989.

[29] J. F. Dorighi, S. Krishnaswamy and J. D. Achenbach, “Stabilization of an Embedded Fiber Optic Fabry-Perot Sensor for Ultrasound Detection”, *IEEE Transactions on Ultrasonics, Ferroelectrics and Frequency Control*, vol. 42, pp. 820-824, 1995.

[30] G. B. Hocker, “Fiber-optic sensing of pressure and temperature”, *Applied Optics*, vol. 18, pp. 1445-1448, 1979.

[31] C. E. Lee, J. J. Alcoz, Y. Yeh, W. N. Gibler, R. A. Atkins, and H. F. Taylor, “Optical fiber Fabry-Perot sensors for smart structures”, *Smart Material & Structure,* vol. 1, pp. 123-127, 1992.

[32] D.J. Webb, “Miniature fiber optic ultrasonic probe”, *Proceedings of SPIE*, vol. 2639, pp. 76-80, 1996.

[33] N.E. Fisher, “Medical ultrasound detection using fiber Bragg gratings”, *Proceedings of SPIE*, vol. 3541, pp. 27-32, 1999.

[34] N. Takahashi, K. Yoshimura, S. Takahashi and K. Imamura, “Development of an optical fibre hydrophone with Fibre Bragg grating”, *Ultrasonics.*, vol. 38, pp. 581-585, 2000

[35] D. A. Jackson, A. B. Lobo Ribeiro, L. Reekie, and J. L. Archambault, “Simple multiplexing scheme for a fiber-optic grating sensor network”, *Opt. Lett*., vol. 18, pp. 1192-1194, 1993.

[36] M. A. Davis and A. D. Kersey, “Matched-filter interrogation technique for fibre Bragg grating arrays”, *Electronics Letters*, vol. 31, pp. 822-823, 1995.

[37] A. B. Lobo Ribeiro, L. A. Ferreira, J. L. Santos, and D. A. Jackson, “Analysis of the reflective-matched fiber Bragg grating sensing interrogation scheme”, *Applied optics*, vol. 36, pp. 934-939, 1997.

[38] I. Perez, H. L. Cui, and E. Udd, “Acoustic emission detection using fiber Bragg gratings”, *Proceedings of SPIE*, vol. 4328, pp. 209–215, 2001.

[39] A. D. Kersey, T. A. Berkoff, and W. W. Morey, “High resolution fiber Bragg grating based strain sensor with interferometric wavelength shift detection”, *Electronics Letters.,* vol. 28, p. 236, Jan. 1992.

[40] A. D. Kersey, T. A. Berkoff, and W. W. Morey, “Fiber-optic Bragg grating strain sensor with drift-compensated high-resolution interferometric wavelength-shift detection”, *Optics Letters*, vol. 18, pp. 72-74, 1993.

[41] D. C. Betz, G. Thursby, B. Culshaw, and W. Staszewski, “Acousto-ultrasonic sensing using fiber Bragg gratings”, Smart Material & Structure, vol. 12, pp. 122-128, 2003.

[42] D. C. Betz, G. Thursby, B. Culshaw, and W. Staszewski, “Identification of structural damage using multifunctional Bragg grating sensors: I. Theory and implementation”, *Smart Material & Structure*, vol. 15, no. 5, pp. 1305–1312, 2006.

[43] D. C. Betz, W. Staszewski, G. Thursby, and B. Culshaw, “Structural damage identification using multifunctional Bragg grating sensors: II. Damage detection results and analysis”, *Smart Material & Structure*, vol. 15, no. 5, pp. 1313–1322, 2006.

[44] V. Bhatia, K. A. Murphy, R. O. Claus, M. E. Jones, J. L. Grace, T. A. Tran and J. A. Greene, “Optical fibre based absolute extrinsic Fabry - Pérot interferometric sensing system”, *Measurement Science Technology*, vol. 7, pp. 58-61, 1996.

[45] I. Read, P. Foote and S. Murray, “Optical fibre acoustic emission sensor for damage detection in carbon fibre composite structures," *Measurement Science Technology*, vol. 13, pp. 5-9, 2002.

[46] D. -H. Kim, B. -Y. Koo, C. -G. Kim and C. -S. Hong, “Damage detection of composite structures using a stabilized extrinsic Fabry–Perot interferometric sensor system”, *Smart Material & Structure*, vol. 13, pp. 593–598, 2004.

[47] S. Legoubin, M. Douay, P. Bernage and P. Niay, “Free Spectral range variations of grating-based Fabry-Perot filters photowritten in optical fibers”, *Journal of the Optical Society of America A*, vol. 12, pp. 1687-1694, 1995.

[48] E. Town, K. Sugden. J. A. R. Williams, I. Benion and S. B. Poole, “Wide-Band Fabry-Perot-Like in Optical Fiber”, *IEEE Photonics Technology Letters,* vol. 7, pp. 78-80, 1995.

[49] M. G. Xu, J. L. Archambault, L. Reekie and J. P. Dakin, “Discrimination between strain and temperature effects using dual-wavelength fiber grating sensors”, *Electronics Letters*, vol. 30, pp. 1085-1087, 1994

[50] S. W. James, M. L. Dockney and R. P. Tatam, “Simultaneous independent temperature and strain measurement using in-fibre Bragg grating sensors”, *Electronics Letters*, vol. 32, pp. 1133-1134, 1996

[51] H. J. Patrick, G. M. Williams, A. D. Kersey, J. R. Pedrazzani, A. M. Vengsarkar, “Hybrid fiber Bragg grating/long period grating sensor or strain/temperature discrimination”, Photonics Technology Letters, vol.8, pp.1223-1225, 1996

[52] O. Frazao, M. J. N. Lima and J. L. Santos, “Simultaneous measurement of strain and temperature using type I and type IIA fibre Bragg gratings”, *Journal of Optics a-Pure and Applied Optics*, vol. 5, pp. 183-185, 2003

[53] Yi-mo Zhang, Li Chuan, Liu Tie-gen, Li Xin and Yin Yan, “Phase mask technique and its writing for fiber Bragg grating”, *Trans. of Tianjin Uni.,* vol. 7, pp. 217-220, 2001

[54] A. G. Simpson, K. Kalli, K. Zhou, L. Zhang and I. Bennion, ”An idealised method for the fabrication of temperature invariant IA-I strain sensors”, *16th Int. Conf on Optical Fibre Sensors (OFS’2003),* Japan, Postdeadline Papers, pp. 14–17, 2003

[55] X. Shu, D. Zhao, Y. Liu, B. A. L. Gwandu, F. Floreani, L. Zhang and I. Bennion, ”Effectively simultaneous temperature and strain measurement utilising a dual-grating sensor formed by type IA and type IIA FBGs”, *Proc 1st IEEE Int. Conf. on Sensors, Kissimmee, USA*, vol. 2, pp. 1740–1745, 2002

4 Acoustic Emission sensing techniques

4.1 Introduction

Several researchers [e.g.1-3] have reported applications of using fibre gratings for the monitoring of structural strain and temperature. The signal frequency is much higher in a system that is used for detecting ultrasonic acoustic waves are different than the more commonly used strain and temperature systems. The typical values of ultrasonic frequencies used in NDT range from 100 kHz up to several MHz. There is less knowledge about a cost effective interrogation available for high frequency wavelength demodulation. A simple and effective way to avoid this limitation in using fibre Bragg grating for acoustic ultrasonic damage detection is to use intensity-encoded interrogation method [5].

In this chapter, four different sensing techniques and interrogation systems were experimentally studied, that can be used for high frequency AE detection. The primary objective of these experiments was to develop robust, low cost, miniaturised sensors for structural health monitoring (SHM) which can be integrated in the structure. These sensors should have a wide dynamic range coupled with optimal signal-to-noise ratio. Such sensing systems can be developed further into reliable SHM systems that can reduce large structural repairs and safely extend aircraft lifetimes. Optical fibre acoustic emission detection systems have been developed previously, but the technology is still immature. These experiments are focussed to develop fibre Bragg grating based sensing systems that can match the capabilities of a piezoelectric transducer whilst giving further advantages such as integration, multiplexing and cost effectiveness.

4.2 Principle of interrogation method

Converting wavelength shift to amplitude and measuring it is a very common and cost effective way of sensing using optical fibre sensors. The main approach of the interrogation method is to use a narrow line width laser and if the wavelength of the laser matches a certain part of the grating spectrum then any shift of the spectrum will modulate the reflected optical power. The interrogation method concentrates on the part of the spectrum where the function can be assumed to be linear as shown in figure 4.1. For this part of the spectrum, on both sides of the main peak, the slope is constant. In order to achieve the maximum operational range in both directions, the laser should be set to the wavelength that corresponds to the grating's full width half-maximum.

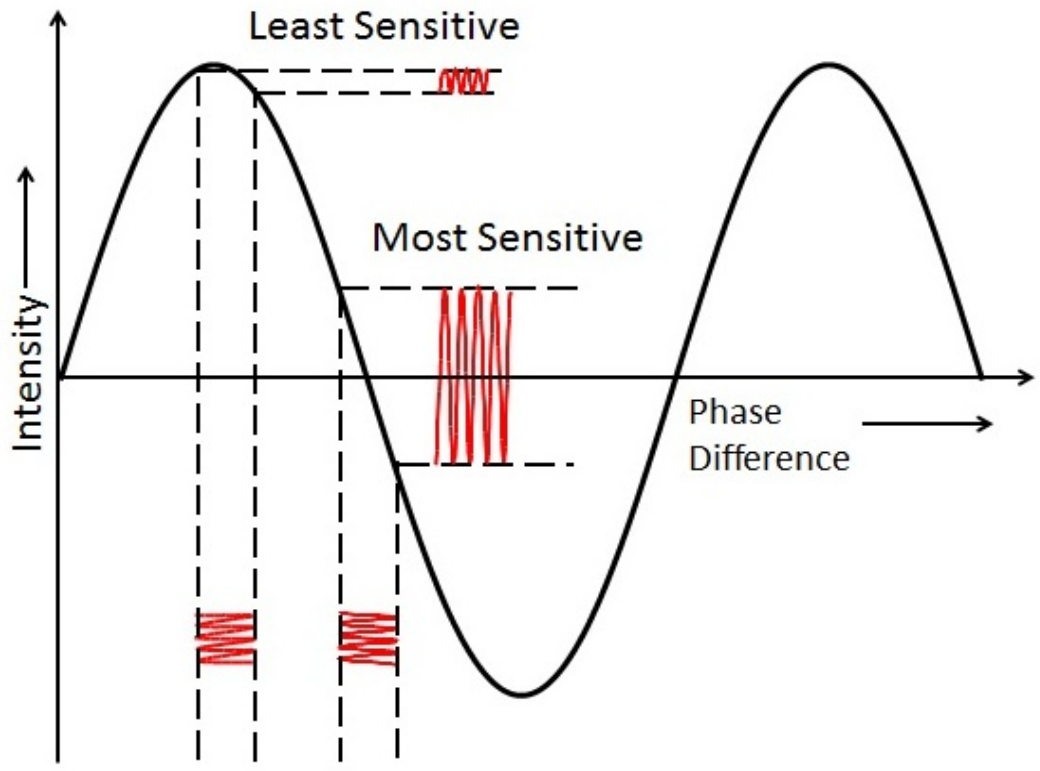

Figure 4.1 Maximum sensitive region and minimum sensitivity region in a grating

This results in a linear relation between the shift of the optical spectrum and the reflected power amplitude, if the wavelength of the laser is kept in this part of the spectrum. However, if the laser is out of this part due to the shift of the optical spectrum of the fibre Bragg grating, the sensor suffers a reduced or complete loss of sensitivity. The sensitivity of the sensor depends on the steepness of the slope. This means that the steeper slope offers the higher sensitivity, but has the disadvantage of a smaller operational spectrum range.

4.3 Matched Fibre Grating Technique

It is already discussed in previous chapters that fibre gratings are sensitive to strain and temperature. They can be used as edge filters. There are several schemes [7-9] proposed that use the FBG as filter. However, using a second FBG for the interrogation of the signal from the sensing FBG is one of the most accepted techniques for demodulation of grating based sensing systems [10, 11]. A second grating in place, can measure wavelength shift in the sensing grating by either tuning reflected optical power [10] or transmitted optical power [12] and operate in a closed loop.

However, the main concern to be taken care of is the SNR of the sensor and the range of frequencies it can detect. In the SHM for aircraft industry, the fibre grating is expected to experience not only ultrasonic acoustic emission but also the loading strain, which causes a much larger spectrum shift than the former does. Moreover, the environmental perturbations like vibration, temperature and pressure variation readily cause a spectrum shift of the fibre grating much larger than its operational range so to put the sensor in non-sensitive region [6]. To overcome the above mentioned limitations an active tracking technique, is

developed in this experiment that offers effective interrogation of high frequency wavelength modulation from fibre grating sensor.

4.3.1 Operation principle

In this experimental work a pair of gratings that have identical (or close to identical) reflection spectra are used, one as sensing grating and the other as a reference grating. The two gratings are connected such that the reflection from the sensing grating will first pass through the reference grating and then received by the photodiode. When the two gratings experience no spectrum shift or the same spectrum shift, the optical signal received by the photodiode will be kept constant and when the two gratings are subjected to some perturbation then the gratings will have a different shift and the received optical signal is modulated by this difference.

As shown in figure 4.2, a square shape reflection spectrum can be assumed for gratings if the gratings are very strong. Then the received intensity by photodiode against the spectrum difference can be calculated, which linearly varies with the absolute value of the wavelength difference of the two gratings. If the wavelength difference is larger than the bandwidth of the gratings the received intensity reaches the maximum and stays constant thereafter. If the basic Gaussian shape is assumed for the reflection spectra of two weak gratings, then the response of received optical power against wavelength change can be simulated.

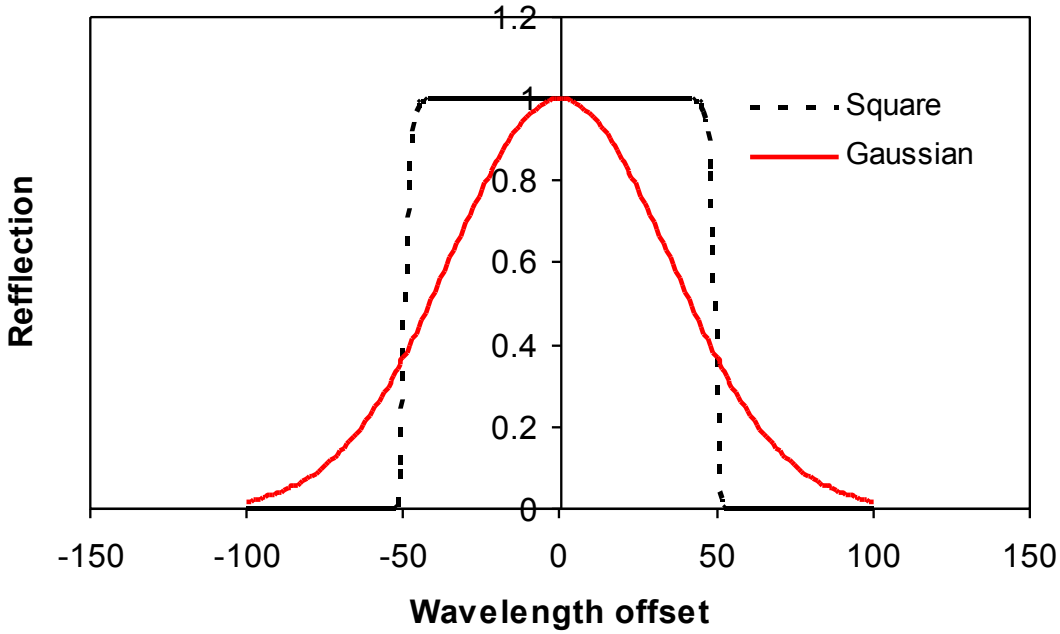

Figure 4.2 Reflection spectra of matched grating pair

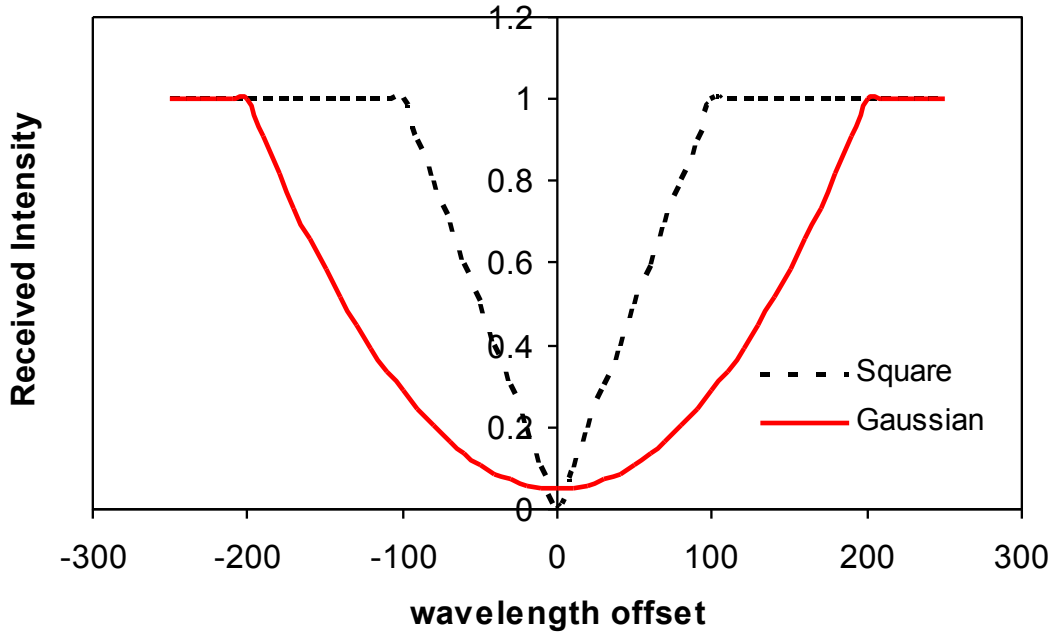

Figure 4.3 Calculated relation between received intensity and spectrum difference

The simulation shows a response that can be approximated as shown in figure 4.3. When the wavelength difference approaches the full bandwidth of the

gratings the received intensity approaches the maximum and then keeps constant.

In whatever case the received optical signal will show the optimum sensitivity to the strain experienced by the sensing grating if these two gratings are halfway overlapped. To track the wavelength change of the sensing grating operation point needs to be set at point where maximum change of the intensity against wavelength change i.e. the optimum sensitive region.

4.3.2 Experimental setup for the matched grating pair technique

The experimental arrangement for the matched pair interrogation technique is shown in Figure 4.4.

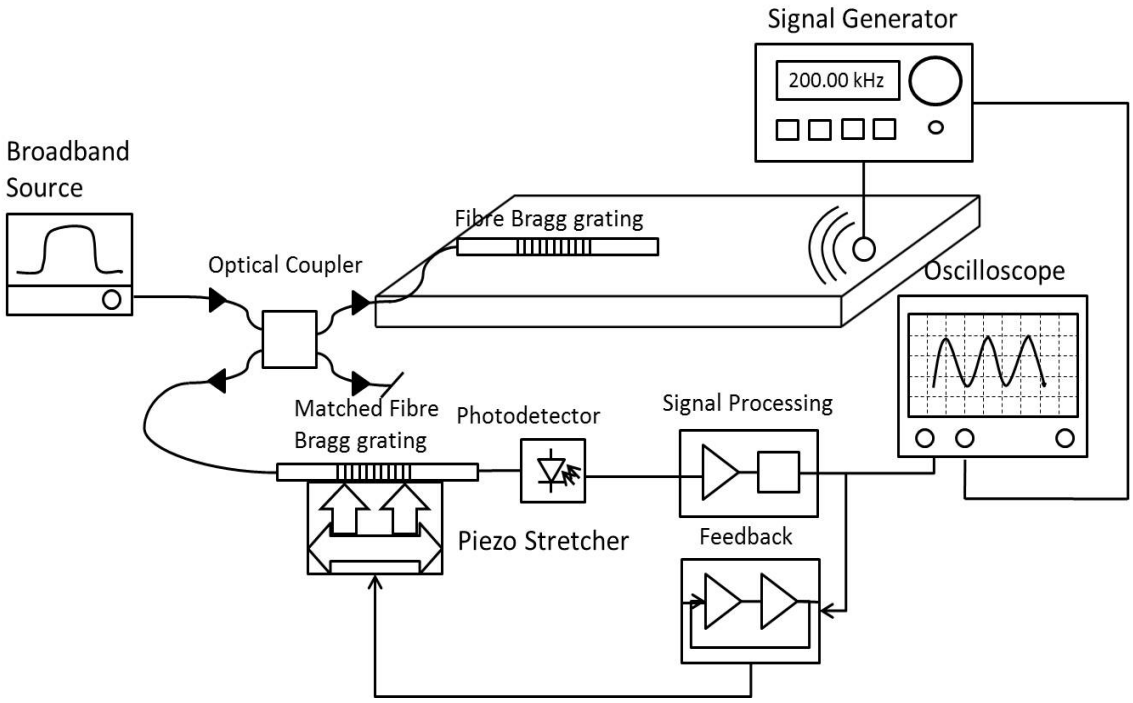

Figure 4.4 Matched pair gratings sensing arrangement

A broadband light source is used to launch a light into the sensing grating via a 3-dB coupler. The gratings used have a length of 3 mm and a 15 dB dip in transmission. The reflection from the sensing grating pass through reference

grating, which is mounted on a piezo stage, and is first filtered by the reference grating and received by a photodiode.

Figure 4.5 shows the spectra of the two gratings that are used in the experiment. A pre-strain (450 microstrain) was applied to the reference grating through the piezo stage to make these two gratings halfway overlapped.

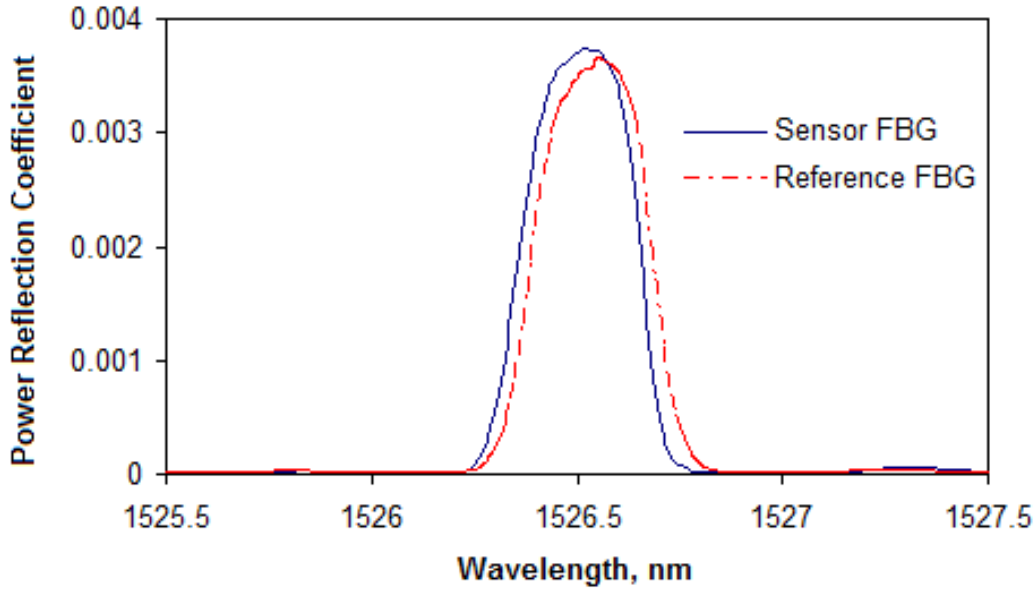

Figure 4.5 Spectra of matched grating pair

Figure 4.6 shows the captured spectra of the received optical signal under various pre-strain values. The double humps in the lowest amplitude curves are due to transmission trough of the second grating. The corresponding intensity of received optical signal is plotted against strain in Figure 4.7. The similarity between Figure 4.7 and the calculated response for the matched grating pair with the Gaussian shape reflection in Figure 4.3 can be clearly seen.

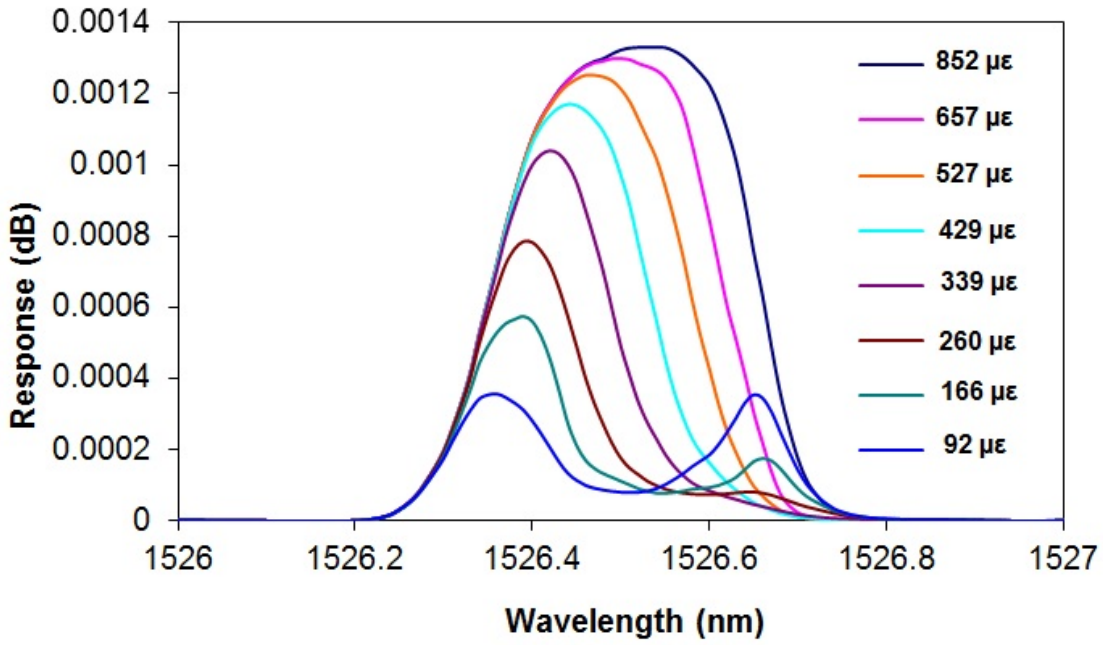

Figure 4.6 Received optical signal under different spectrum shift

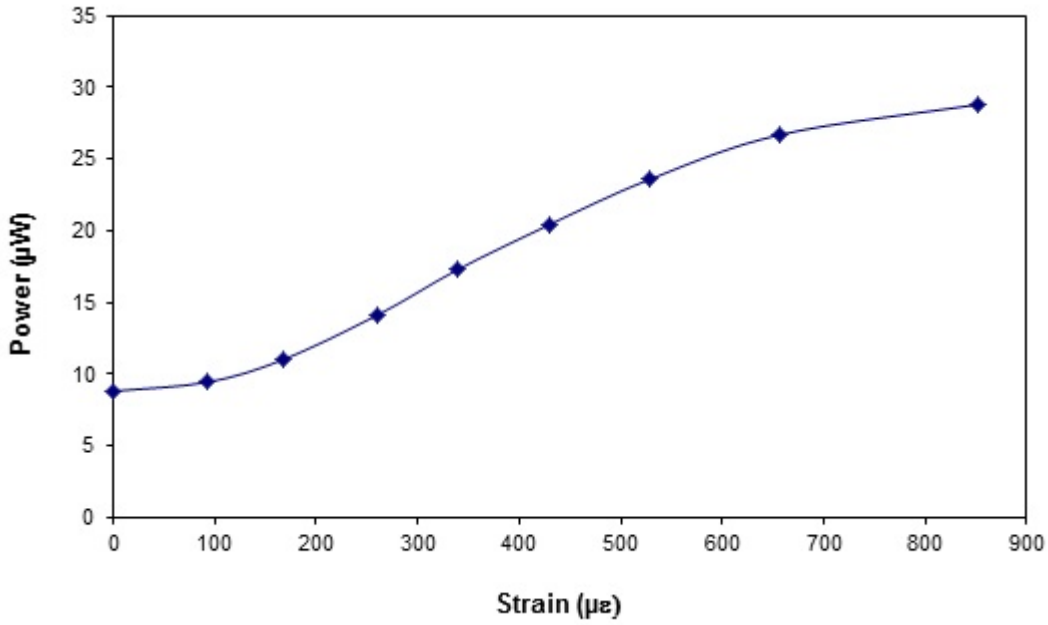

Figure 4.7 Received intensity vs. pre-strain applied to reference grating

4.3.3 Active tracking technique

The principle of this sensor is based on measuring the variation of the reflection from the fibre grating that is induced by acoustic emission. The problem this sensor might face is the wavelength drifting of fibre grating caused by quasi static environmental temperature and strain fluctuation shift sensor from ideal

operating point. A closed-loop electronic circuit is designed to lock the reference grating to the sensor grating so that the reference grating always follows the sensor grating; in the output any low frequency components which usually is related to environmental perturbation is blocked, and the change related to acoustic emission is received by photo detection. The basic arrangement for this scheme and the closed-loop electronic circuit are shown below in figure 4.8. The active feedback circuit was designed with a damping ratio of 0.45 and a natural frequency of 92.7 Hz i.e. any offset below this frequency is offset by the feedback to the piezo, thus ensuring the two gratings always halfway overlapped. The operation point in this experiment is set using the potentiometer in the subtractor stage. The following stage is integrator followed by a proportional integrator. is explained in Chapter 5.

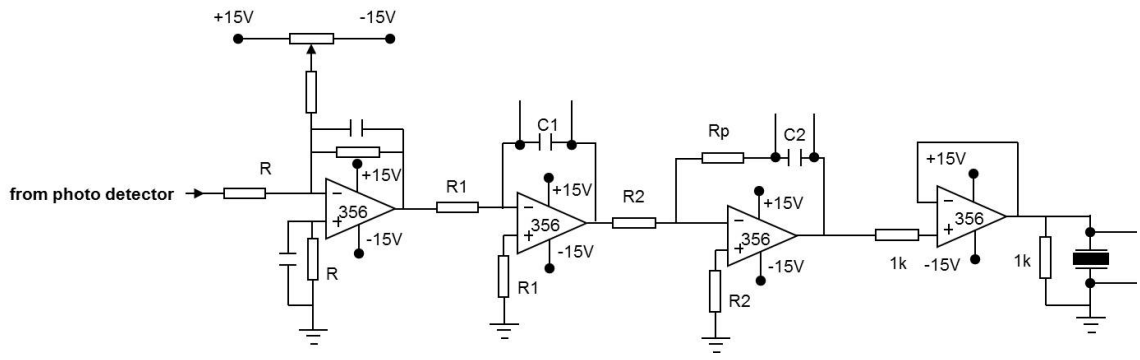

Figure 4.8 Servo Electronic circuit to compensate low frequencies

The derivation of the natural frequency and damping ratio comes from type II feedback system. The detailed working of each stage of this circuit and the derivations are explained in chapter 5 in detail.

Natural Frequency is given by:

$$f_n = \frac{(Ka)^{1/2}}{2\pi}$$ **Equation 4.1**

And the damping ratio of the system is given by:

$$\zeta = \frac{K}{4\pi f_n}$$ **Equation 4.2**

Where,

$$K = K_D K_F K_1 K_2$$ **Equation 4.3**

$\mathrm{K_D}$ is the conversion gain of the photodiode and current- voltage converter

$\mathrm{K_1}$ is the gain of the first integrator

$\mathrm{K_2}$ is the gain of the second integrator

$\mathrm{K_F}$ is the feedback gain.

The gain of the integrators can be given as:

$$K_1 = \frac{1}{R_1 C_1}$$ **Equation 4.4**

$$K_2 = \frac{R_P}{R_2}$$ **Equation 4.5**

$$a = \frac{1}{R_P\, C_2}$$ **Equation 4.6**

C_1 = 4.7nf, C_2 = 4.7nf, f_n = 92.7 Hz , ζ = 0.45, R_1 = 100k, R_2= 100k, R_p = 330k

The higher frequency components are extracted from the received optical signal. Since the environmental perturbations such as the variation of temperature, pressure, strain, and vibration, are of low frequency, the matched grating pair can be kept at a fixed operation point (halfway overlapped with each other) with a high sensitivity to ultrasonic acoustic emission, which is of much higher frequency. The measurement operational range is determined by the tuning wavelength range of the reference grating, which relies on the tuning

range of the piezo. For the piezo used in this work the dimensional change by stretching the piezo i.e. the tuning range is 20 μm, which consequently gives a wavelength shift of 1 nm (tuning range of the grating) to the reference grating. This range is enough to accommodate the wavelength drift of the sensor grating caused by most of the environmental perturbations.

4.3.4 Results and discussion

Figure 4.9(a) is the recorded output when the servo electronics was off; Figure 4.9(b) is the output when the servo electronics was on. It can be very well seen that when the servo electronics is off, the output is fluctuated, indicating that the two gratings were drifted away from the operation point due to the perturbation; when the servo electronics is on, the output keeps unchanged, indicating the immunity to low frequency perturbation and a fixed operation point.

Following this the sensing grating was bonded onto a composite test coupon by using RS epoxy resins. Figures 4.10(a) and 4.10(b) show the sensor responses to a single frequency vibration (6 kHz) induced by a piezo transducer, and the stimulated acoustic emission by breaking a 2H propelling pencil lead [4].

Figure 4.11(a) shows the response when both FBG sensor and piezo sensor are subject to same acoustic emission. The peak responses from two sensors show some difference in frequency and FBG sensor shows some side lobe in response. Figure 4.11(b) shows peak response versus orientation of acoustic emission source. It can be concluded that the boundary reflection causes frequency difference between peak responses and the side lobe may attribute to directional effect of fibre grating. In this matched grating pair the maximum frequency response of the sensor is around 110 kHz.

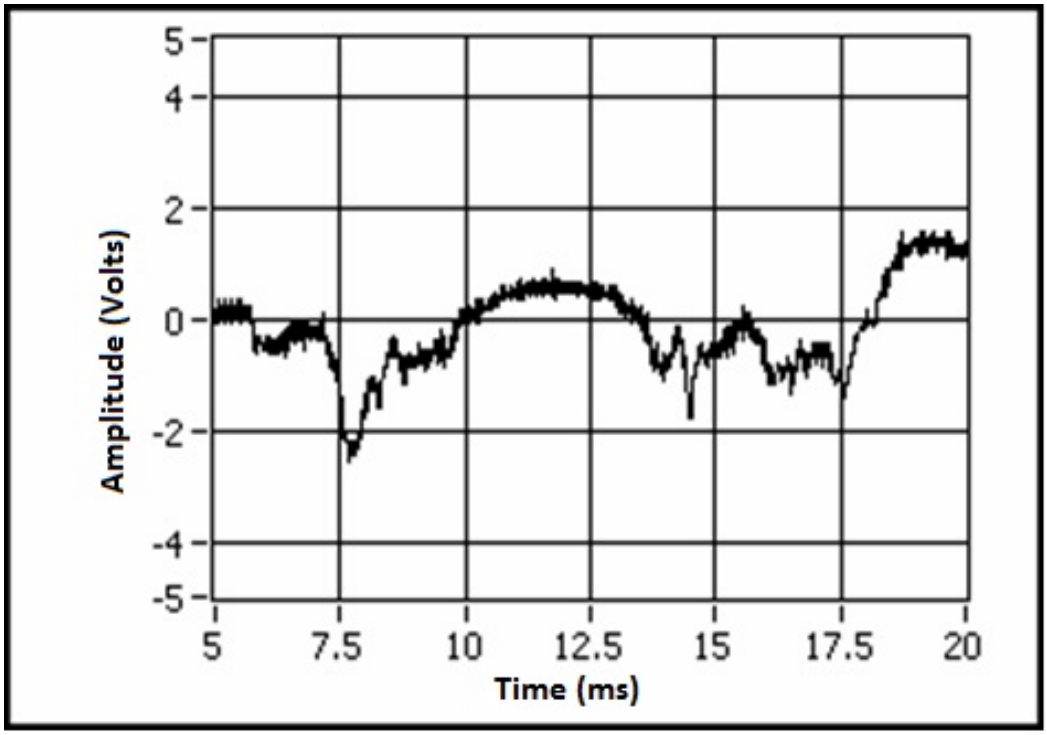

4.9 (a)

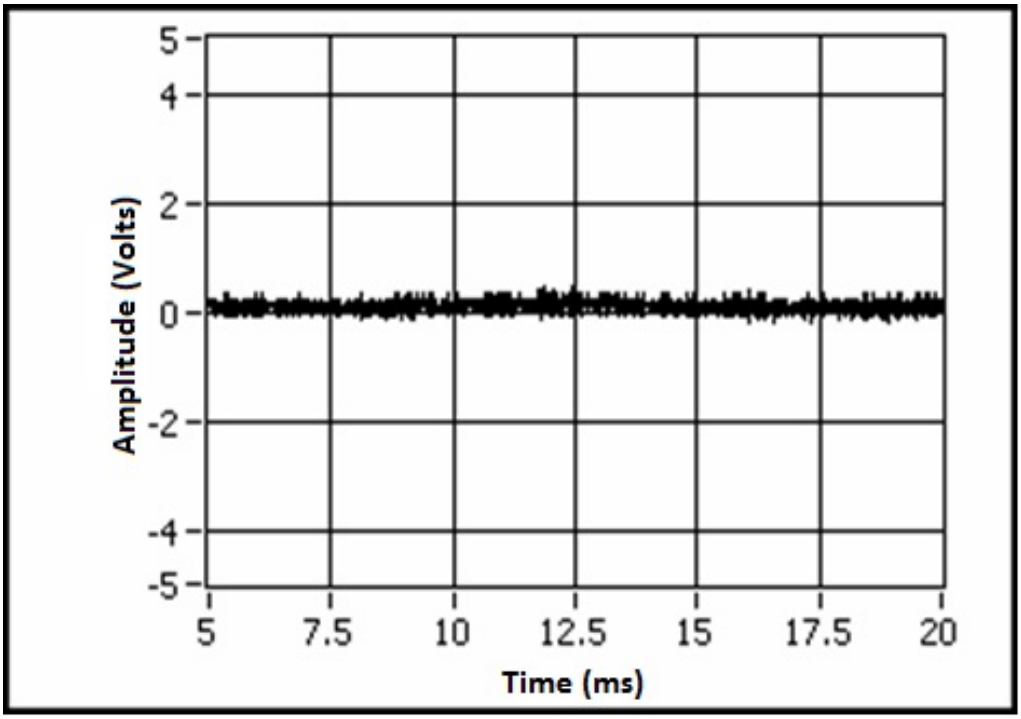

4.9 (b)

Figure 4.9 Detected output with (a) servo off, (b) servo on

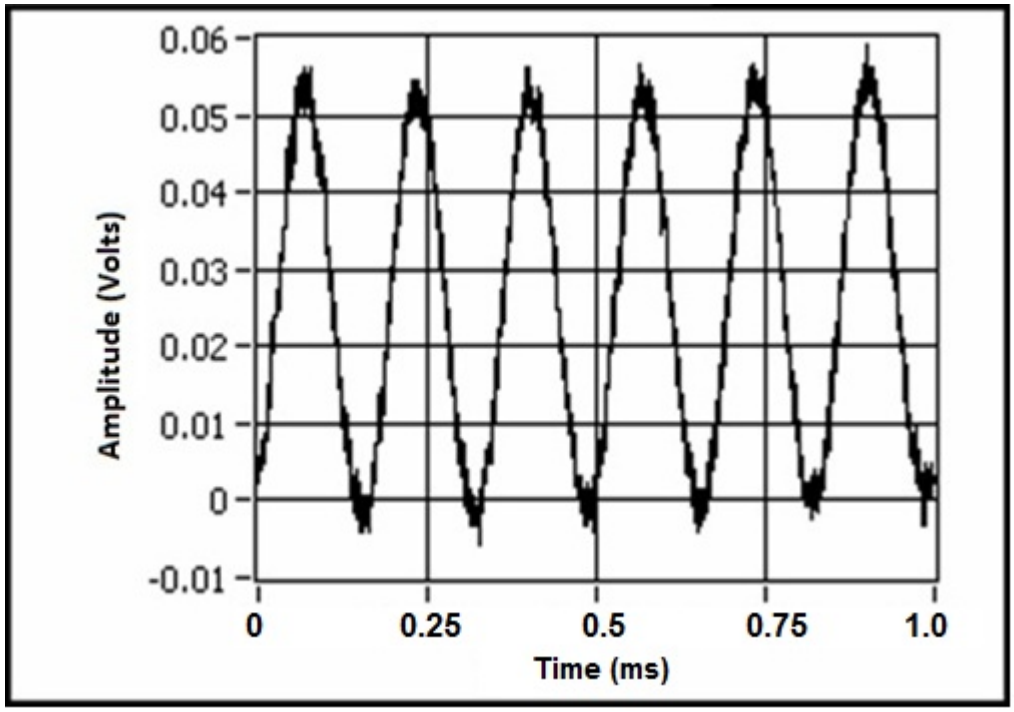

4.10 (a)

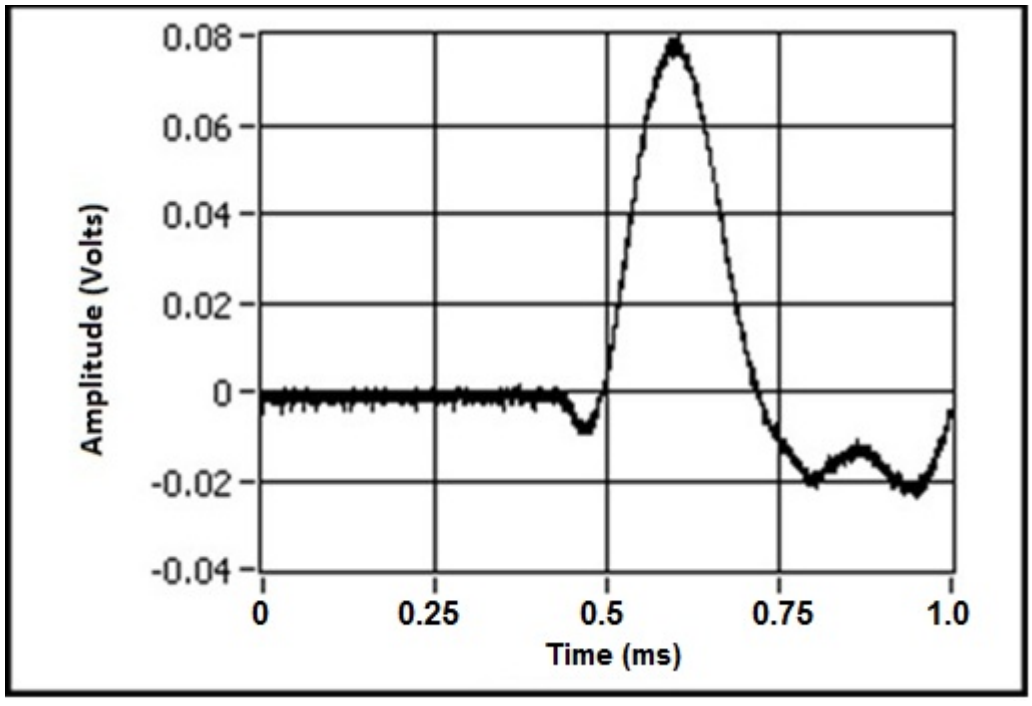

4.10 (b)

Figure 4.10 (a) sensor response to a single frequency vibration (6 kHz), and (b) Sensor response to a pencil lead break

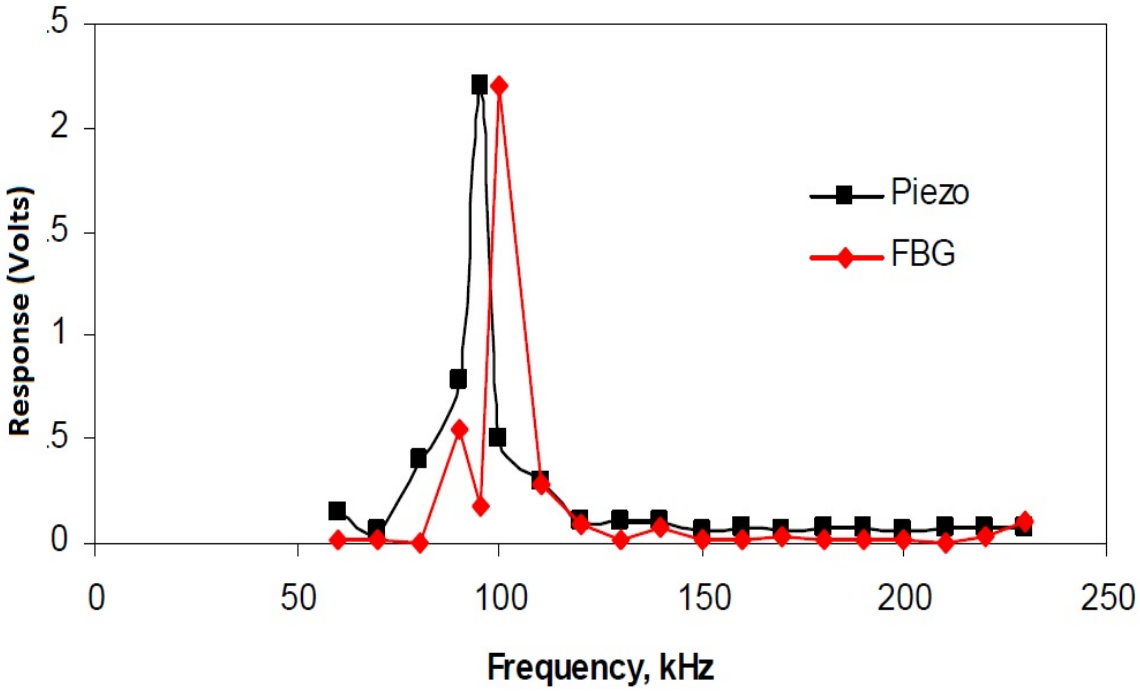

4.11 (a)

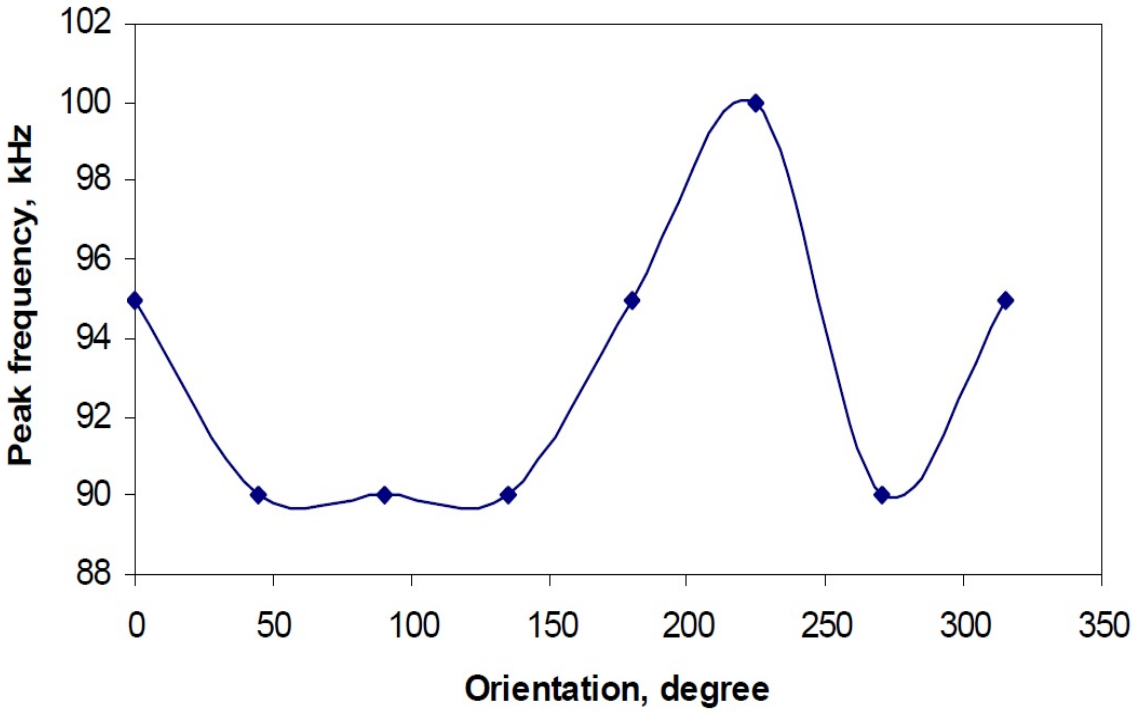

4.11 (b)

Figure 4.11 (a) Comparison of FBG sensor and piezo sensor are subject to same acoustic emission (b) Peak response vs orientation of acoustic emission source

For the higher frequency components of the acoustic emission the response is too low to be detected. This means that the measurement for this proposed sensor cannot cover the whole frequency range of the acoustic emission. In order to detect weak signal at higher frequencies the system signal-to-noise ratio is crucial, which is directly related to the received intensity of the optical signal by the photo detector. In the case of using matched grating pair, high optical intensity means that the gratings used have strong reflection and large bandwidth. On the other hand the measurement sensitivity of the sensor is proportional to the ratio of the received intensity change to the wavelength change of the gratings induced by the acoustic emission, which inevitably requires narrow bandwidth of the grating.

An option to achieve both high intensity and narrow bandwidth is to use Fibre grating laser (FBG laser) as sensing element. The following section discusses the use of FBG laser as sensor.

4.4 Fibre Grating Laser Based Sensor

The use of FBG laser has been proposed by several researchers [e.g. 13-16]. AE detection with FBG laser can offer advantages that can be offered by FBG sensors and also have the potential to measure AE signals with a higher sensitivity than FBG sensors. The linewidth of fibre lasers is typically a few tens of kilohertz, corresponding to a coherence length of the order of tens of kilometres. Ye and Tatam [16] used the FBG laser configuration along with a path-length imbalanced readout Mach–Zehnder interferometer (MZI) to measure the laser frequency shift induced by ultrasonic vibration. The Laser cavity is perturbed by the AE signals and modulates the lasing frequency.

4.4.1 Experimental setup for fibre Grating laser based sensor

In active fibre grating sensors, gratings form part of a fibre laser and offer a higher accuracy than passive Bragg grating sensors. A Fibre DFB laser [16] was then constructed. The active part of the laser consists of a phase shifted grating, written on Er-Yb co-doped Fibre and was replaced with the sensor grating in the matched-grating pair technique discussed in previous section. The sensing arrangement using the Er-Yb DFB fibre laser deployed for AE detection is shown in the figure 4.12.

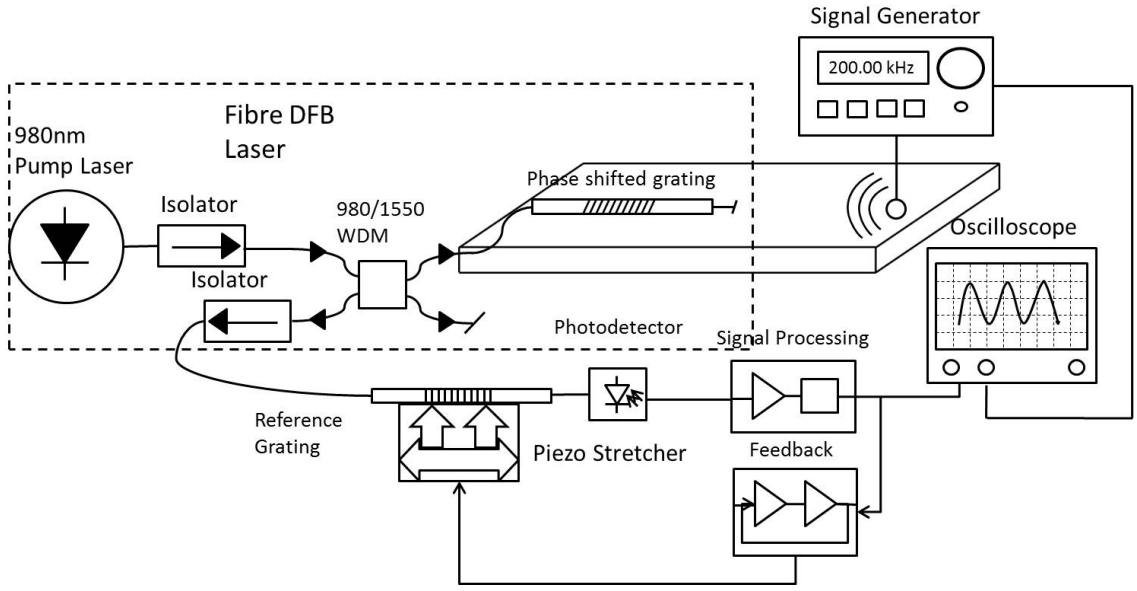

Figure 4.12 Sensing arrangement using Fibre grating laser as sensing element

The phase-shifted FBG written into an Er3+/Yb3+ co-doped fibre is used as the laser head. A 980 nm fibre pigtailed solid state pump laser was coupled into the Yb3+/Er3+-co-doped fibre through a 980/1550 nm fibre wavelength division multiplexer (WDM). A 980 nm optical isolator is used at the output of the pump laser in all cases to prevent undesired optical feedback from destabilising the pump diode. 1550 nm optical isolator is placed at output fibre laser to ensure avoiding any unintended feedback effects into the DFB laser.

The laser has high output as shown in figure 4.13 and a narrow linewidth in range of tens of kilohertz. High intensity gives a high SNR, high change in intensity to wavelength ratio gives high sensitivity and a narrow linewidth gives a high resolution.

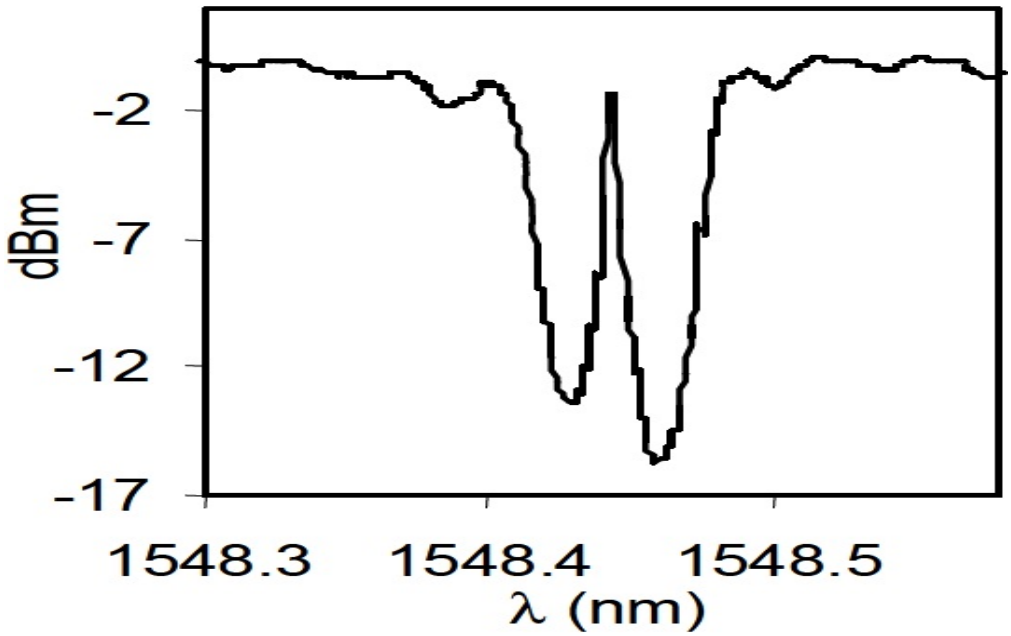

4.13(a)

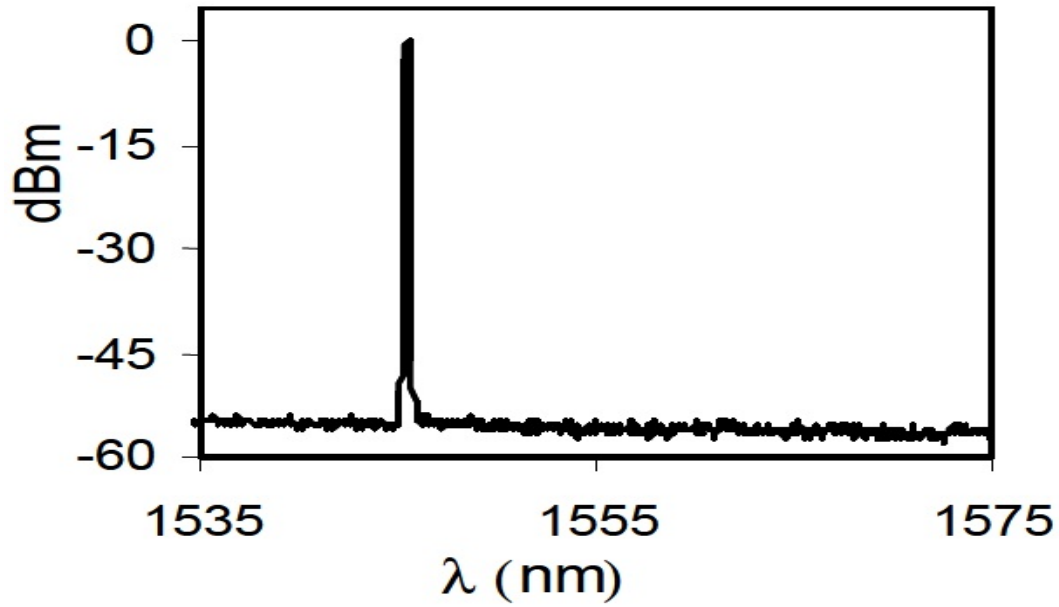

4.13(b)

Figure 4.13 FBG laser output

The wavelength of the FBG laser is set in the middle of the rising/falling edge of the reference grating, as illustrated in figure 4.14. This is the operation point of the sensor. Any drift away from this point is detected by the photo detector and compensated by the counter-moving the reference grating which is mounted on the piezo and controlled by the servo electronics. The servo electronics still tracks any low frequency change caused by environmental perturbation and leaves alone any changes higher than the natural frequency of 92.7 Hz, therefore the acoustic emission induced change will be detected at the output.

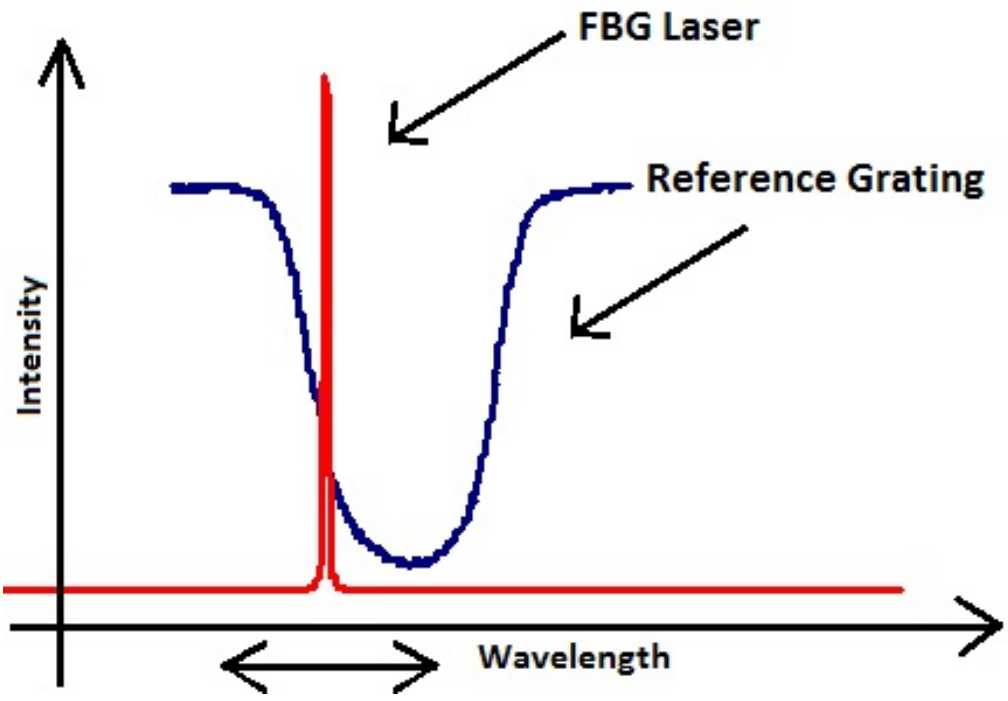

Figure 4.14 Operation point of the sensor

4.4.2 Results and discussion

The FBG laser then was bonded onto the same composite test coupon. A low profile piezo buzzer was mounted 65 cm away from the FBG laser to simulate an ultrasonic acoustic emission source. A commercially available broad band PZT transducer with an integrated amplifier built in (WDI-PAC ltd.) as placed beside the FBG laser to detect the acoustic emission as a comparison.

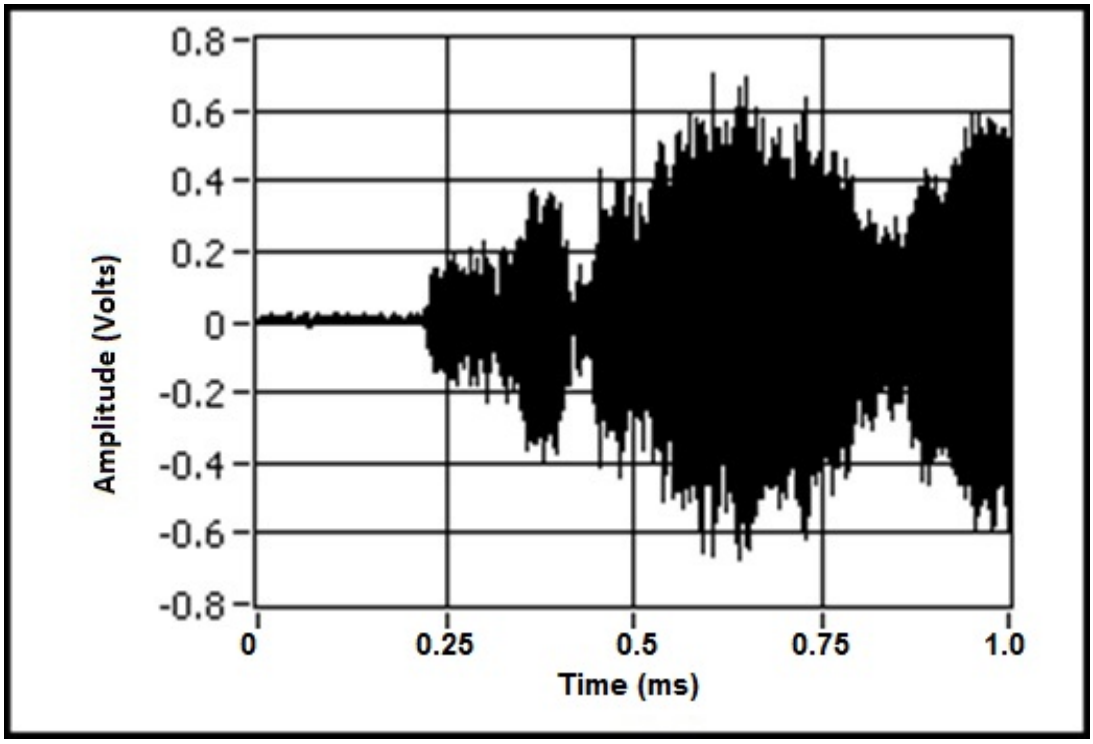

(a)

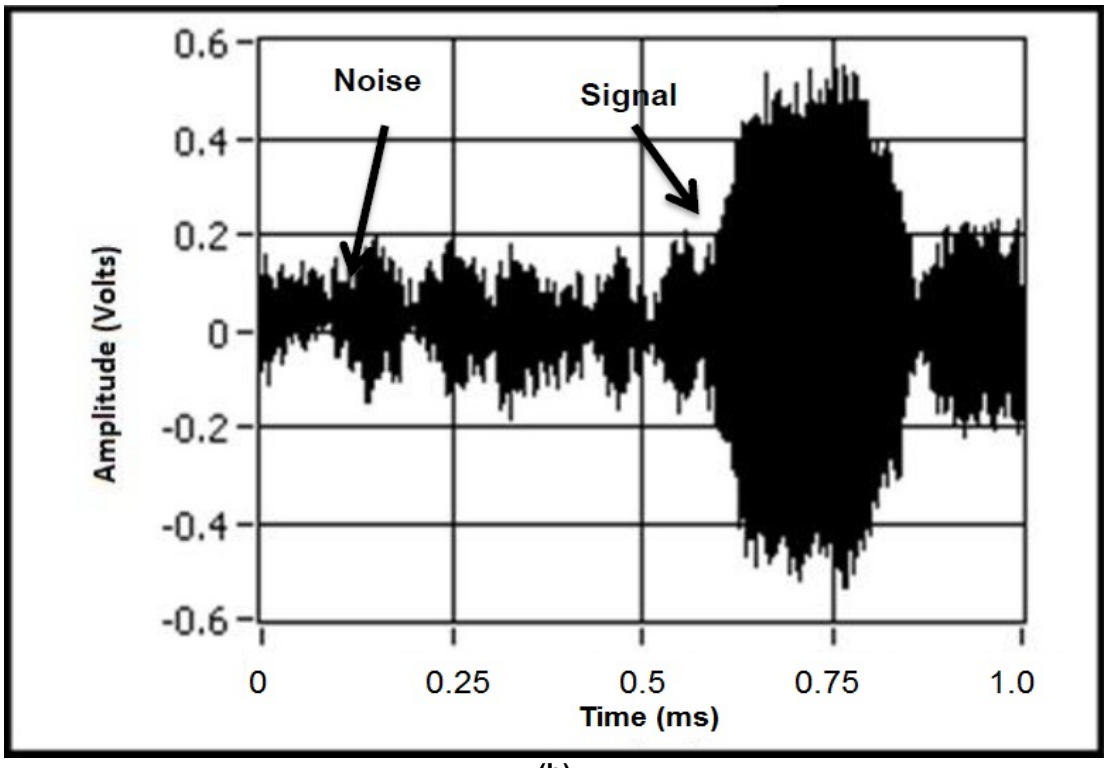

(b)

Figure 4.15 Waveforms of a burst of sine signal (a) measured by WDI transducer, (b) measured by FBG laser based sensor

To look at the typical responses of the sensor to ultrasonic acoustic emission a burst of sine signal of 270 kHz was applied to the piezo buzzer. The measured

results are shown in Figure 4.15. From the waveforms it can be seen that the noise level in the WDI is very low but background noise is present in the signal measured by the FBG laser. It is very important to suppress such noise to improve the SNR of the sensor. This noise might be from the electronics or some pick up from external perturbations. Obviously the measurement frequency range of the sensor has been much improved due to the use of FBG laser sensing element. The acoustic emission signal with a frequency up to 300 kHz has been detected by using this proposed sensing technique. The measurement frequency range could be higher, which, however, is limited by the performance of the piezo buzzer used. The response difference between the WDI transducer and the FBG laser sensor mainly attributes to the difference between the sensor structures (the FBG laser sensor shows distinct features in the directionality of the measurement).

As a part of CONSTRUCT, the fibre laser interrogation technique was further developed by Insensys. During the cross comparison tests [17], where in a FBG, FBG – Fabry Perot and FBG laser were compared against the piezo sensors performance. It was found during the tests that the fibre laser sensor's offer good sensitivity and wide dynamic range. They have large coherence length and allow the use of an interrogating interferometer with a very fine free-spectral-range. However, a compact optical configuration that can offer a higher sensitivity and even higher dynamic range is still of interest.

An all optical configuration technique, using 3 by 3 coupler in Mach-Zehnder Interferometer configuration [18, 19] is proposed. This technique is expected to monitor the wavelength variation of the fibre grating with a frequency response up to 1MHz. This system is capable of measuring both FBG and fibre laser and very cost effective.

4.5 3 X 3 coupler experiment

The characteristic parameters of fibre grating such as reflection, time delay and wavelength, all can be used as the measurand in acoustic emission detection. Among these monitoring wavelength change still is much of interest. Most known interrogation schemes for measuring fibre grating wavelength are of static and low frequency response.

Interferometric fibre optic sensors are high sensitivity sensors and are able to detect very small variations in the measurand. But they require a suitable signal processing technique that can provide real time output for the measured parameter [20].

Out of several demodulation techniques [21, 22] available, the use of a 3 by 3 coupler-based demodulation, where the output maintains a relative phase shift of 120 degrees, offers a number of advantages, including high resolution over a large dynamic range, good environmental stability, and polarization insensitivity and thus, can be considered for practical applications [20].

4.5.1 Operation Principle

The working principle of this experiment is to use an unbalanced Mach-Zehnder interferometer, terminated by a 3 by 3 coupler, to recover the wavelength shift of an FBG. A 3 by 3 coupler has an advantage over 2 by 2 coupler as it has the same power transfer ratios at the output ports and provide a 120-degree phase-shifted signal without an active component and thus they are in quadrature. The 3 by 3 coupler-based interferometric demodulator is highly sensitive and also has high measuring frequency compared with the interferometer terminated by two 2 by 2 couplers [23-25].

The change of wavelength of the fibre Bragg grating is directly proportional to the change in the optical phase shift induced by signal that is caused because of perturbation and can be given as [18]:

$$\Delta\phi(\lambda) = \frac{-2\pi nd}{\lambda^2}\Delta\lambda \qquad \textbf{Equation 4.7}$$

where,

$\Delta\phi$: phase change of MZI

$\Delta\lambda$: wavelength change of FBG

d: path difference of MZI

A typical optical Fibre Mach–Zehnder interferometer with a 3 by 3 coupler is shown in figure 4.14.

The three outputs from the interferometer, assuming the 3 by 3 coupler is lossless, are given by the following equations [18, 19]:

$$P_1 = -2B_2\,(1 + \cos\phi) \qquad \textbf{Equation 4.8}$$

$$P_2 = B_1 + B_2\cos\phi + B_3\,sin\phi \qquad \textbf{Equation 4.9}$$

$$P_3 = B_1 + B_2\cos\phi - B_3\,sin\phi \qquad \textbf{Equation 4.10}$$

where, B_1, B_2, B_3 are constants that are dependent upon coupling coefficients. Adding and subtracting equations (Eq 4.9) and (Eq 4.10) respectively,

$$P_2 + P_3 = 2(B_1 + B_2\cos\phi) \qquad \textbf{Equation 4.11}$$

$$P_2 - P_3 = 2\,B_3\sin\phi \qquad \textbf{Equation 4.12}$$

Multiplying equation (Eq 4.11) and (Eq 4.12) with signal from local oscillator

$$P'_2 = 2B_3 \sin\phi . \cos\omega_c t \quad \textbf{Equation 4.13}$$

$$P'_3 = 2(B_1 + B_2 \cos\phi). \sin\omega_c t \quad \textbf{Equation 4.14}$$

Adding equations (Eq 4.13) and (Eq 4.14)

$$P' = 2B_3 \sin\phi . \cos\omega_c t + 2(B_1 + B_2 \cos\phi). \sin\omega_c t$$

Assuming $B_2 = B_3$ and since, B_1 is the dc output of P_2 and P_3 and can be reduced to zero by introducing offset in the electronics.

$$P' \approx \sin(\omega_c t + \phi) \quad \textbf{Equation 4.15}$$

Where, ω_c is determined by local oscillators.

From equation 4.15 we can see that P' contains information of the phase and phase change of the MZI is directly proportional to change in wavelength and can be given by equation 4.7. It can be noted that unless the electronics are properly balanced i.e. B_1 = 0 and B_2 = B_3, distortions will be present in the output and that will affect the phase measurement due to wavelength change.

4.5.2 Experimental setup

Figure 4.16 (a) and (b) below shows the experimental arrangement of the 3 by 3 Mach Zehnder experiment. Light is launched through a circulator into the FBG and the light from reflection of the grating is fed into the Mach Zehnder interferometer. The outputs ports (P_2 and P_3) are connected to photo detectors. The light is converted to current and then to voltage by the current to voltage converters. These quadrature output from the photodetectors is than fed into the signal processing unit which is designed to recombine both the outputs and derive phase information from it. Any perturbation to the FBG results in change

of phase of the Mach Zehnder. This phase carries information of the wavelength change of the FBG.

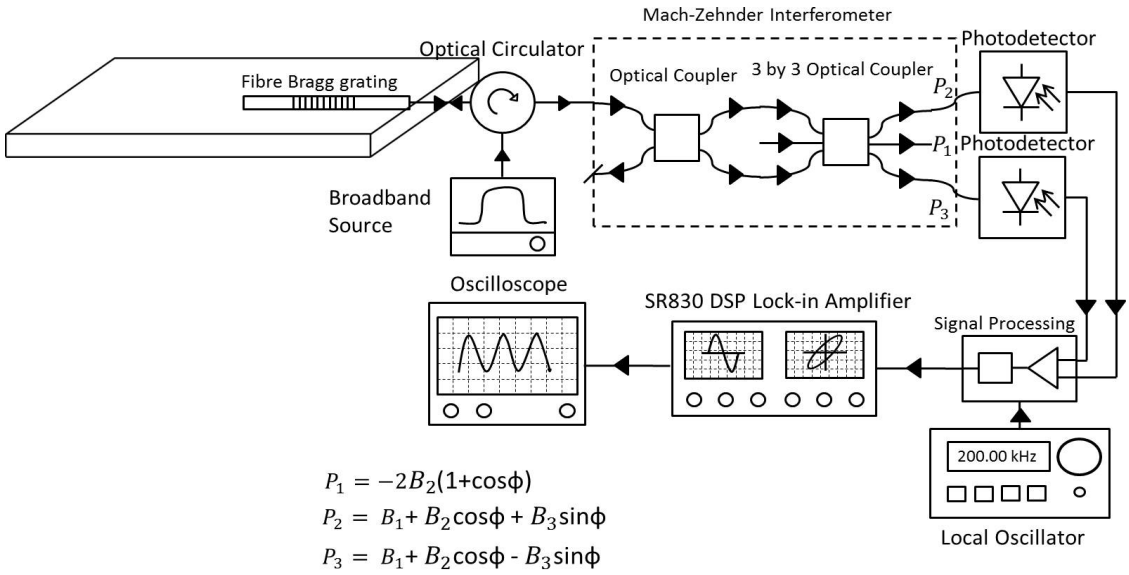

4.16 (a)

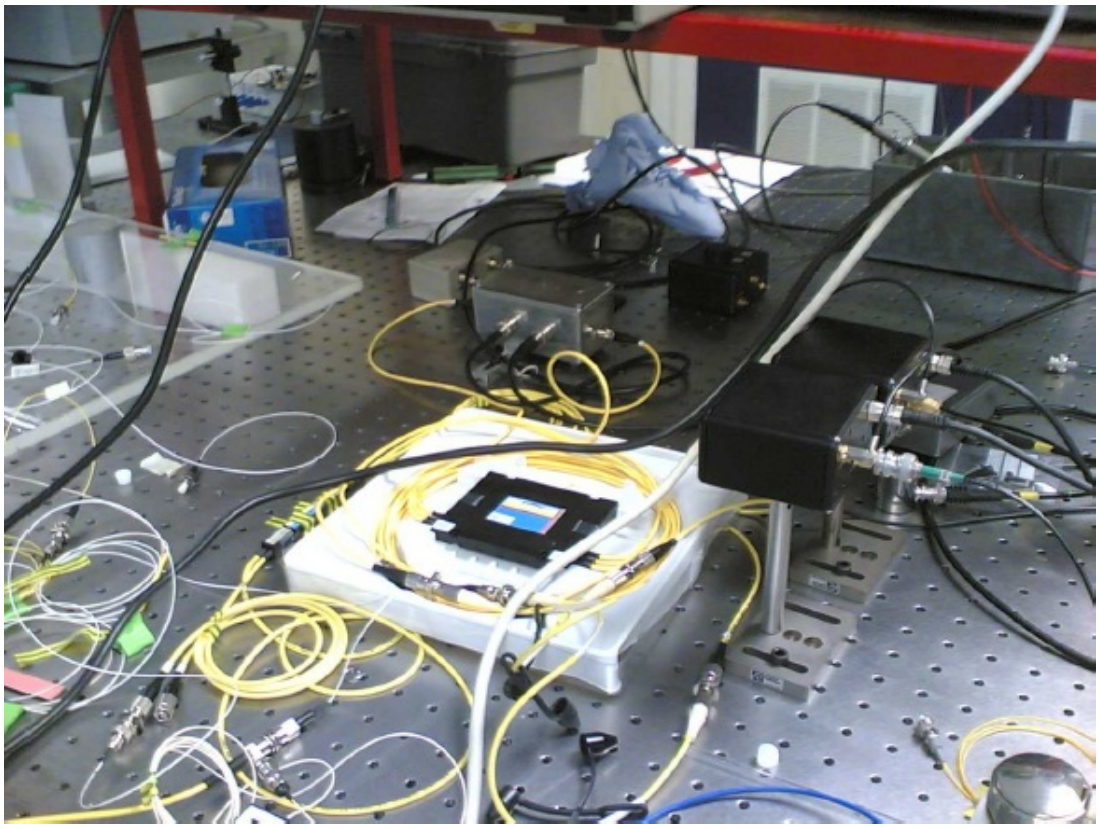

4.16 (b)

Figure 4.16 (a) Experimental Set up of 3 by 3 coupler MZI experiment (b) Laboratory setup of the experiment

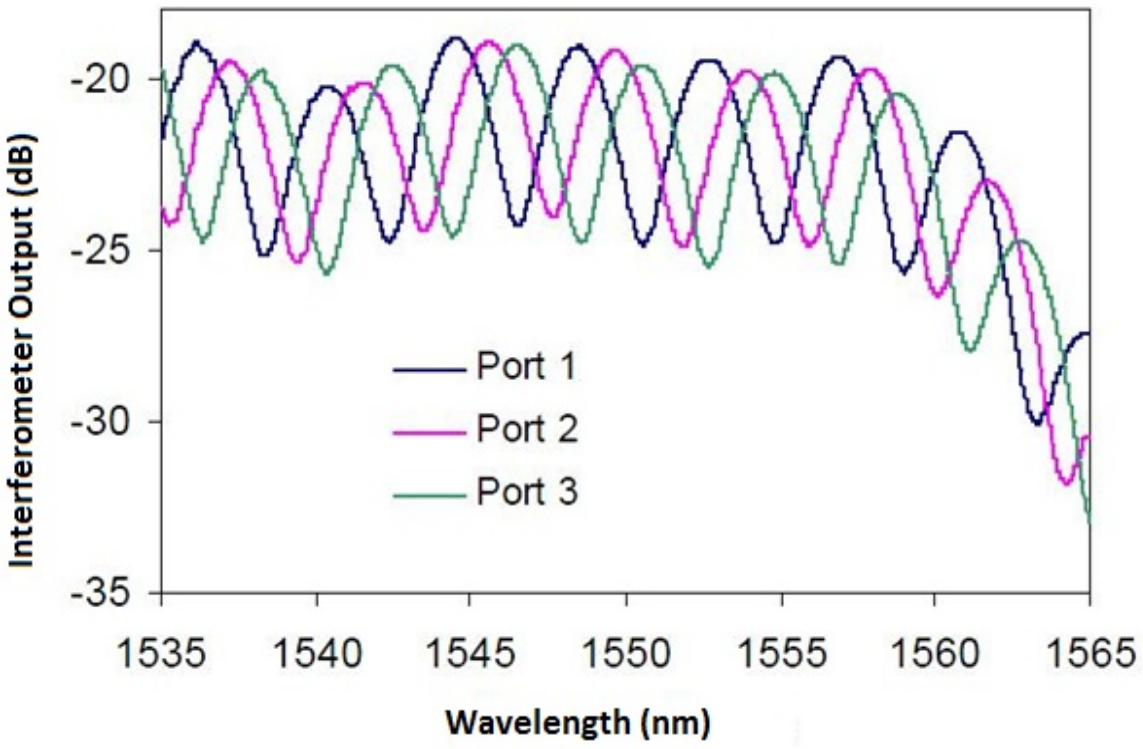

Figure 4.17 Output spectra of the Mach-Zehnder Interferometer

Figure 4.17 shows the output of the Mach Zehnder interferometer which are in quadrature.

4.5.3 Quadrature recombination electronics

The idea is to derive phase information from the signal and the electronics in this experiment as shown in figure 4.18 are designed for that purpose. The equations discussed earlier to achieve *P'* as in equation 4.15 are realised by using quadrature recombination electronics. This circuit consists of two current to voltage converters that pick the photodetector output and change the current to voltage. The outputs P_2 and P_3 from the photodetectors are added to achieve an output consisting cosine term and are subtracted at the same time to achieve a sine term as shown in equation 4.11 and 4.12. A dc offset in adder amplifier is used to nullify the effect of B_1. The next stage consists of multipliers. An external oscillator is used to provide a signal of 1 MHz to the multiplier circuit and a phase shifter is used to change the oscillator phase signal by 90 degrees

thus getting a sine and a cosine component. These sine and cosine components are multiplied to cosine and sine output respectively, from previous stage and is represented in equation 4.13 and 4.14. These processed signals are added and fed to lock in amplifier. The phase of this signal coming from the Mach Zehnder interferometer, which contains information on the wavelength shift in the FBG, is recovered by using this lock-in amplifier.

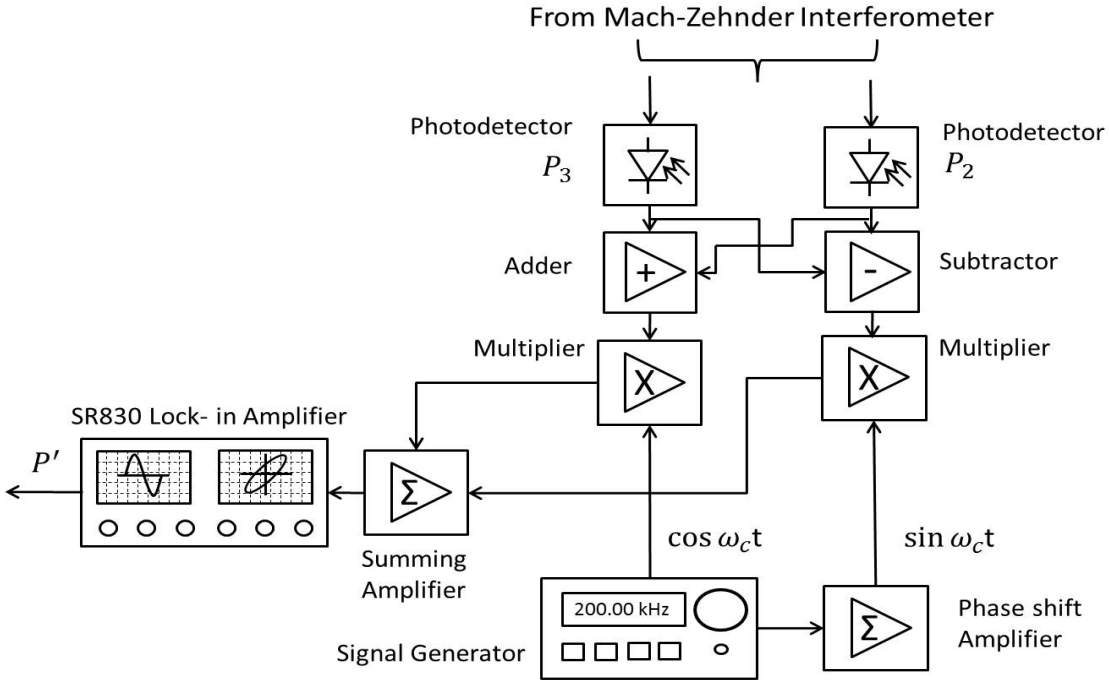

$$P_2 = B_1 + B_2 \cos\phi + B_3 \sin\phi$$
$$P_3 = B_1 + B_2 \cos\phi - B_3 \sin\phi$$
$$P' = \cos\omega_c t . \sin\phi + \sin\omega_c t \cos\phi$$

Figure 4.18 Quadrature Recombination circuit [Ref: Appendix Figure 1]

3.5.4 Results and discussions

The FBG was bonded on a small test composite. Figure 4.19 shows the tapping response of the sensor when a metal piece was tapped 20cm away from the FBG on to the test coupon where the FBG was mounted.

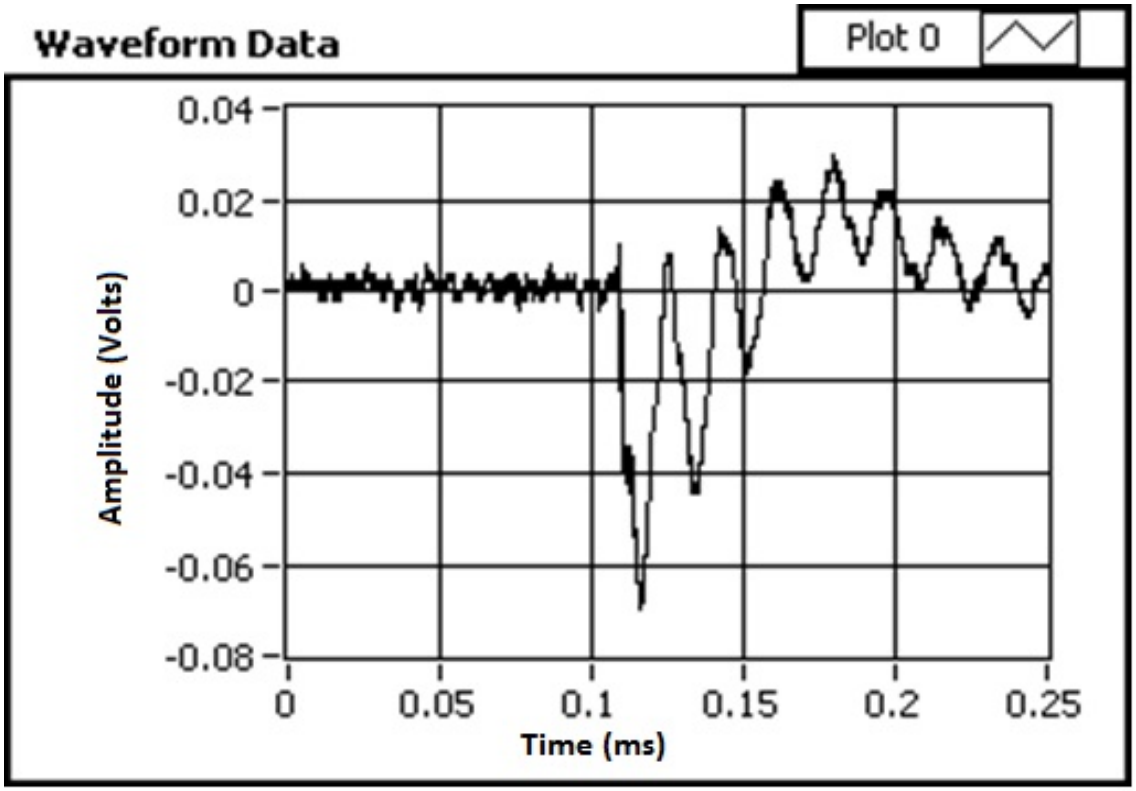

Figure 4.19 Tapping Response of the FBG sensor

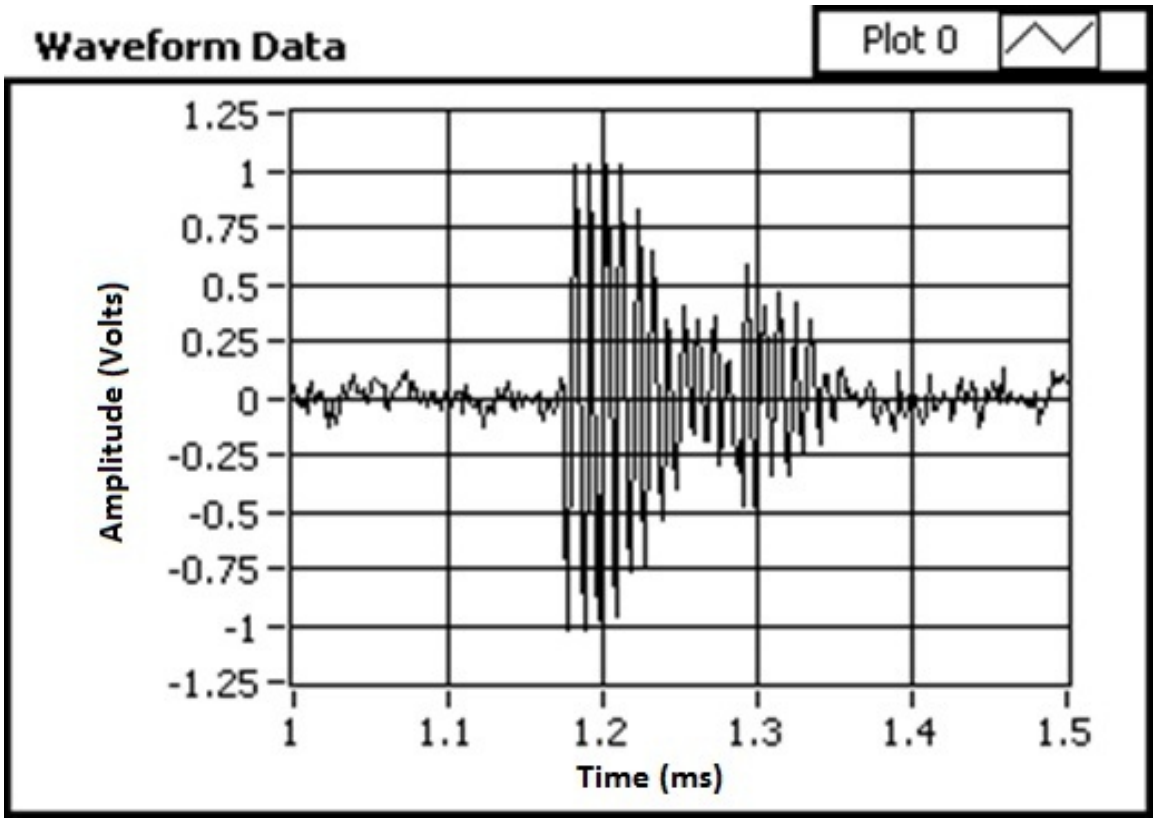

Figure 4.20 Wavelength shift for strike response

Figure 4.20 shows the strike response from the system at a distance of 20 cm. The signal level has increased in comparison to matched pair grating technique. However, the tapping response has a weaker response in comparison to strike. This method is capable of detecting high frequencies and is highly sensitive. The limitation of this experiment is that the output power ratio of 3×3 fibre coupler changes due to variable polarisation state in fibre. Thus the phase and wavelength relation is not satisfied that leads to reduced sensitivity and distortion in response. To overcome this, a method by using two lasers and a single coupler was proposed [5]. This method can also be used for high frequency detection.

When one laser's output is at optimal sensitivity the other can be tuned at lowest sensitivity and vice versa. By using both outputs for tracking, multiple grating can be scanned through enhancing dynamic range and avoiding signal fade out associated with positions of minimal sensitivity.

4.6 Two Laser method

Fibre grating based Fabry-Parot cavity is used as acoustic emission sensor, which can provide higher sensitivity than normal fibre Grating. The FBG Fabry-Perot cavity with pseudo-sine response has been made and tested. Response of a short cavity FBG Fabry-Perot is shown in figure 4.21. These FBG Fabry-Perot devices consists of 2 chirped FBGs with a cavity length of 14mm giving free spectral range ~60pm (theoretically calculated FSR ~58pm). These have been designed with low reflectivity so that the responsivity is more uniform than previously tested devices.

The pair of laser diodes with wavelength spacing of a quarter of free spectral range of Fabry-Perot cavity has been used to interrogate the spectral response

of the FBG Fabry-Perot cavity in which the acoustic emission information is carried.

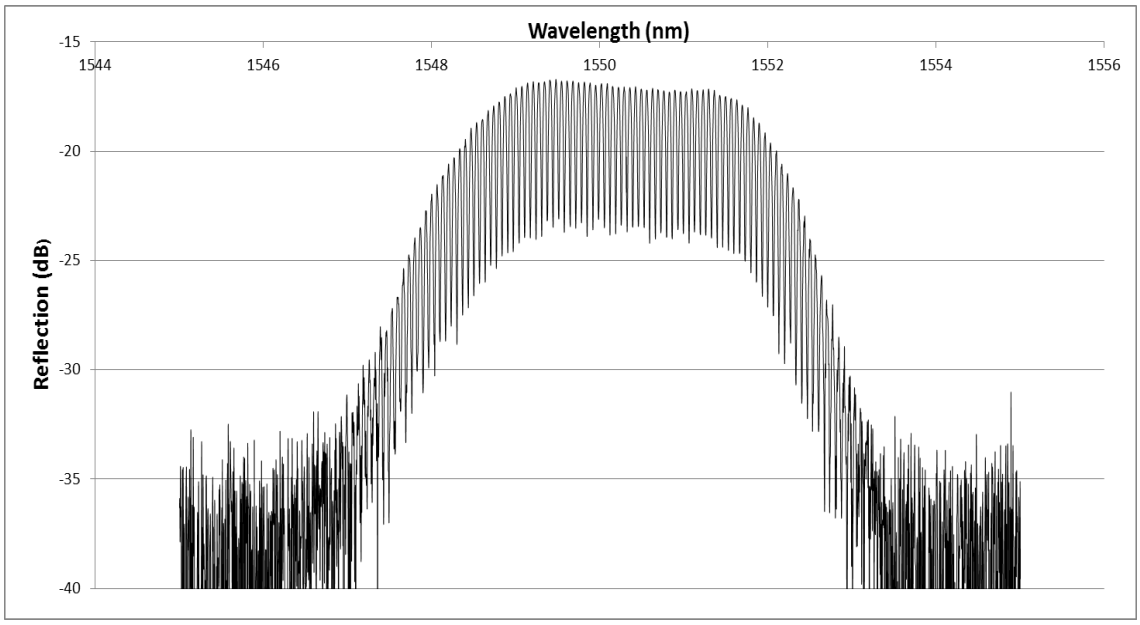

Figure 4.21 Reflection spectrum of 14mm FBG Fabry-Perot

This system is based on the same principle as the wavelength interrogation system using 3 by 3 coupler therefore it is compatible with the signal processing unit of the 3 by 3 coupler experiment. FBG Fabry-Perot's are able to attain high sensitivities than the normal FBG's. However, the sensitivity of the system depends on what part of FBG Fabry-Perot spectrum the laser is tuned to and the main concern with this approach lies in the varying sensitivity of the sensor when the spectrum of the Fabry-Perot cavity shifts due to environmental perturbations.

4.6.1 Operation principle

The main working principle in this work is to combine and launch two lasers via a 3dB coupler in a low finesse FBG Fabry-Perot as shown in figure 4.22. To ensure that the system detects all the acoustic emission events i.e. any wavelength shift in the FBG Fabry-Perot due to perturbation or acoustic

emission, it is necessary that the wavelengths of the two laser are set in quadrature, for example, one laser is tuned to the most sensitive region and the other to the least sensitive region, as shown in figure 4.23.

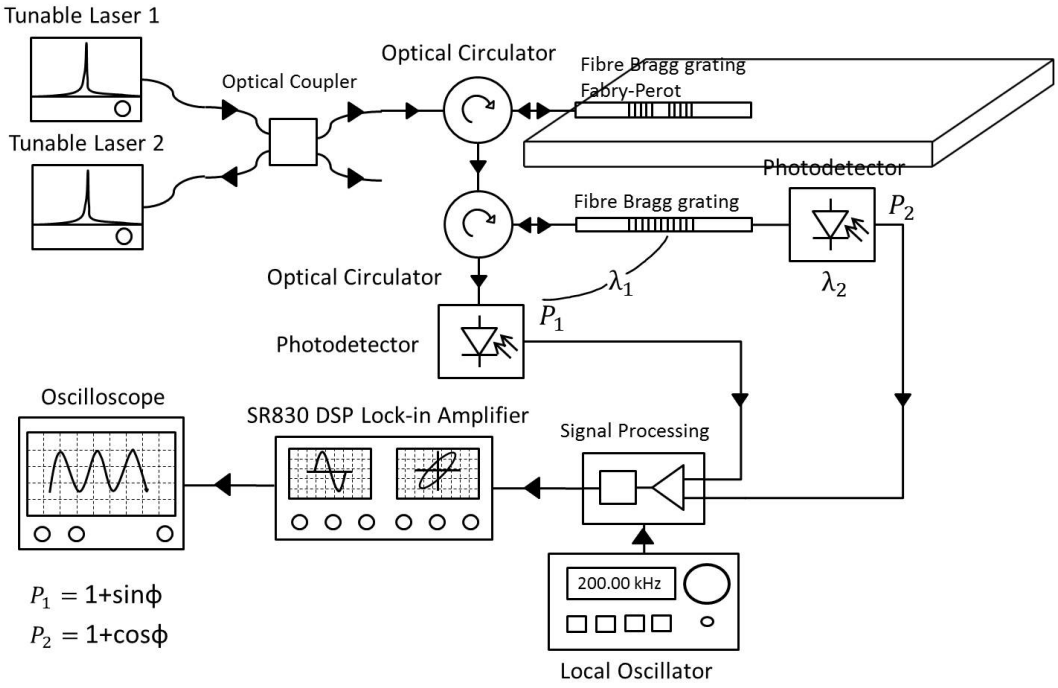

Figure 4.22 Experimental set up for two laser method

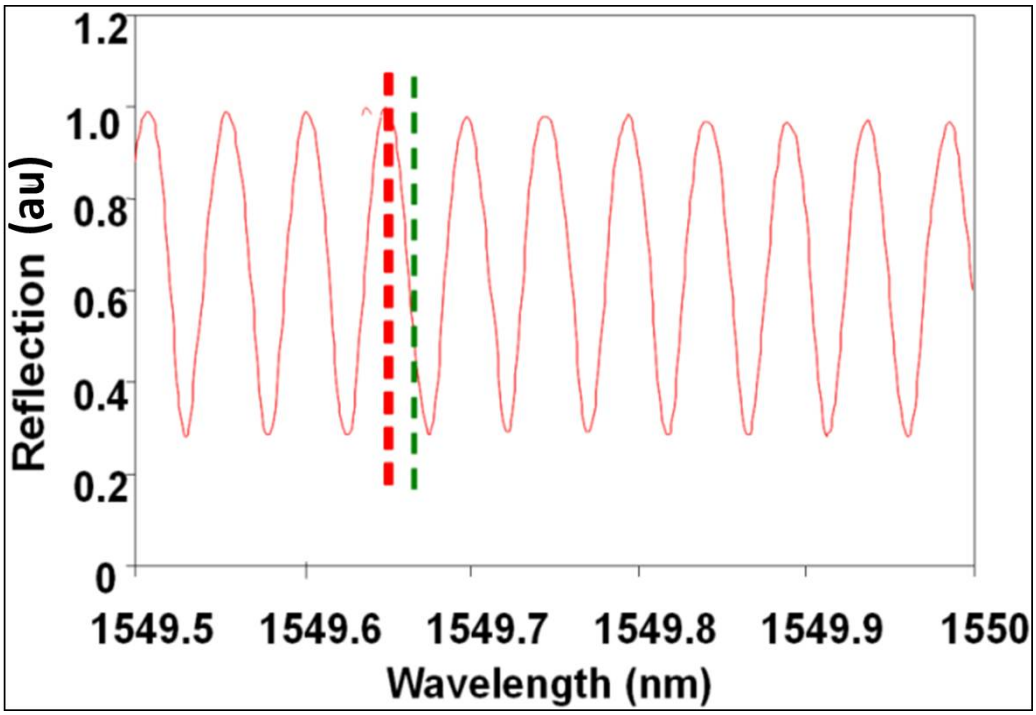

Figure 4.23 Reflection profile of the FBG Fabry-Perot and tuning up of two lasers in quadrature

The responses from the two lasers can be expressed in terms of sinϕ and cosϕ which is explained below, where ϕ is the phase change proportional to the wavelength change of the FBG Fabry-Perot caused by environmental perturbation and acoustic emission.

The output from the photodetectors can be expressed as P_1 and P_2, where,

$$P_1 = (1 + \sin\phi) \quad \textbf{Equation 4.16}$$

$$P_2 = (1 + \cos\phi) \quad \textbf{Equation 4.17}$$

where, $\phi = 2\pi\, l/\lambda$ and l is the optical path difference between the two arms

Multiplying P_1 and P_2 with signal from local oscillator

$$P'_1 = (1 + \sin\phi) * \cos\omega_c\, t \quad \textbf{Equation 4.18}$$

$$P'_2 = (1 + \cos\phi) * \sin\omega_c\, t \quad \textbf{Equation 4.19}$$

Adding equations (Eq 4.18) and (Eq 4.19)

$$P' = (\sin\phi) * \cos\omega_c\, t + (\cos\phi) * \sin\omega_c\, t \quad \textbf{Equation 4.20}$$

$$P' = \sin(\omega_c\, t + \phi) \quad \textbf{Equation 4.21}$$

where ω_c is determined by local oscillators.

4.6.2 Experiment

The quadrature signals from the two lasers are reflected to the photodetectors. From there the signals are processed and recombined using signal processing electronics as shown in figure 4.22. At this point a local oscillator generates a sine wave and cosine wave with a frequency of ω_C and these are recombined with the two received signals to generate a signal proportional to $\sin(\omega_c\, t + \phi)$. The phase of this signal, which contains information on the wavelength shift in

the FBG Fabry-Perot due to the environmental perturbation or acoustic emission, is recovered by using lock-in amplifier, same as in previous experiment.

4.6.3 Results and discussions:

Tests were carried to test the response of the FBG Fabry-Perot by tapping the optical bench and also by using a low profile buzzer as acoustic signal generator. Figure 4.24 shows response for a signal of 1 kHz and figure 4.25 and 4.26 shows a typical response of the measured output when the table was gently tapped at a distance 20cm away from the FBG Fabry-Perot sensor.

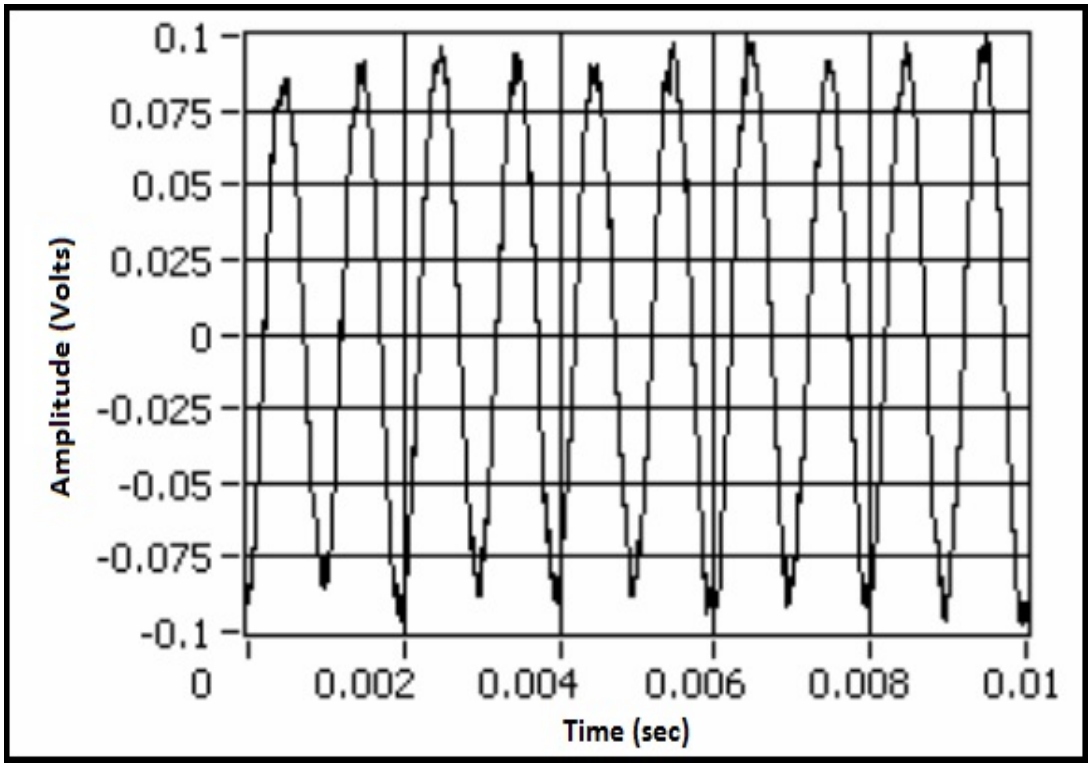

Figure 4.24 Response for a signal of 1 kHz

The SNR has improved a lot in comparison to the response in Figure 4.19. This technique is principally better as the signal fadeout problem is reduced and also the processing electronics design is simple. In summary, this technique can detect the high frequency wavelength changes of an FBG Fabry-Perot induced by the acoustic emission events.

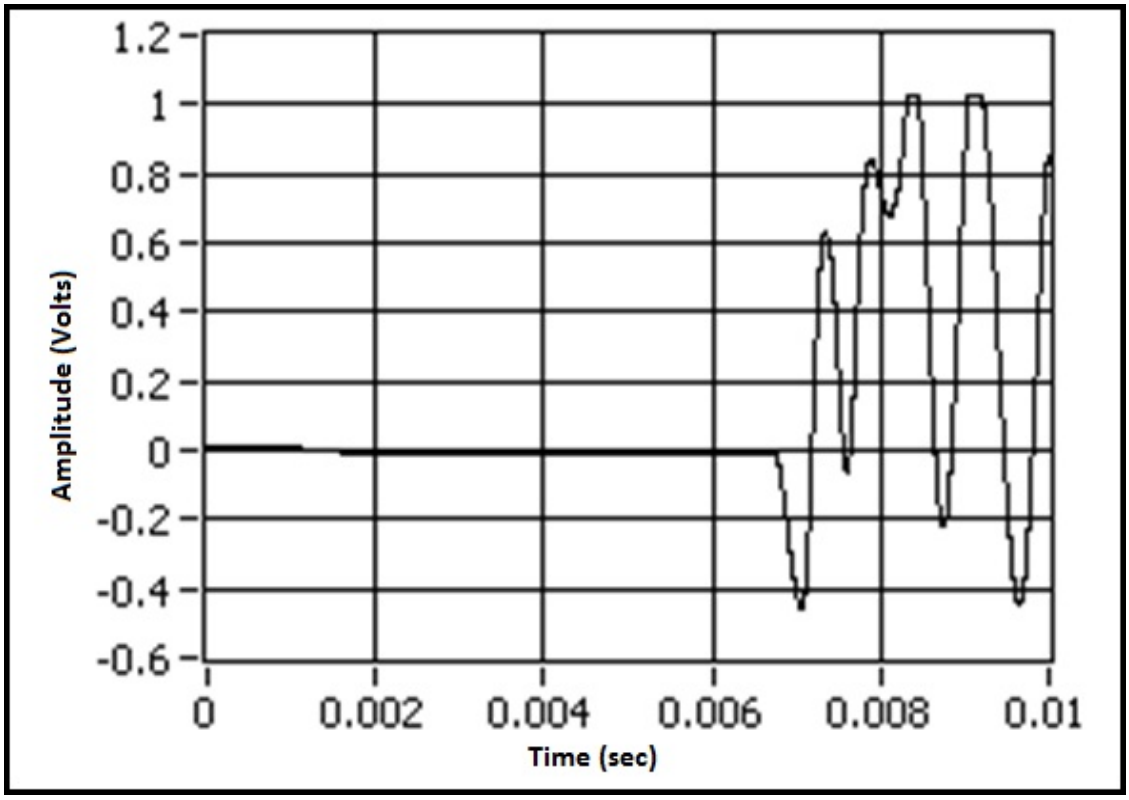

Figure 4.25 Tapping Results at distance 20cm

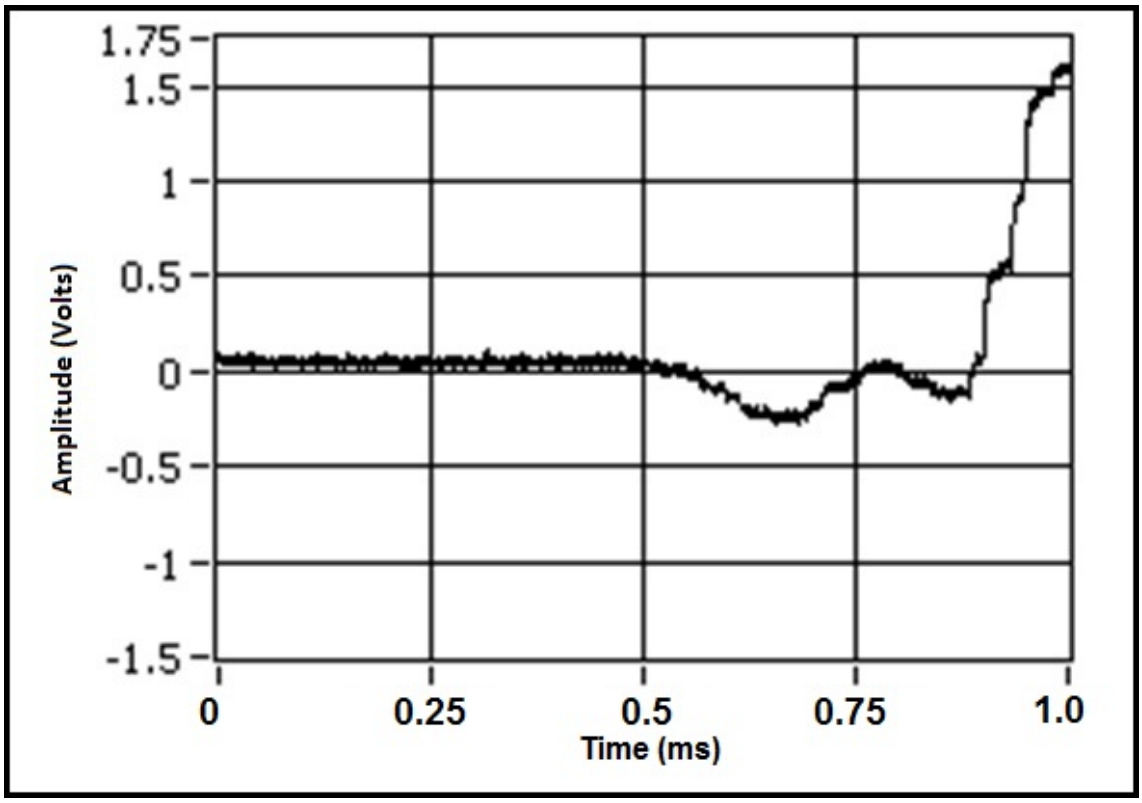

Figure 4.26 Tapping Results at distance 20cm

By setting the wavelengths of the two lasers in quadrature the measurement sensitivity can be maintained in spite of environmental perturbation, making this approach practical for real time applications.

However, to keep both the lasers in quadrature they have to be tuned after any event has occurred and recorded. The lasers used don't have modulation input to feedback and track the wavelength change. Also using two lasers increase the overall cost of the system and thus not very practical in applications where multiple sensors have to be used.

4.7 Chapter conclusions

In this chapter four new interrogation techniques have been proposed that are used for AE detection by wavelength interrogation. Novel interrogation systems namely, active tracking technique and quadrature recombination technique were developed. Active tracking technique ensures that the sensor, which is subjected to acoustic emission, is always working at an optimised sensitivity without suffering the impact from environmental perturbations.

In the matched pair grating experiment the maximum detectable frequency is 110 kHz. This technique is very simple and offers multiplexing of sensors. But it was unable to detect high frequencies thus, doesn't cover the dynamic range of frequencies that need to be measured. In order to overcome the issue of range, enhance the signal to noise ratio, achieve both high intensity and narrow bandwidth a fibre grating based laser has been designed and fabricated. This fibre laser acts as acoustic sensor based on the same principle as FBG acoustic sensor in matched pair technique. Due to its lasing feature it can provide much narrower linewidth and higher output intensity than FBGs, thus higher sensitivity and signal-to-noise ratio. It can be seen that it can detect high

frequencies up to 300 kHz and this range is limited due to the piezo buzzer used. This technique has immense potential as it offers higher sensitivity and simple interrogation system. Fibre lasers are sensitive to environmental perturbations but the active tracking technique makes sure that it operates at optimum region cancelling the changes due to environment. Designing a compact system with the sensitivity equivalent to electrical transducers with low noise is still a primary target.

An all fibre interrogation method using 3 by 3 coupler was proposed to demonstrate high sensitivity, provide a dynamic range and very cost effective. Quadrature recombination technique was developed to recover the wavelength change by monitoring the change in phase of the Mach Zehnder interferometer. This technique detected low frequency signals up to 10kHz from tapping tests but remains immature with huge potential. The high frequency signals detected were burried in the noise and making the signal to noise ratio very low then expected. Future work should concentrate on enhancing the signal to noise ratio. Also, the frequency measured is limited by the electronics and the buzzer as rest of the components are passive. However, this method has potential to detect frequencies up to 1MHz, but the output power ratio of 3 by 3 fibre coupler changes due to variable polarisation state in fibre and the phase and wavelength relationship doesn't stand correct in such case.

To overcome this a two laser method was designed and demonstrated. This technique has been proposed to detect high frequencies and the electronics are same as in the previous technique. The signal to noise ratio has improved in comparison to previous experiments. But still it doesn't cover the frequency range and the issue of remains outstanding. There is another disadvantage of

this method as the lasers used have to be manually tuned everytime an event occurs and the overall system is not compact. Further work should be carried to make the system compact and to potentially design a locking technique for optimum performance of such system. Also, testing embedded sensors in conjunction with the interrogation methods discussed in the chapter should be carried out.

In these experiments, Fibre laser sensor, interrogation with 3 by 3 coupler and two laser technique offers better sensitivity along with dynamic range. However, the incumbent piezoelectric technology remains the target for the optical sensors to match. The compactness of the sensor is another issue that needs to be taken into consideration. The fibre Bragg grating Fabry-Perot sensor is marginally better than a fibre Bragg grating and remains a device of great potential. The sensitivity can be matched to the application quite easily and the interrogation requirements are also simple. A novel compact, low cost, active, highly sensitive sensor with fibre Bragg grating Fabry-Perot can be realised as the solution. The active tracking technique offers a solution to eliminate noise due to natural and environmental perturbation and thus can be used to track the wavelength changes. So, a technique using a Fabry-Perot sensor along with active tracking technique can be a potential sensing technique for the aerospace application and has been developed further.

4.8 References

[1] E. Udd, “An overview of Fibre Optic Sensors", Review of Scientific Instruments, vol. 66, pp. 4015-4030, 1985.

[2] T. G. Giallorenzi, J. A. Bucaro, et al., “Optical Fiber Sensor Technology”, IEEE Journal of Quantum Electronics, Vol. QE-18, pp. 626-664, 1982.

[3] R. M. Measures, M. LeBlanc, K. Liu, S. Ferguson, T. Valis, D. Hogg, R. Turner and K. McEwen, "Fiber optic sensors for smart structures", Optics and Lasers in Engineering, vol. 16, pp. 127-152, 1992.

[4] G. J. Hamstad, "On the far-field structure of waves generated by a pencil lead break on a thin plate," J. Acoust. Emiss. Vol.12, pp. 157, 1994

[5] I. Read, P. Foote and S. Murray, "Optical fibre acoustic emission sensor for damage detection in carbon fibre composite structures," Measurement science & Technology, vol.13,pp. N5-N9, 2002

[6] W. Zhang, K. Sugden, R. P. Pappu, D. J. Webb, and I. Bennion, "Acoustic Emission Sensor Using Matched Fibre Bragg Gratings and Active Tracking Technique", Proc. of Mediterranean Photonics, Italy, 2008.

[7] S. M. Melle, K. Liu, and R. M. Measures, "A passive wavelength demodulation system for guided-wave Bragg grating sensors," IEEE Photon. Technol. Lett., vol. 4, pp. 516–518, 1992.

[8] M. A. Davis and A. D. Kersey, "All-fiber Bragg grating strain-sensor demodulation technique using a wavelength division coupler," Electron. Lett., vol. 30, pp. 75–77, 1994.

[9] Q. Zhang, D. A. Brown, H. Kung, J. E. Townsend, M. Chen, L. J. Reinhart, and T. F. Morse, "Use of highly overcoupled couplers to detect shifts in Bragg wavelength," Electron. Lett., vol. 31, pp. 480–482, 1995

[10] D. A. Jackson, A. B. Lobo Ribeiro, L. Reekie, and J. -L. Archambault, "Simple multiplexing scheme for a fiber-optic grating sensor network," Opt. Lett., vol. 18, pp. 1192–1194, 1993.

[11] L. A.Ferreira, JL Santos, and F. Farahi, Pseudoheterodyne demodulation technique for fiber Bragg grating sensorss using two matched gratings, IEEEPhoton. Technol. Lett., 9, 4, pp. 487–489, 1997

[12] M. A. Davis and A. D. Kersey, “Matched-filter interrogation technique for fiber Bragg grating array”, Electron. Lett., vol. 31, pp. 822–823, 1995.

[13] A.D.Kersey, T.A.Berkoff and W.W.Morey, "High-resolution fibre-grating based strain sensor with interferometric wavelength-shift detection", Electronics Letters, vol.28, pp.236-238, 1992.

[14] K. P. Koo, A. D. Kersey, "Bragg grating-based laser sensors systems with interferometric interrogation and wavelength division multiplexing," Journal of Lightwave Technology, vol.13, pp.1243-1249, 1995.

[15] G.A.Ball, W.W.Morey, P.K.Cheo, "Single- and multipoint fiber-laser sensors", IEEE Photonics Technology Letters, vol.5, pp.267-270, 1993.

[16] C-C Ye and R P Tatam, "Ultrasonic sensing using Yb3+/Er3+-codoped distributed feedback fibre grating lasers", Smart Mater. Struct., vol.14, pp 170-176, 2005.

[17] A. Main and I. Read, “CONSTRUCT: Optical fibre sensor cross-comparison testing”, 2008 – Restricted Access

[18] S. K. Sheem, T. G. Giallorenzi, and K. Koo, "Optical techniques to solve the signal fading problem in fiber interferometers," Appl. Opt., vol.21, pp.689-693, 1982.

[19] K.P.Koo, A.B.Tveten and A.Dandridge, "Passive stabilization scheme for fiber interferometers using (3×3) fiber directional couplers," Applied Physics Letters, vol.41, pp.616-618, 1982.

[20] Y.Jiang, Y.Xu and C.K.Y.Leung, "3*3 Coupler-Based Mach-Zehnder Interferometer and Its Application in the Delamination Detection in FRP Composite", Applied Optics, vol.21, pp.689-693, 1982.

[21] K. Liu and R.M.Measures, ‘‘Signal Processing Techniques for Interferometric Fiber-Optic Strain Sensors,’’ J. Intel. Meter. Syst. Struct., vol.3, pp.432–461, 1992.

[22] D. A. Brown, C.B.Cameron, R.M.Keolian, D.L.Gardner and S.L.Garrett, ‘‘A Symmetric 3*3 Coupler Based Demodulator for Fiber Optic Interferometric Sensors,’’ SPIE, vol. 1584, pp. 328–335, 1991.

[23] Y.Jiang, "Stabilized 3×3-coupler-based interferometer for the demodulation of fiber Bragg grating sensors", Opt. Eng., vol.47, 015006, 2008.

[24] M. D. Todd, M. Seaver, and F. Bucholtz, “Improved, operationallypassive interferometric demodulation method using 3*3 coupler", Electron. Lett., vol.38, pp.784–786, 2002.

[25] G. A. Johnson, M. D. Todd, B. L. Althouse, and C. C. Chang, “Fiber Bragg grating interrogation and multiplexing with a 3*3 coupler and a scanning filter”, J. Lightwave Technol., vol.18, pp.1101–1105, 2000.

5 Acoustic Emission sensing and development of Active tracking technique

5.1 Introduction

Chapter 4 focussed on four sensing techniques that involved detection systems using lasers without any feedback control (free running) except matched fibre grating technique that uses a feedback control but also multiple gratings to detect the acoustic emission. Using multiple gratings and multiple light sources increase the system's operational cost, it is also difficult to achieve system stability because the operational parameters have to be precisely adjusted. This chapter focuses on overcoming the problems that were observed in the previous experiments and also covers the development of a compact active tracking feedback sensing system.

From the previous chapter it can be inferred that a uniform fibre Bragg grating sensor is unsuitable for this kind of application. The Bragg shift is very small to allow detection. The Fabry-Perot sensor's offers sensitivity that can be matched to the application and has simple interrogation requirements. Thus it becomes an obvious choice for such sensing applications. However, the main concern for optical sensors is still to match the existing piezoelectric technology and demonstrate an optimal signal-to-noise ratio coupled with a wide dynamic range. Here in this chapter, the main focus will be on the working of laser diode tracking system for interrogating high sensitive fibre grating Fabry-Perot cavity. The circuitry is same as used in the matched pair fibre grating experiment. But it has been improved to overcome the issues of tracking range of laser diodes,

normalising power, increase in sensitivity and improvement in SNR of the system.

5.2 Principle & theory of experiment

The wavelength of the laser diode can be tuned by varying operating current to lock to the chosen operation point irrespective of external perturbation. The output optical phase of the Fabry-Perot cavity is modulated by the cavity length change which in turn is modulated by the acoustic emission applied to the Fabry-Perot cavity. The response of the sensor depends on both the cavity length and the coupling efficiency between the Fabry-Perot cavity and the structure to be monitored. A low-finesse fibre grating based Fabry- Perot sensor such as the one shown in figure 5.1 produces a pseudo-sinusoidal signal under cyclic loading conditions and it is easy to detect acoustic emission signal using a laser and interrogation system. However, the sensitivity varies depending on the part of the spectrum that the laser spectrum overlaps The principle of the concept that we propose here is to tune the laser to the most sensitive region on one of the fringes and lock its wavelength in this position.

A servo-mechanism has been designed in the same lines of the matched pair grating experiment is used for locking the wavelength to maximum sensitivity and any wavelength offset away from the optimum operation point will be detected by this system. If the frequency of the wavelength offset is below this natural frequency, it will be compensated by feeding back an error signal into the laser diode control. Any wavelength offset with frequency above that will be detected by the system. Usually the frequency of the environmental perturbation is less than 100 Hz. Therefore the acoustic emission signal above this frequency can always be detected using this system.

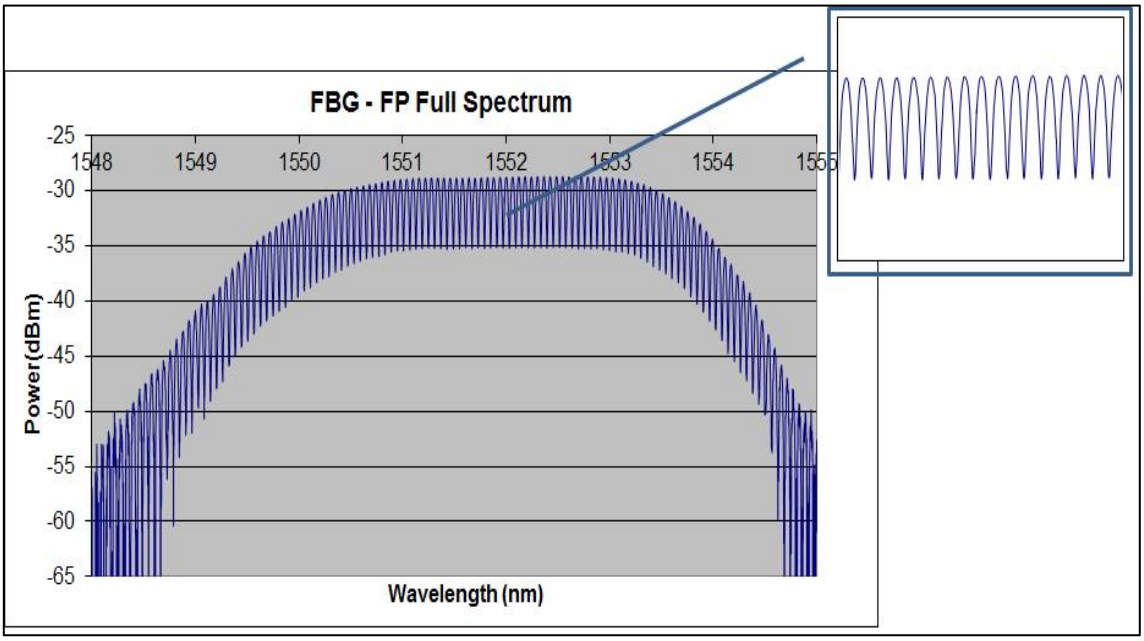

Figure 5.1 Fibre Bragg Grating Fabry Perot Full Spectrum

5.3 Circuit Design and Implementation

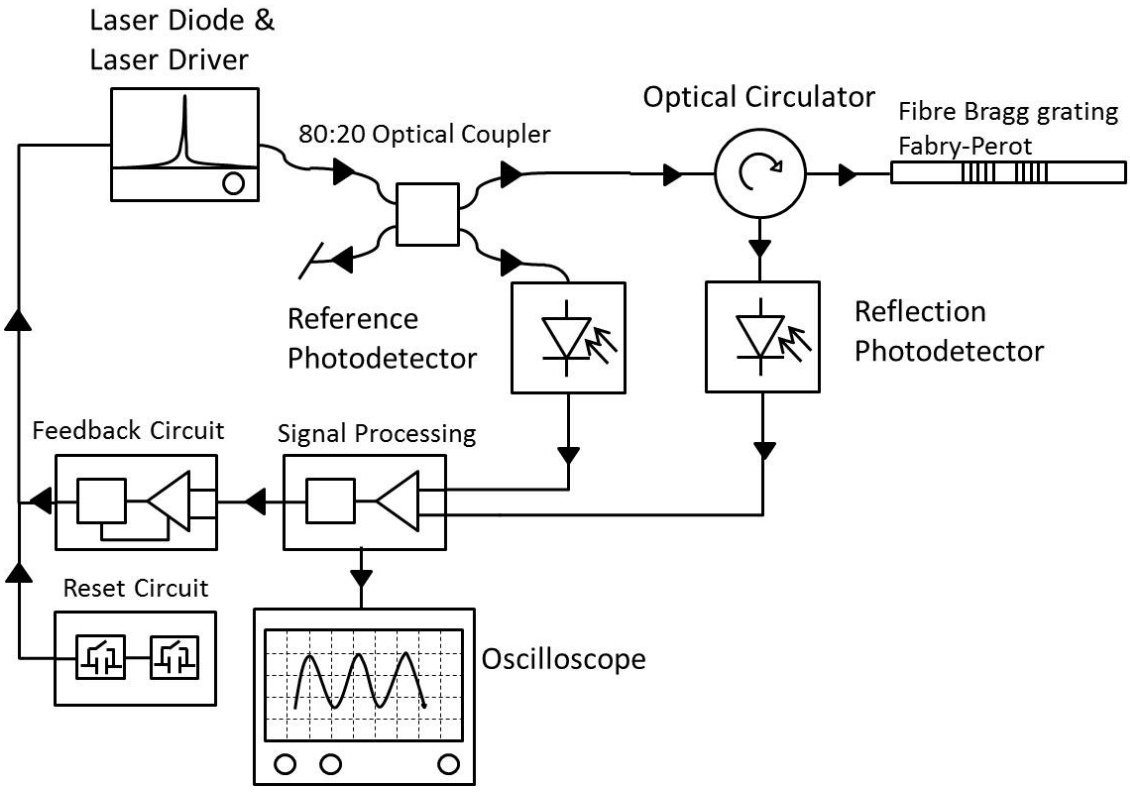

Figure 5.2 Experimental arrangement for the acoustic emission detection using active tracking technique

This section will try to explain various components and functionality of the feedback system. The system contains three parts:

i) Feedback Circuit

ii) Reset Circuit

iii) Optical System

5.3.1 Feedback Circuit

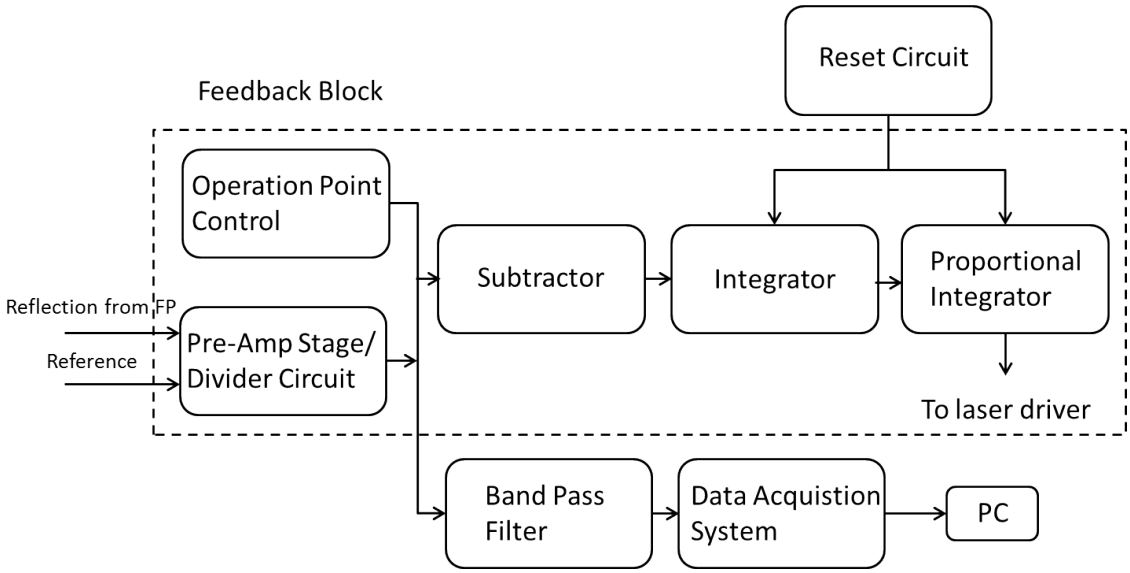

Figure 5.3 Block diagram of active feedback technique showing feedback control and reset mechanism

Figure 5.4 shows the block diagram of the feedback circuit that has been used in the experiment. The circuit is designed for a damping ratio ζ of 0.45 and natural frequency f_n of 93 Hz [2]. All the calculations are explained further in this chapter. There are two input current to voltage converters that are connected to photodiodes and have very low input impedance. Because of the low input impedance the photodiodes operate essentially as short circuit. The photodiode current which is proportional to the incident light is converted to voltage. One photodiode is used to collect the light from the reflection of the grating under test and the other is used as a reference which collects the incident light from

the coupler. Both photodiodes are used in photovoltaic mode and they are unbiased to reduce the dark current and flicker noise. The output from both the current to voltage converters are fed into a divider so that output power from the laser diode is also normalized, so as to remove the effect of any output power change caused by the wavelength tuning of the laser diode. The output from the divider is connected to the subtractor circuit and a potentiometer RV1 is connected to other input of the subtractor.

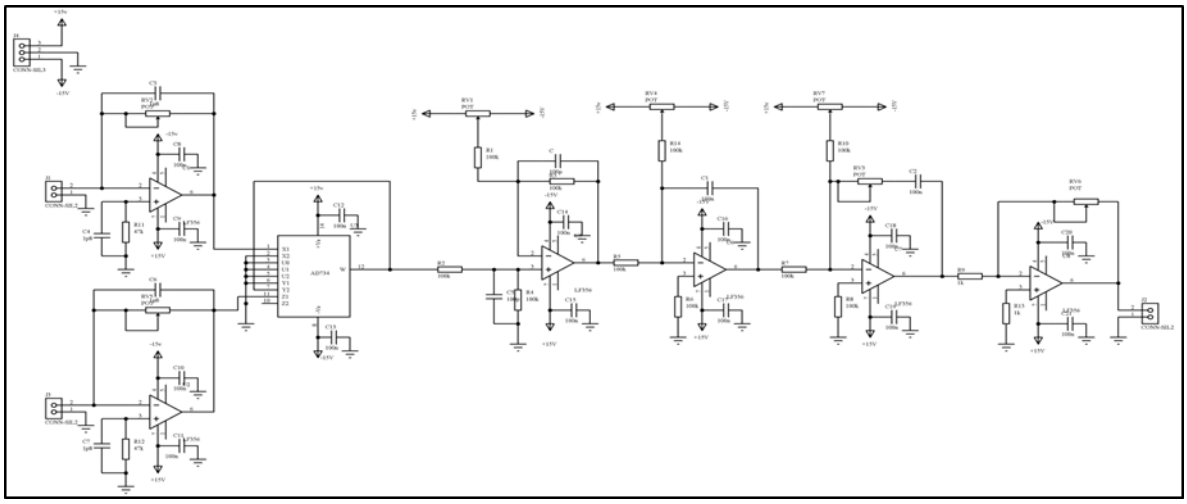

Figure 5.4 Circuit diagram of the feedback circuit [Ref: Appendix Figure 3]

This potentiometer is used to set the operation point of the system. This difference output is fed to first integrator and a second integrator follows which stabilises the loop.

Any offset below the natural frequency caused by environmental perturbation is compensated for and is fed back into the laser diode thus allowing only the higher frequency components to be detected.

5.3.2 Feedback Analysis

Consider a simple feedback system in complex domain that can be shown as below figure 5.5:

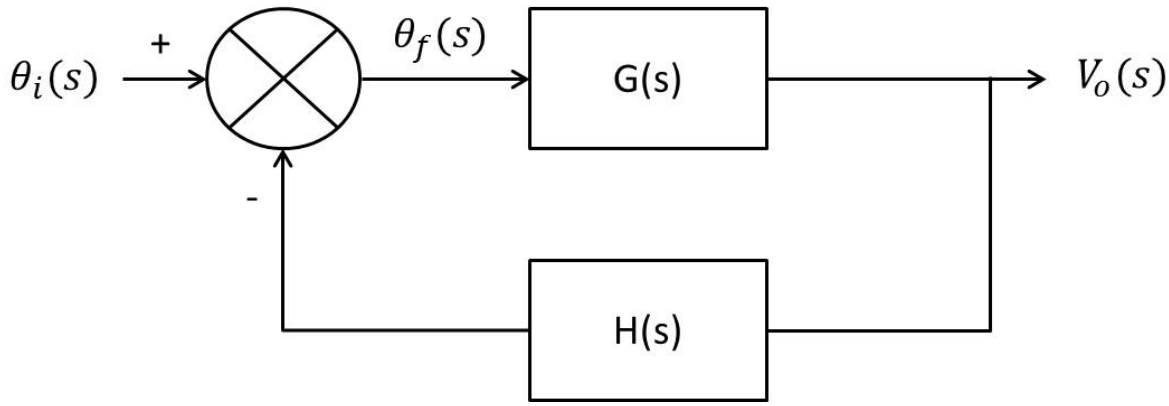

Figure 5.5 Basic feedback system

where,

$\theta_i(s)$ Laplace transform of phase input

$\theta_f(s)$ Laplace transform of the phase error

$V_o(s)$ Laplace transform of the output voltage

$G(s)$ Laplace transform of forward gain (product of individual forward transfer functions)

$H(s)$ Laplace transform of feedback (product of the individual feedback transfer functions)

Using control electronics theory [1] we can obtain the following relationships for the above control system:

$$\theta_f(s) = \frac{1}{1 + G(s)H(s)}\,\theta_i(s) \qquad \textbf{Equation 5.1}$$

$$V_o(s) = \frac{G(s)}{1 + G(s)H(s)}\,\theta_i(s) \qquad \textbf{Equation 5.2}$$

$\mathrm{G(s)\ H(s)}$ is the loop transfer function.

Fig. 5.4 shows the block diagram of the feedback system. This can be represented in terms of the feedback parameters as shown in below figure 5.6 that will make it easy for feedback analysis.

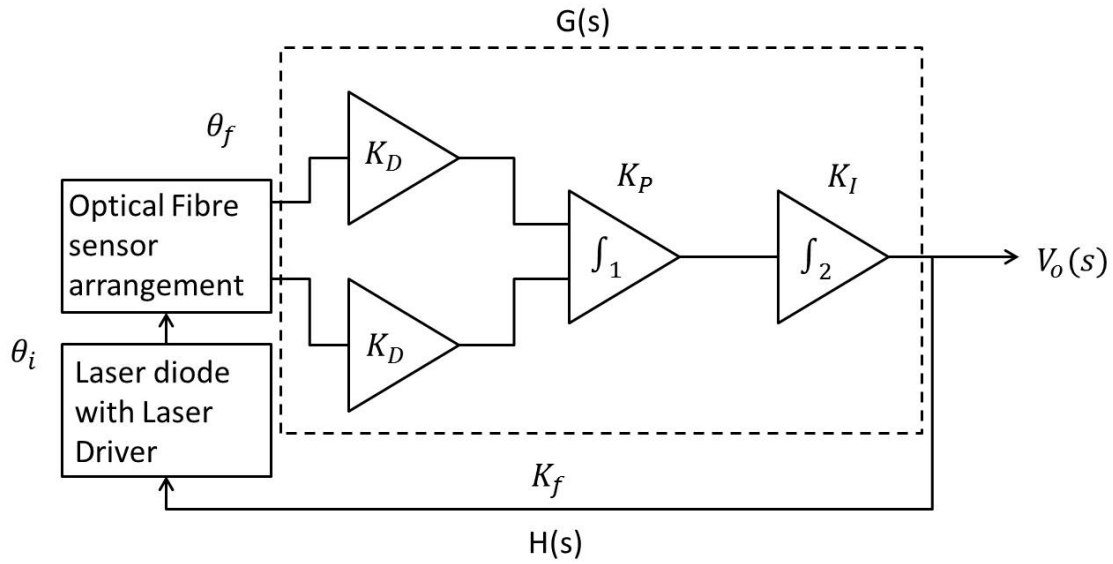

Figure 5.6 Block diagram of feedback circuit

$G(s)$ can be represented as :

$$G(s) = K_D\, K_P(s) K_I\,(s) \qquad \textbf{Equation 5.3}$$

where,

$\mathrm{K_D}$ is the conversion gain of the photodiode and current- voltage converter

$\mathrm{K_P(s)}$ is the transfer function of the first integrator

$\mathrm{K_I\,(s)}$ is the transfer function of the second integrator

$\mathrm{H(s) = K_F}$ is the feedback gain.

The integrators are being used as the loop filter and their gains $\mathrm{K_P(s)\ and\ K_I\,(s)}$can be represented as:

$$K_P(s) = \frac{-K_1}{s}$$ **Equation 5.4**

where,

K_1 is the gain of the first integrator

$$K_I(s) = \frac{-K_2\ (s + a)}{s}$$ **Equation 5.5**

where,

K_2 is the gain of the second integrator

Now, the loop transfer function can be re-written as:

$$G(s)\ H(s) = K_D\ K_F\ K_P(s) K_I\ (s)$$ **Equation 5.6**

Replacing $K_P(s)$ and $K_I\ (s)$ in equation (7), we get

$$G(s)\ H(s) = \frac{K_D\ K_F\ K_1\ K_2\ (\ s + a\ )}{s^2}$$ **Equation 5.7**

$$G(s)\ H(s) = \frac{K(\ s + a\ )}{s^2}$$ **Equation 5.8**

where,

$$K = K_D\ K_F\ K_1\ K_2$$ **Equation 5.9**

From equation (5.8) we can say that the systems loop is a type-2 loop. The characteristic equation can be given as:

$$1 + G(s)\ H(s) = 0$$ **Equation 5.10**

The roots of the characteristic equation become the closed loop poles of the overall transfer function.

Replacing the characteristic equation with equation (5.8), we get,

$$1 + \frac{K(s+a)}{s^2} = 0$$

$$s^2 + Ks + Ka = 0 \qquad \textbf{Equation 5.11}$$

This is a second order system and a second order characteristic equation can be represented in a normalised form:

$$s^2 + 2\zeta\omega_n s + \omega_n{}^2 \qquad \textbf{Equation 5.12}$$

Comparing it with equation 5.11 we get,

$$\omega_n{}^2 = K\,a$$

$$f_n = \frac{(Ka)^{1/2}}{2\pi} \qquad \textbf{Equation 5.13}$$

which is the natural frequency of the second order system.

and,

$$2\zeta\omega_n = K$$

$$\zeta = \frac{K}{4\pi f_n} \qquad \textbf{Equation 5.14}$$

which is damping ratio of the system.

The gain of the integrators are:

$$K_1 = \frac{1}{R_1 C_1}$$

$$K_2 = \frac{R_P}{R_2}$$

$$a = \frac{1}{R_P\, C_2}$$

5.3.3 Reset Circuit

A laser diode whose wavelength is tuned by changing operating current is wavelength set to the operation point where the FBG Fabry-Perot cavity shows maximum wavelength shift against external perturbation. Any drift of the wavelength from the operation point is monitored by a photo detector and feedback to the laser diode driver through servo electronics. However, this approach is limited by the amount that one can tune the laser. To overcome the limit in wavelength tuning a fast responding resetting circuit has been designed. The principle of this resetting is to reset the LD wavelength to the initial value once the LD reaches its tracking limit. Since the reset time is in the order of ~10 ns there will be minimal effect.

The output voltage of the feedback circuit is compared to a reference voltage Vref using comparators LM 311. Two comparator ICs are used in the reset circuit, one for negative and one for positive feedback voltage comparison. When output voltage of the feedback circuit is negative it is compared with negative Vref that can be set manually, on one of the comparator and the output of the comparator C1 is -5V, if Vref < Vout or 0 if Vref > Vout. If the feedback voltage is positive then second comparator is used. Positive Vref is set manually and output of comparator C2 is +5V, if Vref < Vout or 0 if Vref > Vout. The output of both the comparator goes into a OR gate. The pulse from the OR gate triggers two monostable pulse generator.

The D input of the flip flop is tied to +8V (high) while the S (Set) input is tied to -8V (low). Initially Q is low and Q' is high. Whenever the flip flop is clocked due to any pulse from the output of the comparator 311, it's Q output will go high and Q' will become low.

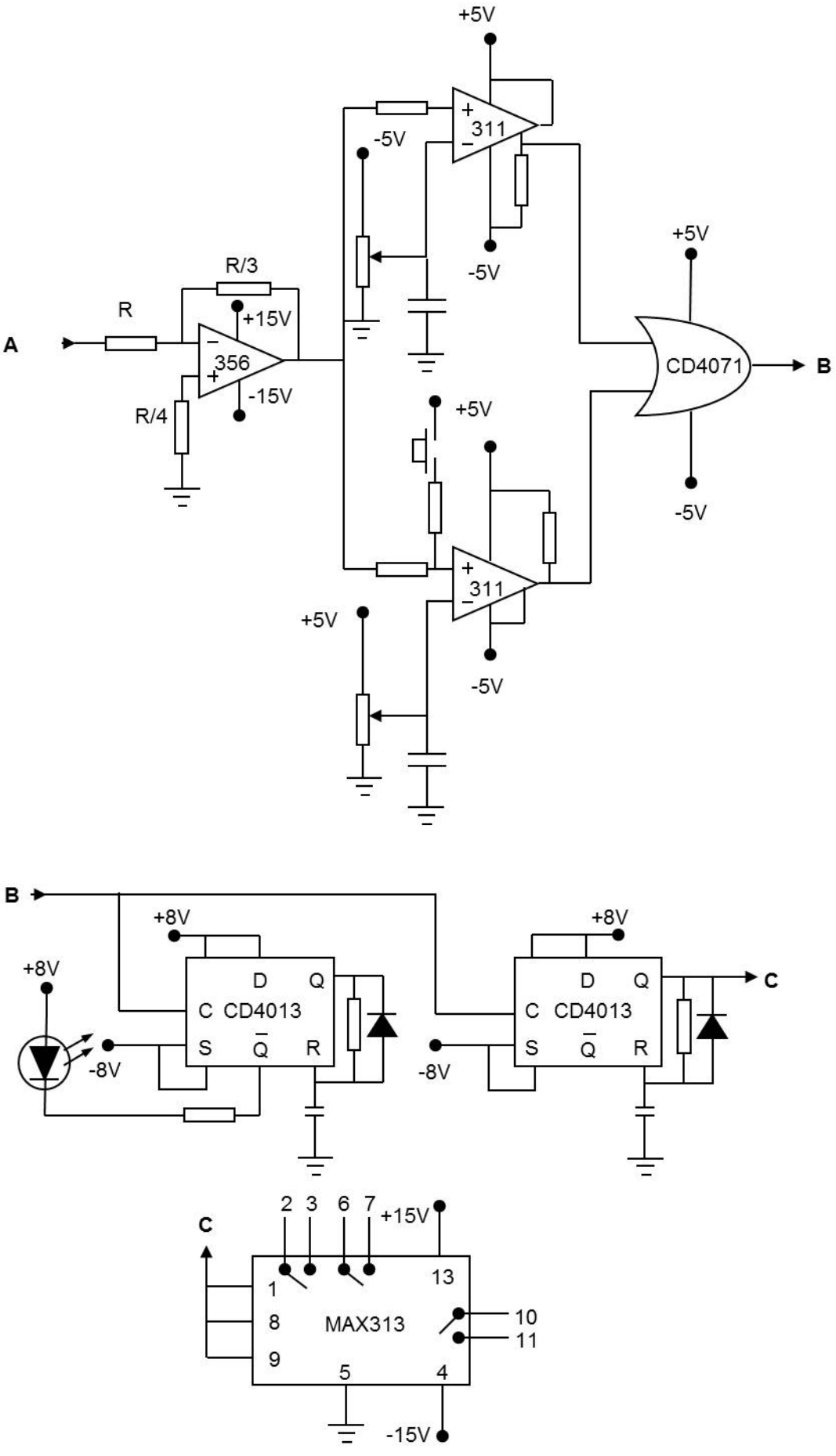

Figure 5.7 Circuit diagram of Reset Circuit [Ref: Appendix Figure 2]

In case of first flip flop, Q' will turn on the LED (active low configuration) while Q outputs will start charging the 0.22uF and 510pF capacitors for first and second flip flop via their respective resistors (22M and 56K).

The moment R(reset) input trigger threshold is reached, Q will become low and Q' will become high. The diode connected across the RC combination is now forward biased and discharges the capacitor instantly for enabling the circuit to sense the next trigger pulse. Without it, the capacitor would be discharged through its series resistor. This would result in uncertainty for the next monostable pulse duration due to partially charged state of capacitor if another pulse comes before it is fully discharged. One monostable is used as an indicator to check if any reset has taken place. The LED on the monostable is triggered for four seconds indicating that a reset has taken place. The second monostable closes the CMOS switches in MAX 313. The switch is closed for 10ns and it allows discharging the capacitors on the integrator, if they are saturated. The voltage across the capacitors reaches to zero during this time. Thus, the circuit is reset and ready there is no loss of vital information.

5.3.4 Optical System

The laser diode used in the experiment is CQF975/508 series laser manufactured by JDS Uniphase. It has polarisation maintaining fibre, an inbuilt wavelength locker that stabilises the laser wavelength and a built in optical isolator that prevents any feedback and allows unidirectional transmission of light.

Typical values of the laser diode recorded at case operating temperature of 25^{O} C and thermistor resistance 10kΩ are listed in the table5.1:

Parameter	Min	Max
Power output from the pigtail	20 mW	-
Operating current	-	200 mA
Operating Temperature	20^{O} C	35^{O} C
Spectral Linewidth	< 5 MHz	20 MHz
Central Wavelength	1527 nm	1610 nm

Table 5.1 Typical values of the Laser diode JDS Uniphase CQF975/508

The current-power-wavelength characteristics are plotted in figure 5.8. The tuning range of the laser diode used here is 0.36nm, shown in below figure. The power output of the laser diode is up to 20mW but in the characteristic plot it is severely reduced.

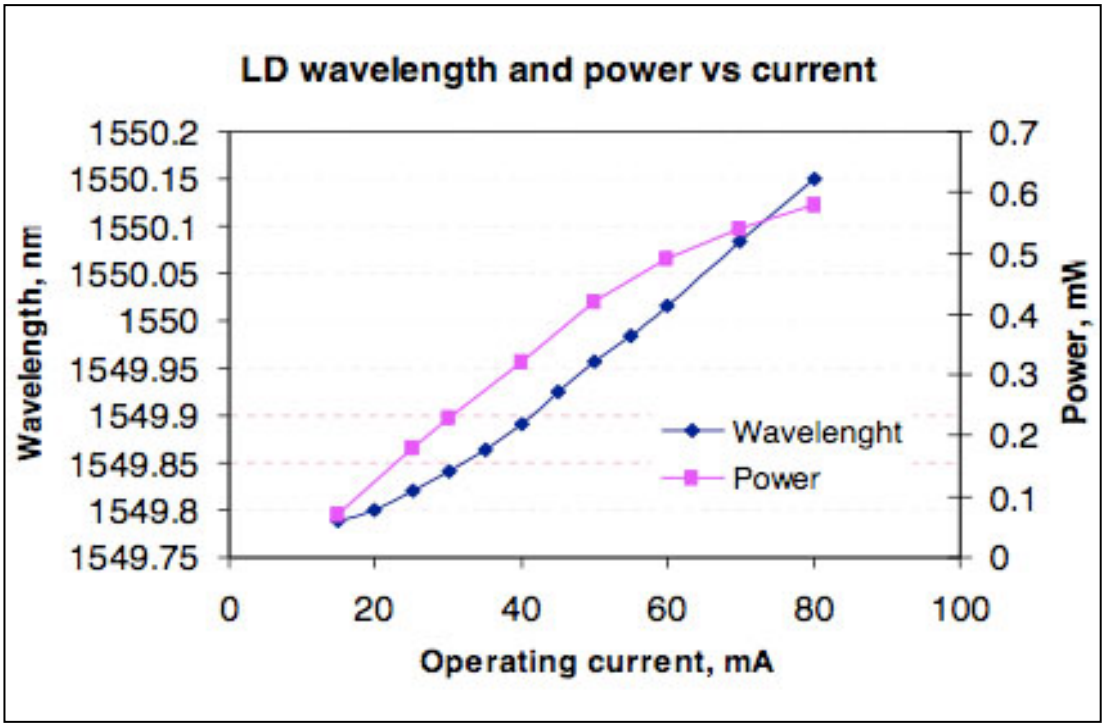

Figure 5.8 Graph showing Wavelength and power with respect to the current tuning

This is because of two reasons one is the linewidth of the laser diode and other is the use of optical attenuator to control the power. It is necessary to use an optical attenuator as it ensures that the output from the trans-impedance amplifier is not saturated and thus, the tracking electronics operate in non-saturated region (< ±5 volts) by keeping the power output low.

In most cases this is enough to cover the perturbation induced wavelength shift of the Fabry-Perot cavity as shown in figure 5.9. In some cases where this perturbation induced wavelength shift is larger than 0.36 nm, the servo will be reset using a reset mechanism, to lock the wavelength of the laser diode in most sensitive region of another fringe.

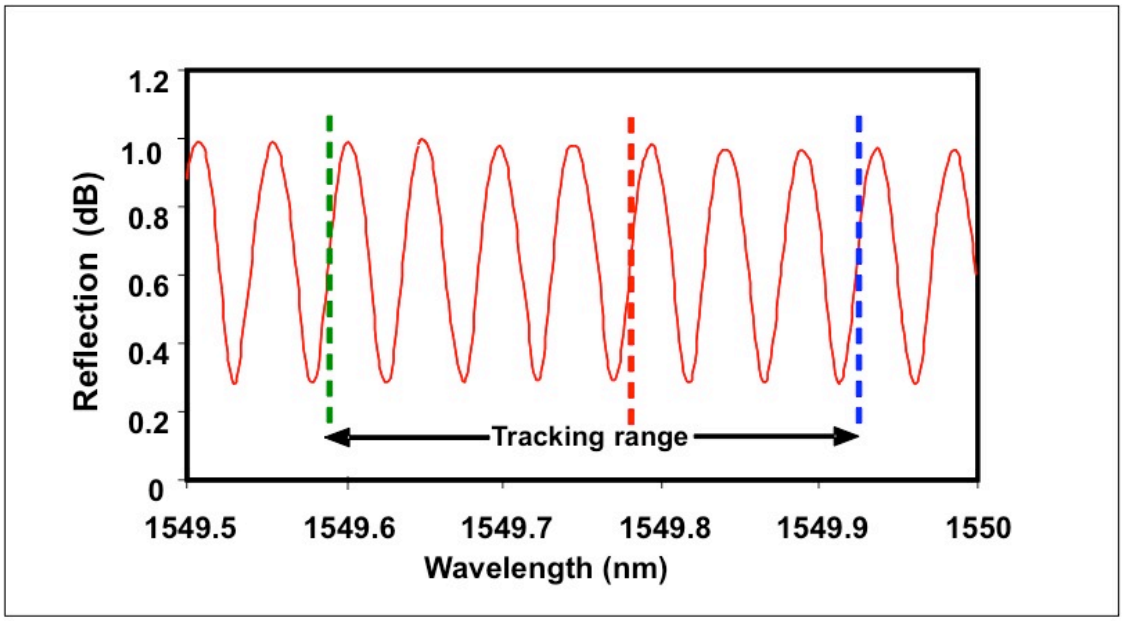

Figure 5.9 Tracking range of the Laser diode

Over the central part of the spectrum the fringes show a near identical response, the system ensures the laser diode always operates in an optimum operation region but may over time track different fringes. The reset time is in the order of nano-second, far faster than any concerned acoustic emission signals, this ensures minimal effect while the sensor is in use.

5.4 Experiment, Results & Discussions

The experimental setup is shown in Figure 5.2. The FBG Fabry-Perot resonators were made using a chirped phase mask to have a flat top using a UV laser and designed to have a bandwidth of 4nm. Each grating had a reflectivity of ~10%. Figure 5.10 shows a FBG Fabry-Perot with a cavity of 15.5mm and a free spectral range of 60pm which is measured from the reflection spectrum that was characterized by an ANDO optical spectrum analyser with measurement resolution of 10pm (minimum resolution of OSA). This means that the spatial distance between peaks must be at least 10 pm in order to be distinguished.

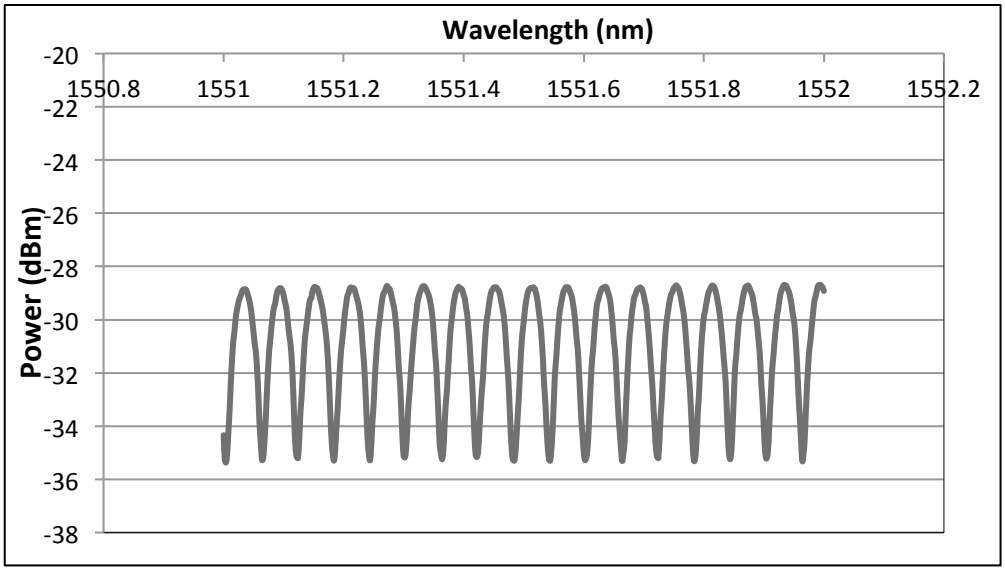

Figure 5.10 FBG Fabry-Perot cavity of 15.5 mm with FSR = 60pm

The FBG Fabry-Perot resonators were bonded onto a test panel (a glass plate) using epoxy resin. Light from a laser diode is launched into the system via an 80:20 optical fibre coupler. 80% of the light is directed towards the low finesse Fabry-Perot resonator that has a short cavity (different Fabry-Perot cavities between 13.5mm – 25mm were tested) via a fibre optic circulator. The remaining 20% of the light from the optical coupler is received by a photodiode and is used as a reference. The reflected light from the Fabry-Perot resonator is

received by a second photodiode. The output from both photodetectors is amplified and fed to the divider circuit.

The ratio of sensing arm and reference arm provides the wavelength information without suffering any intensity variation. It can be seen from the characteristics of laser diode that both power and wavelength are changed when the operating current is changed. And with reference arm in place and the circuit locked to optimal region the power can be kept constant with change in the wavelength.

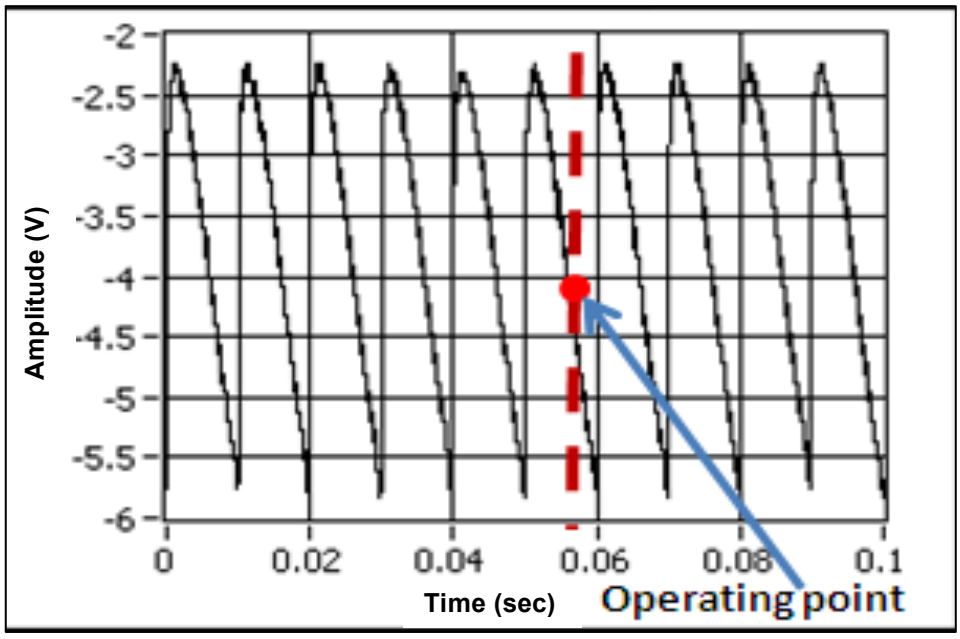

Figure 5.11 Operation point for the sensor

To keep the sensor always working in optimum operation point it is required to set the operation point which can be determined by applying a small external modulation say, 250mV 100Hz ramp signal to the laser diode controller and which repeatedly tunes the laser wavelength over half FSR (in this case 30pm). Figure 5.11 shows the sensor output for the aforementioned ramp signal applied. The operation point can be set at 40 – 60% of the slope of the falling edge. Once the operation point is set the system can be locked to the optimum sensitive region.

Figure 5.12 shows the comparison of the relative level of sensor output measured with the feedback circuit ON to that measured with the feedback OFF, when a continuous wave at 339kHz is fed through the piezo buzzer. For a 25 mm FBG- Fabry-Perot sensor, it can be seen that when the feedback is OFF, both the signal and the noise levels are fluctuating due to the sensor moving away from its optimum operation point. But when the feedback is ON, the output is stable, and noise level is lower indicating a fixed operation point and a maximum sensitivity and the noise floor is also stable. A change of 10 db in SNR can be seen clearly.

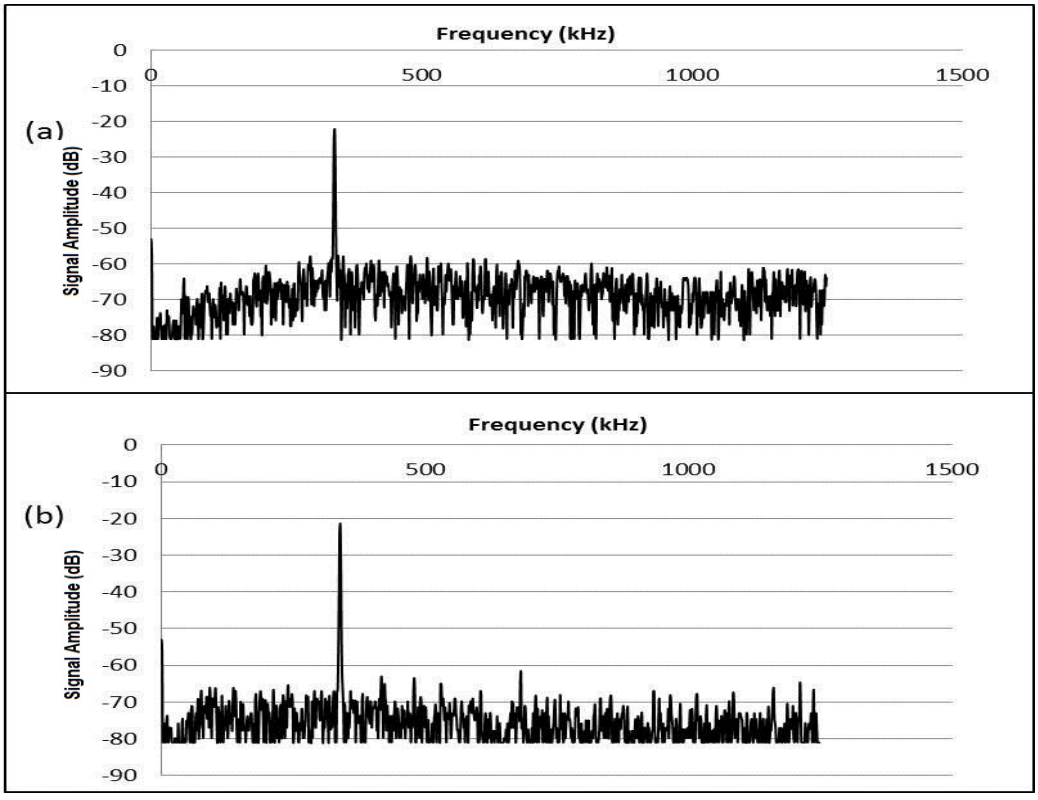

Figure 5.12 Sensor output when (a) the feedback is OFF (b) the feedback is ON

5.4.1 Testing Methods

5.4.1.1 Low profile source

A low profile piezo (P-876 DuraAct™ piezoelectric patch) was bonded using Superglue onto the test structure 60 cm away from the Fabry-Perot sensor to

simulate ultrasonic acoustic emission signal, and excited using a programmable function generator. In this way the piezo sensor could be used to generate a range of different frequencies and amplitudes. The typical response of the Fabry-Perot sensor to the ultrasonic acoustic emission was monitored by applying to the piezo buzzer a continuous burst with small signal amplitude at different frequencies. Only the AC component of the AE signal is recorded as the DC component with magnitude of several volts does not carry any vital information relevant to AE signal. Figure 5.13 shows the FFT of a CW signal at 258kHz and signal amplitude of 500 mVpp for a short cavity Fabry-Perot.

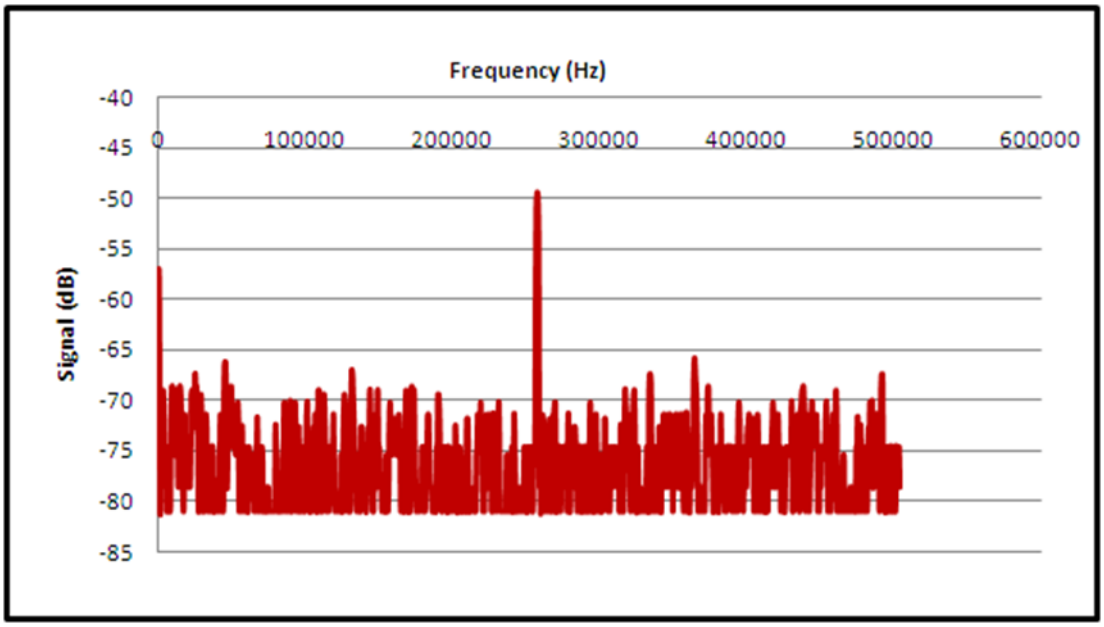

Figure 5.13 Output of the sensor system when a 500mV signal is applied to the piezo

5.4.1.2 *Pencil break test*

A pencil break source can generate frequencies close to a real acoustic emission event [3]. This type of test does not require a piezoelectric transducer to introduce the signal into the test structure and is therefore more likely to spread the acoustic energy between the propagation modes of the test structure similar to real acoustic emission. However, these tests are likely to be more variable than the other tests described here as it is difficult

to simulate similar events for comparison of results. To compensate this variability these pencil break tests are performed repetitively. Pencil breaks generate a range of frequencies unlike the other stimuli used in these tests. Figure 5.14 and 5.15 shows the time responses from one of the pencil break tests carried out to measure the acoustic emission generated with free running laser system and LD interrogation system. In this case a 2H propelling lead pencil was used, the pencil break was performed at a distance of 100 mm away from the sensor. The response is shown in figure 5.14 and 5.15 below:

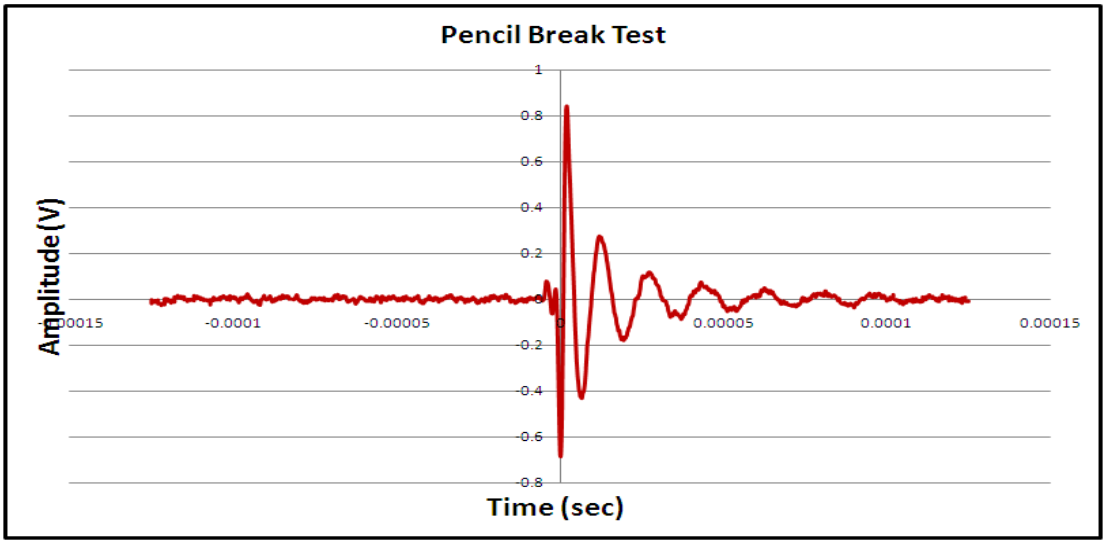

Figure 5.14 Response of pencil break test at 100mm away from sensor LD tracking

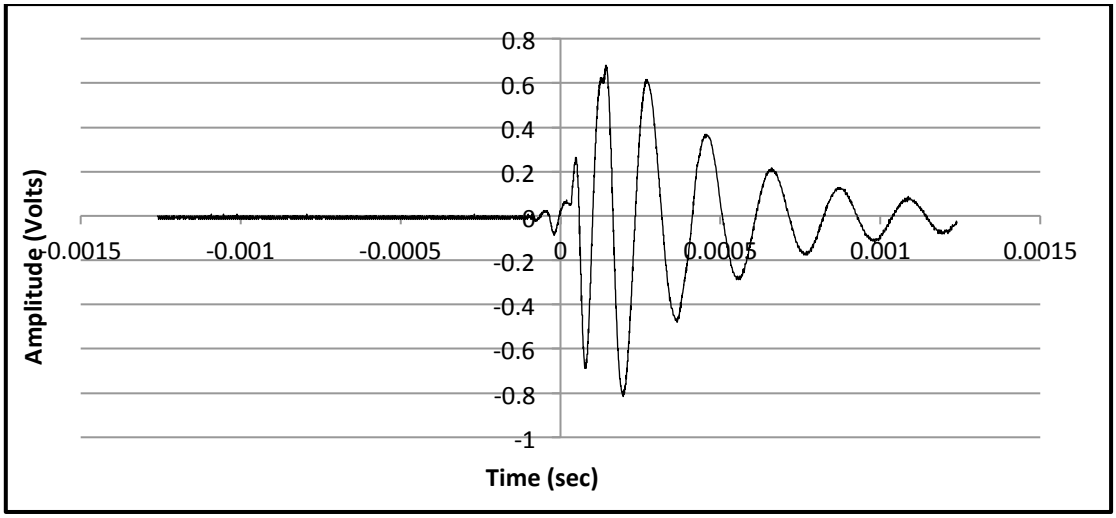

Figure 5.15 Response of pencil break test at 100mm away from sensor from free running tunable laser

5.4.2 Packaging and design of various sensors

Various sensors have been tested for sensitivity and performance. The Fabry-Perot cavity has been deployed in both straight and coiled form. Long cavity FBG- Fabry-Perots were coiled on various materials such as aluminium disks and Polyphenylene sulphide (PPS) and were tested.

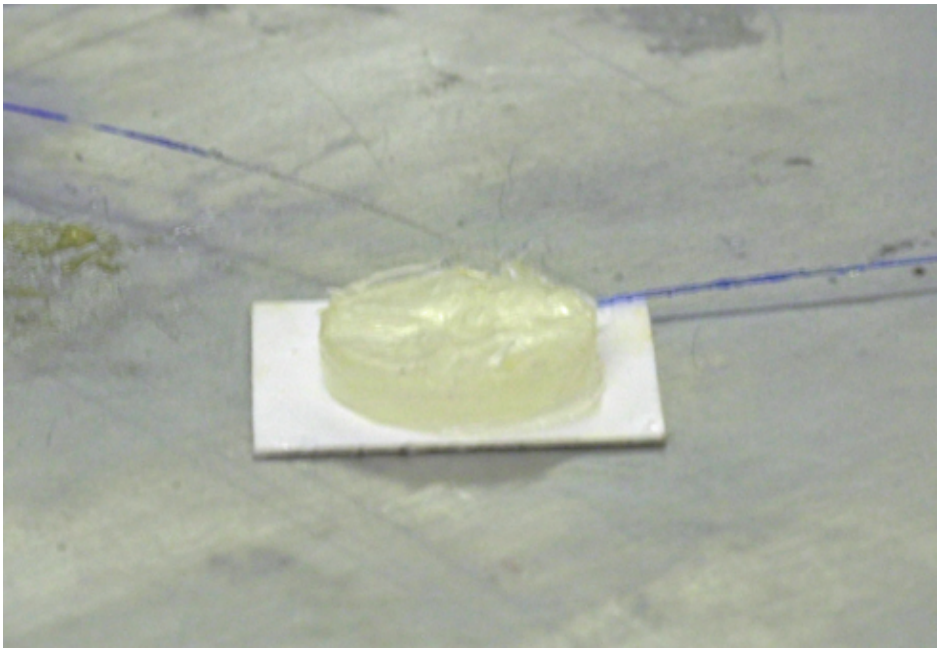

Figure 5.16 Long cavity FBG Fabry-Perot Cylindrical Sensor Courtesy: Dr. Ian Read

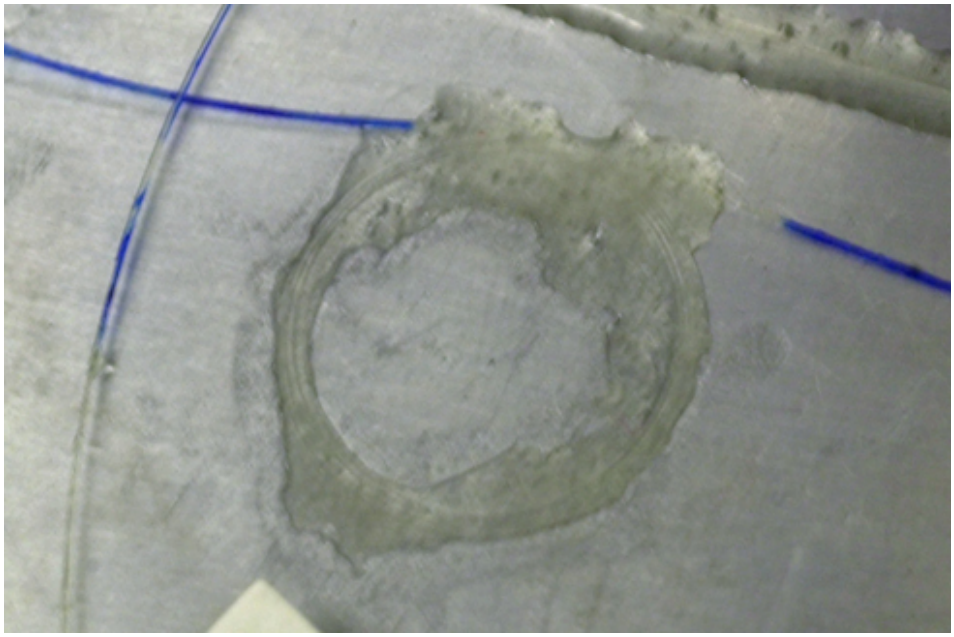

Figure 5.17 Long cavity FBG Fabry-Perot flat spiral Sensor Courtesy: Dr. Ian Read

Apart from that BAE (courtesy: Dr. Ian Read) has designed cylindrical sensors and spiral sensor out of long Fabry-Perot cavity that are shown in figure 5.16 and 5.17.

5.4.3 Airbus Tests

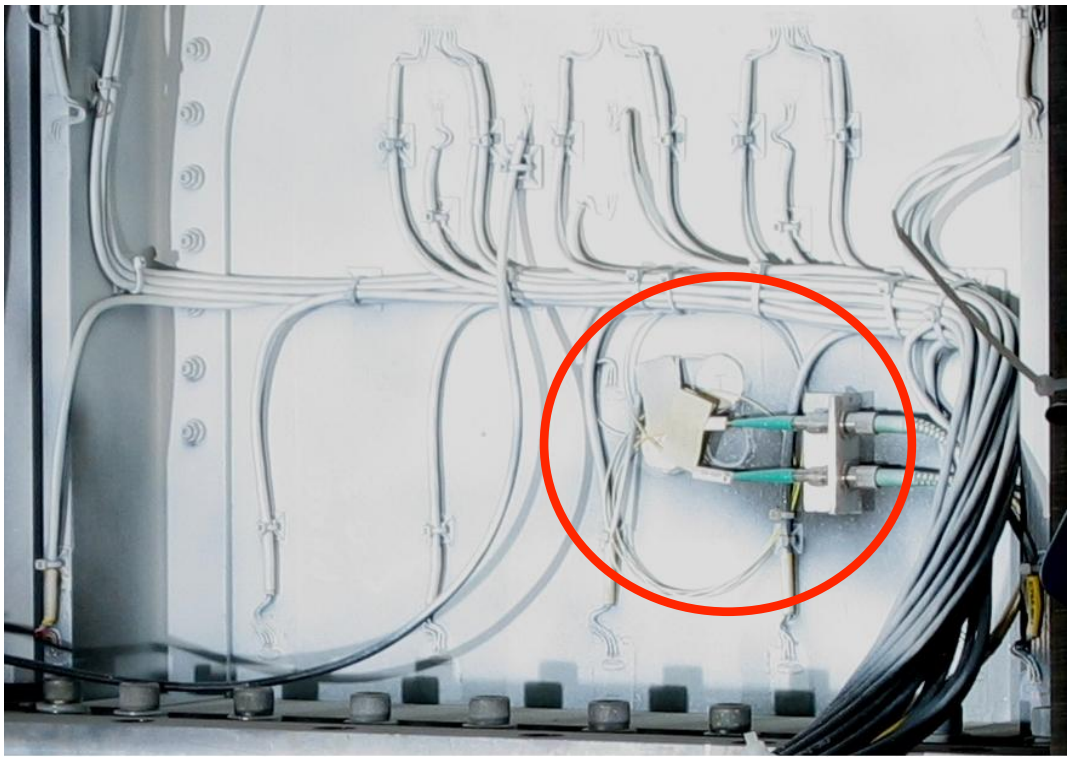

Figure 5.18 Testing at Airbus with the Fabry-Perot sensor mounted on the test rig

The feedback system was tested at the Airbus premises. The system comprised of feedback circuit and optical system. The coiled sensor was mounted on the test coupon. The sensor used in the test is a long 50 cm Fabry-Perot cavity that was made with Draka fibre which allows the sensor to be deployed in coiled form with smaller diameter as it has very low bending loss and offer high responsivity and good spatial resolution can be achieved using it. Optical disks are more susceptible to perturbation and can pick both longitudinal and transverse emission signals. Figure 5.18 shows the sensor mounted on specimen under test.

The optical coiled disk is firmly bonded to the test plate using superglue®. The sensors currently used at Airbus are Resonant Sensors manufactured by Ultra Electronics. It is already discussed in Chapter 2.

The below figure 5.19 shows the RS sensors mounted on the specimen. The complexity in placement of sensors can be clearly seen, however, if optical fibre based sensors are used they can be embedded into the structure thus getting rid of the complex and expensive infrastructure.

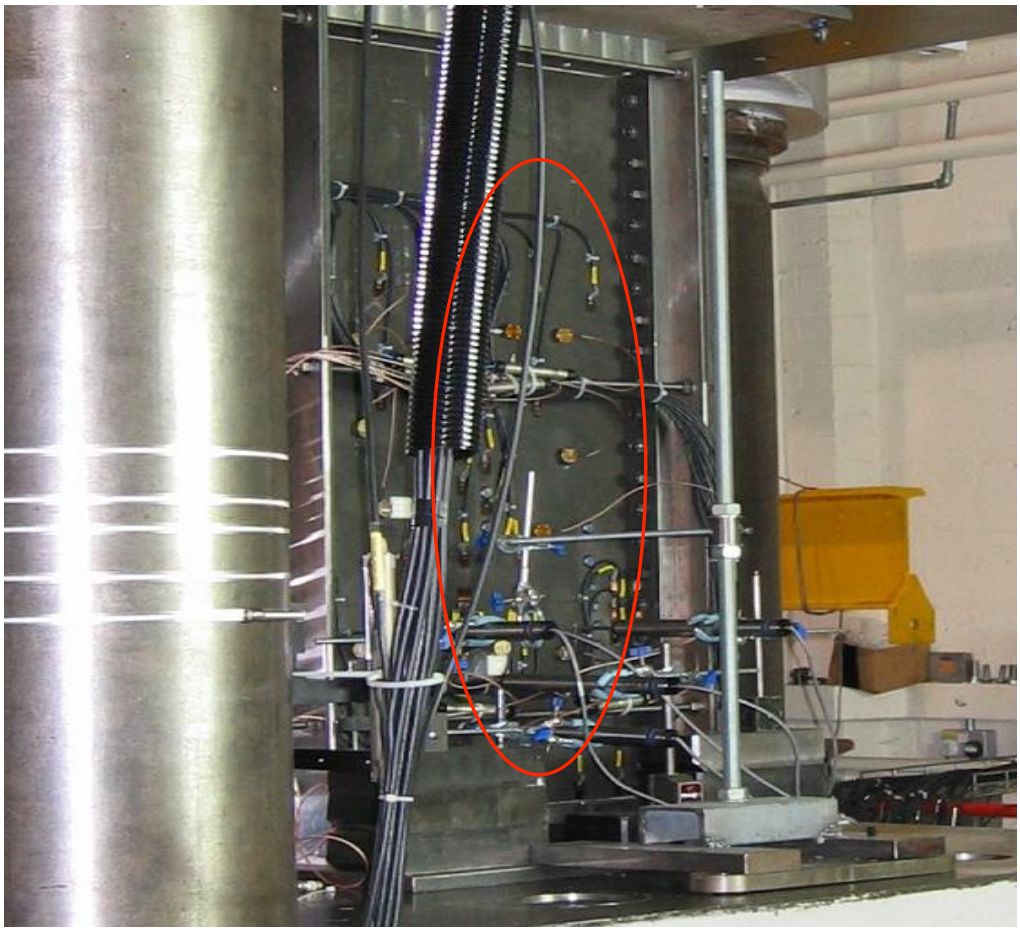

Figure 5.19 Airbus Rig mounted with resonant sensors for compression to failure tests.

Figure 5.20 shows the demonstrator that was used in Airbus test. This was one of the final tests to demonstrate the technologies that were developed within CONSTRUCT project.

Airbus selected a series of composite stringer run-out components to test

the detection while the structure was subjected to destruction.

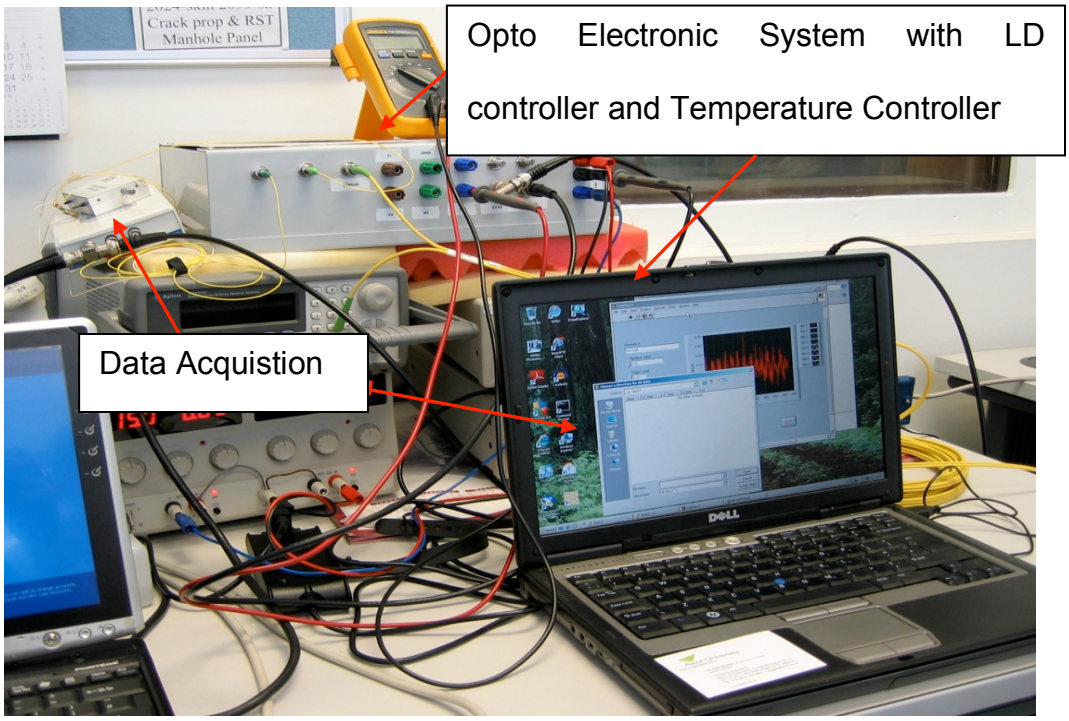

Figure 5.20 Demonstrator at Airbus Tests

Figure 5.21 shows some typical acoustic emission events captured by the demonstrator during the test. More than 50 events were captured and they had good signal to noise ratio and more events were captured but showed presence of large background noise. The number of captured events was limited by the threshold value set by the data acquisition software.

The testing started with application of strain to the structure and it took place in different stages. The number of events recorded until the specimen was loaded to first crack, were very less. Once this threshold had been reach many events were captured.

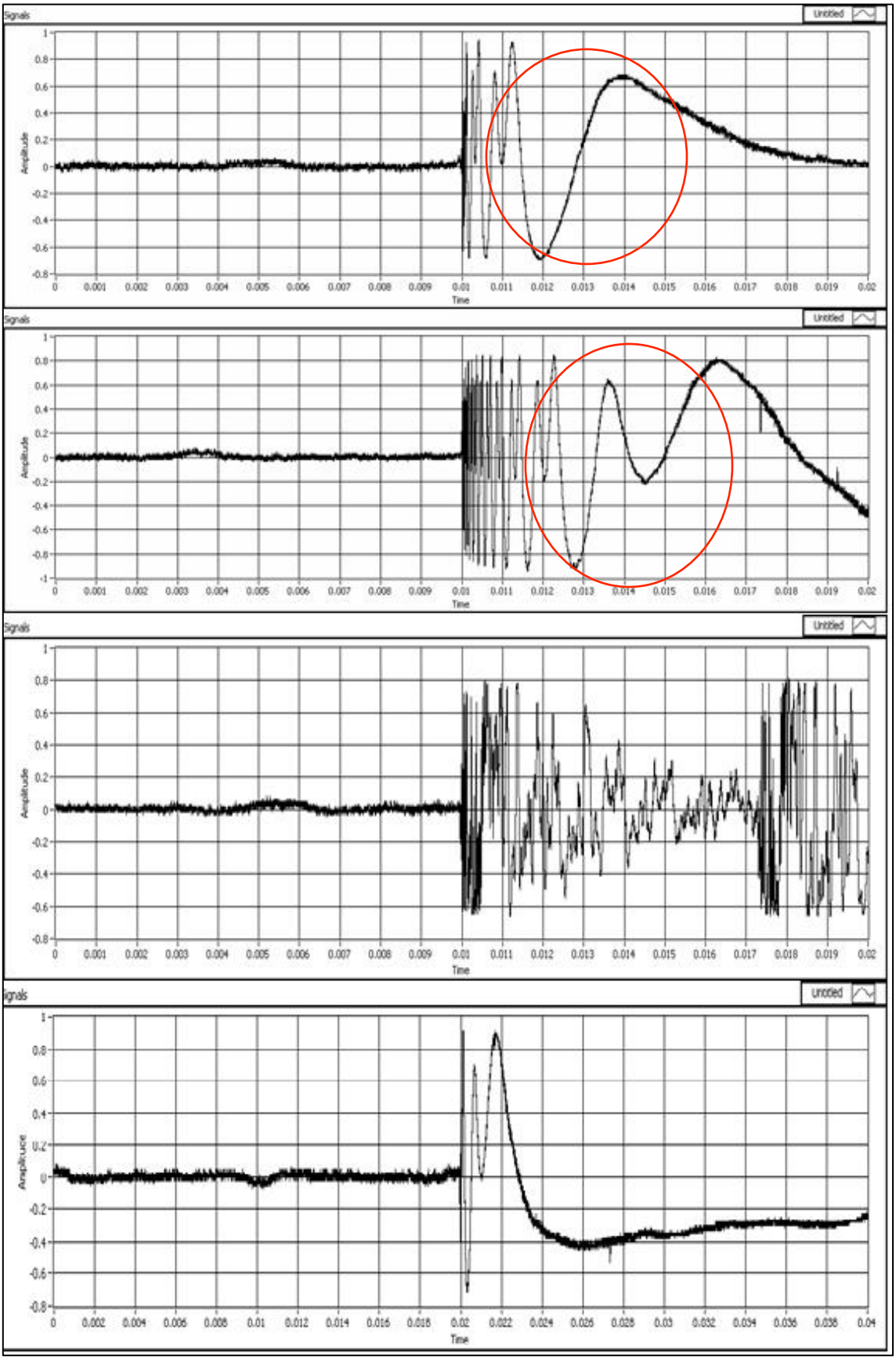

Figure 5.21 Acoustic emission events captured by demonstrator

The first three events in the figure 5.21 show the release of high energy and last the event shows release of moderate energy. In the first two events it can be seen that the acoustic event envelope is different from a normal acoustic envelope. The reason being the system, while the structure was continuously loaded was near to saturation and the LD current was manually adjusted to bring the system to normal operation condition. The system when locked manually again was ready to capture the acoustic events. This was a drawback in the system as it was almost in saturation region with any large event with high energy release taking place.

To overcome this, the system was redesigned and a reset circuit as discussed in the beginning of the chapter was added to the system that enabled the system to work with optimum performance under severe loading conditions. However the sensor still requires a limited loading condition where loading caused wavelength change should be within ±2nm. If a sudden change whacks the sensor out of this range the tracking will be unable to cope. Although, we were unable to test the new demonstrator in the live environment but it was tested in the lab. The results are discussed in further sections.

Figure 5.22 shows some typical acoustic emission events capture by the BAE system for the same sensors. Their system was free running and the laser used had a very narrow linewidth. The first acoustic event trace in the above figure shows an event with moderate energy. The bottom trace shows a double event which has higher energy.

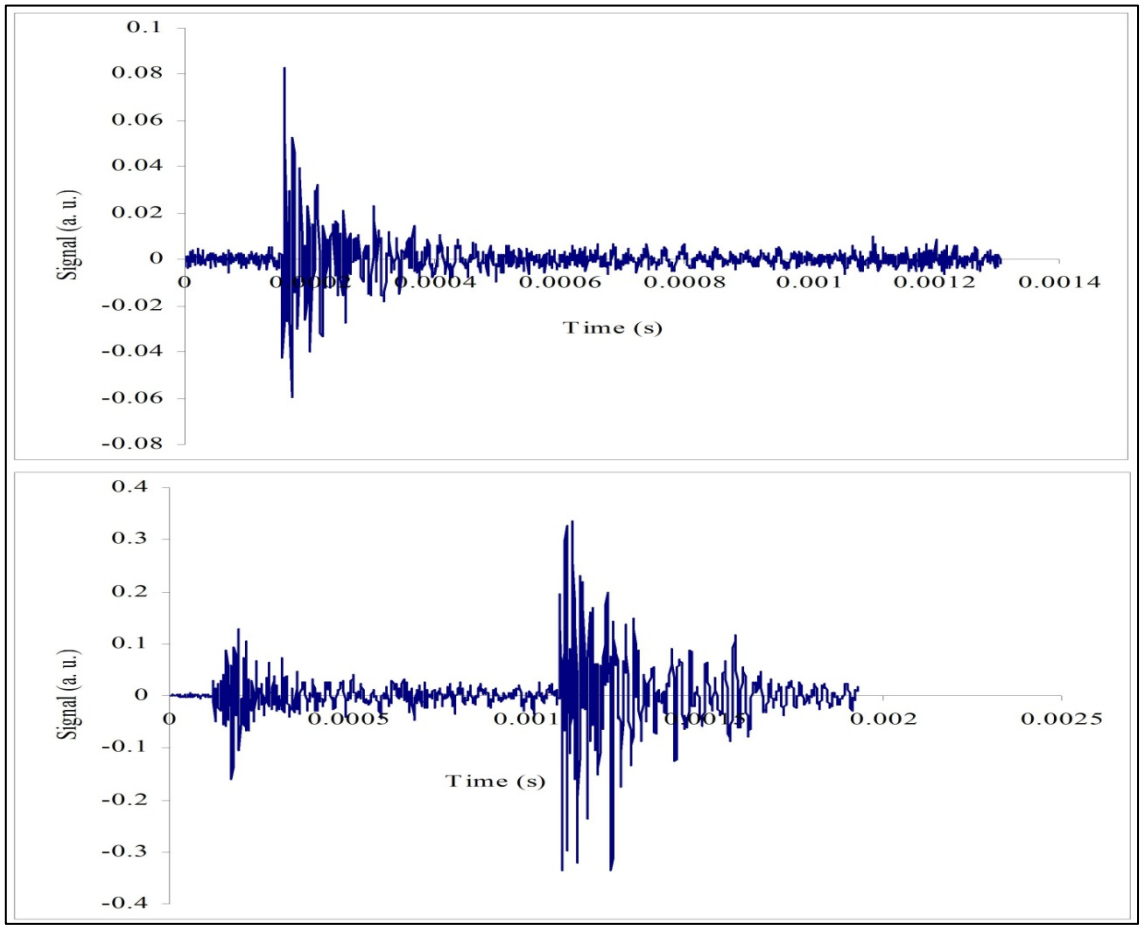

Figure 5.22 Acoustic emission events captured by BAE Systems

Courtesy: Dr. Ian Read, BAE systems

5.4.4 Comparison of sensors at BAE

Acoustic emission tests were carried jointly at BAE along with Dr. Ian Read to test the performance of coiled disk sensors with both BAE system and feedback system developed at Aston. The 30cm FBG Fabry-Perot was used as test sensor and was firmly bonded to the metal plate under test using epoxy. The aim of the test was to analyse the performance of coiled sensor in comparison with the WDI sensor and the straight sensor. The test comprised of Burst signal testing which was generated using an actuator and pencil break test. The amplitude of burst signal was < ~ 500mV. The idea was to monitor the response of the sensor at low amplitude bursts which will make it easier to comment on the sensitivity of the sensor.

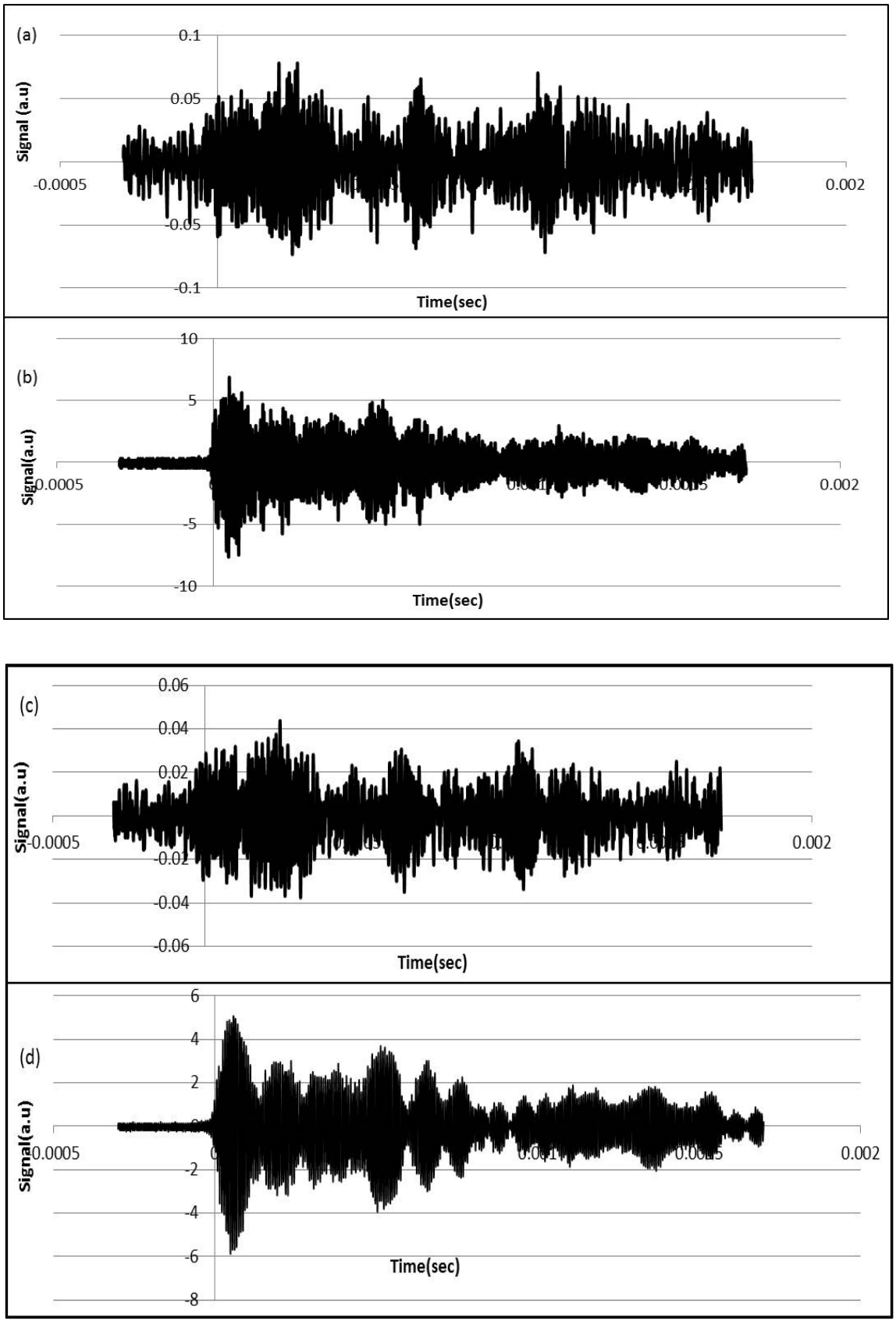

Figure 5.23 Responses from (a) Interrogation system locked (b) WDI when system is locked (c) Interrogation system free running (d) WDI when system is free running

It was also important to analyse the performance of the feedback system and comparing it's functionality with BAE's system and to choose the best sensing technique. The other aim of the tests was to monitor the performance of long cavity coiled sensors with the interrogation systems, which were found to be more sensitive than the short cavity sensors. Long cavity sensors can be easily coiled and are sensitive to the transverse as well as longitudinal waves whereas the straight Fabry-Perot sensors are more sensitive to the longitudinal emissions. BAE's interrogation system is free running and has a narrow Linewidth tunable laser and sensor. All the results at BAE are compared with the standard WDI sensor. The first test was to monitor performance of coiled sensor when the system is locked to its optimum operational point. It may be seen from figure 5.23 (a) & 5.23(c) that the response from the long cavity sensor that was connected to our interrogation system was very noisy. The SNR was very low. The SNR of WDI was good for the burst signal when laser was locked and when it was free running as shown in 5.23 (b) & 5.23(d). There can be several reasons behind this one being the Linewidth of the laser diode which is in range of 5 – 20 MHz, the electronics of the feedback circuit or the wrong selection of operation point.

To check whether it is an issue of electronics or the laser diode the system was set as free running but still the presence of noise was there which was reducing the SNR. It was evident from this test that coherence might be an issue as BAE's system yielded good SNR response and can be seen in figure 5.24 (c). It was from a pencil break test. Figure 5.24(a) and 5.24(b) show the burst signal response of the sensor when laser diode was connected to the BAE detector. The SNR seems to be improved but still the WDI response remained better. The duration of burst signals in all the tests was same.

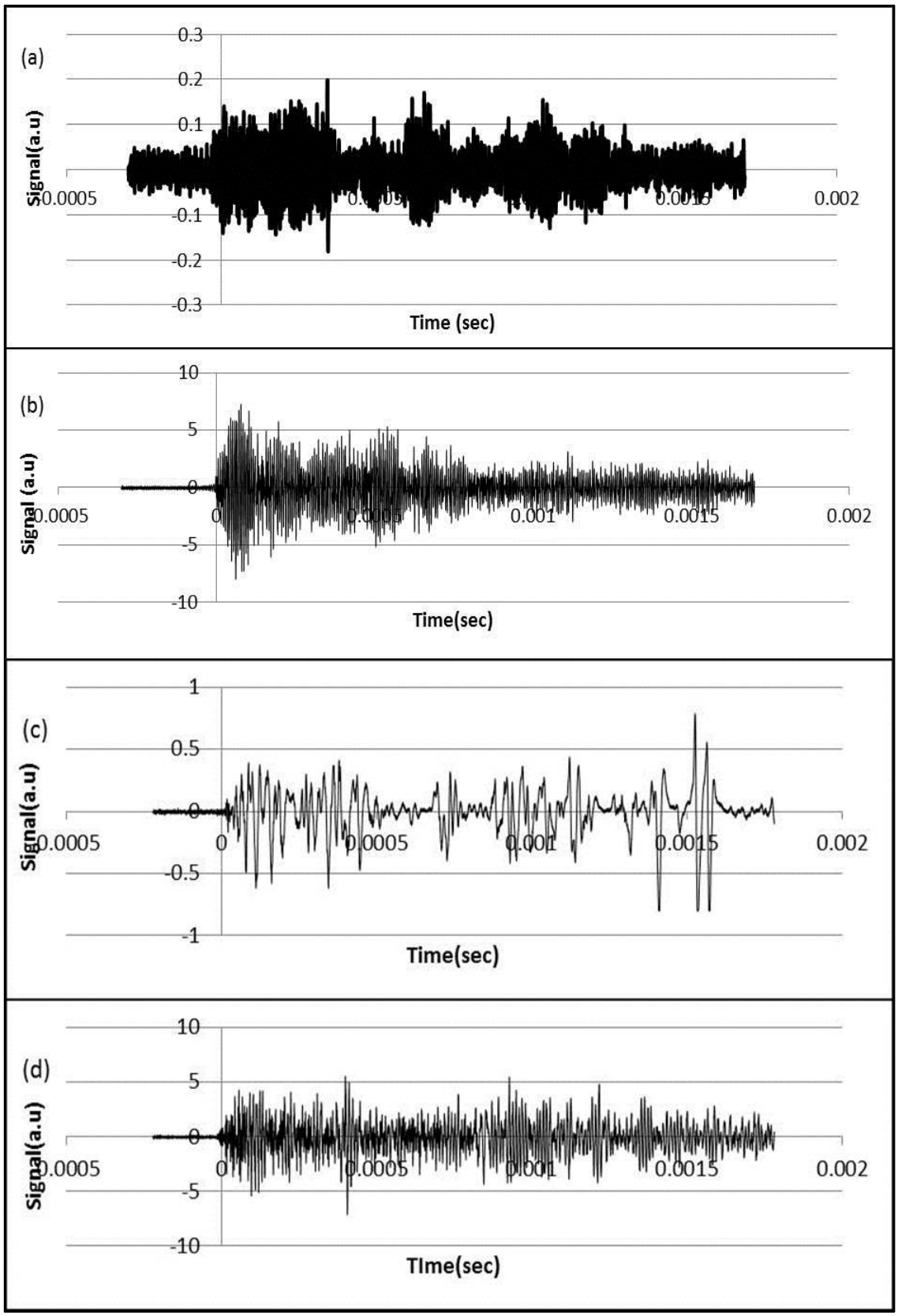

Figure 5.24 Response from (a) LD laser with BAE detector (b) WDI with BAE detector (c) Pencil break with BAE laser (d) Pencil Break with WDI sensor

It would have been an excellent move to test the BAE laser with Aston's interrogation system for comparison results of both the lasing sources, but since it doesn't had an external modulation input our system was incompatible with it.

5.4.5 Tests at Lab with different sensors and discussions

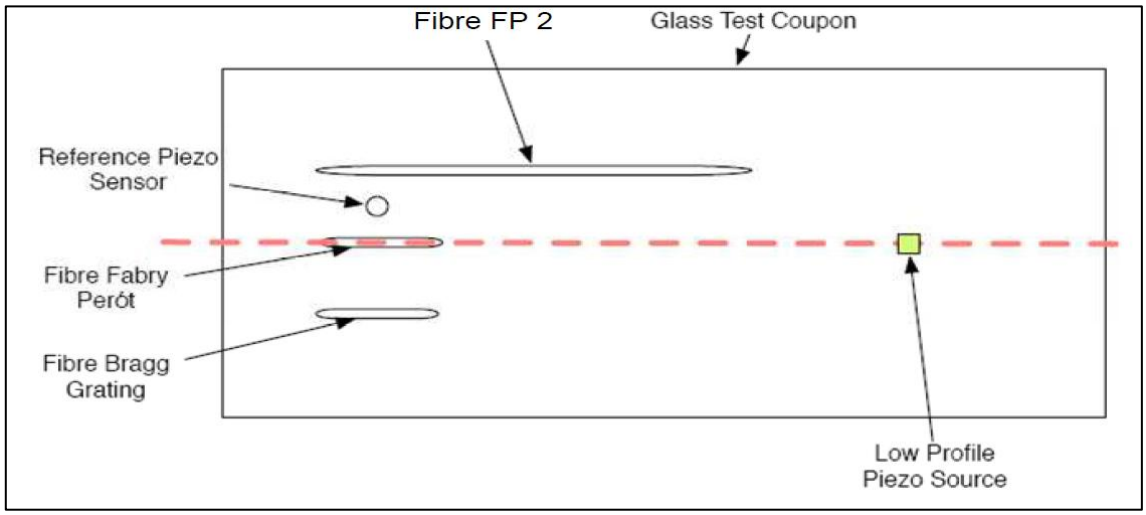

Figure 5.25 Arrangement of sensors and actuators on the glass test coupon

Figure 5.25 above shows the sensor arrangement in the lab. The sensors are mounted on a glass mirror plate. A low profile Dura Act ® piezo source is mounted on the glass test coupon. The sensors for the test were glued on the glass test coupon as shown in the above diagram. To characterise the interrogation unit, Fabry-Perot sensors with different cavity lengths were tested. The interrogation system is compatible with mostly all the Fabry-Perot sensors of different cavity lengths. Fabry-Perot cavities fabricated with different lengths (14mm, 15mm, 15.5mm, 25mm, 20cm, 30cm, 50cm and 100cm etc.) were used in the experiment. However, the sensitivity of the Fabry-Perot depends upon the cavity length, shape, placement and effect of noise sources. Most of the results were compared with WDI sensor and RS sensor. Figure 5.26 compares all the three sensors over a frequency range of 0-600kHz. The response of WDI and RS sensor are similar and the SNR is also large. However, it can be very well

noticed that the frequency response profile of the three sensors closely match. The signal level of other two devices is very good and that is one noticeable limitation of the FBG Fabry-Perot based feedback system.

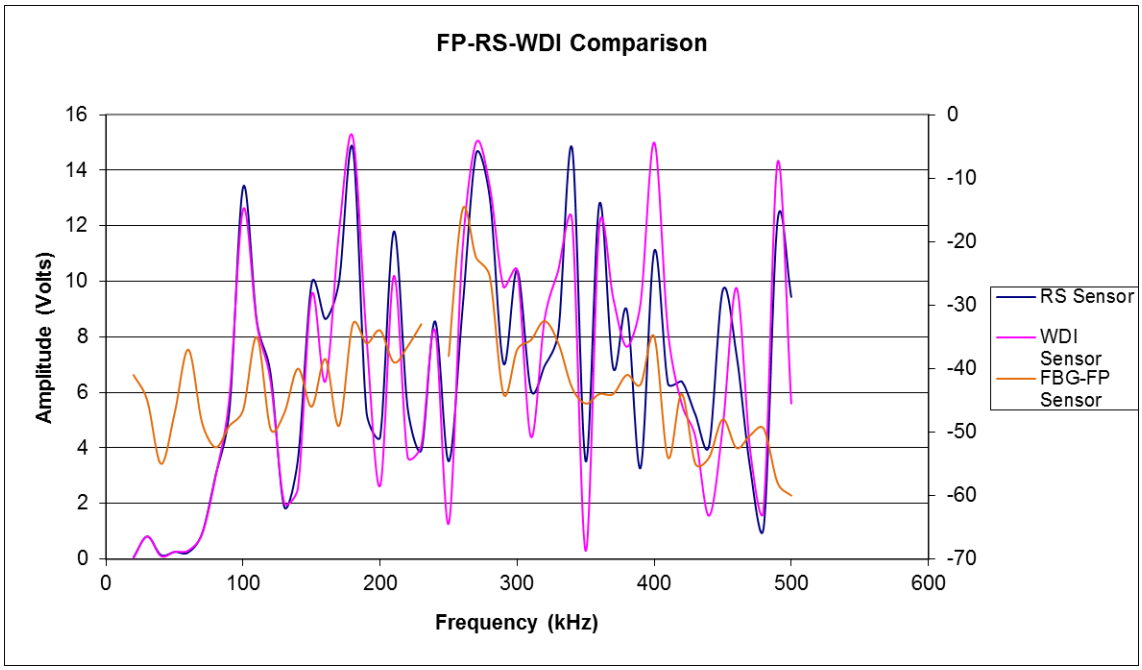

Figure 5.26 Comparison of responses from RS sensor, WDI sensor and FBG Fabry Perot sensor

Figure 5.27 shows typical frequency response of the sensing system to a signal applied to the piezo of 500mVpp signal amplitude. The line shows the characteristic response of the sensor for various frequency measurements. The frequency response is very peaky due to the influence of the plate to which the transducer and sensors are bonded. The frequency range that can be detected using the tracking system is up to 600 kHz. It is limited to 600 kHz because of Band Pass filter that has upper cut-off frequency of 600 kHz. Also, tests were carried out to test whether the reset mechanism locks the wavelength once the system is out of tracking range. To test the functionality of the reset mechanism a pressure was applied on the glass plate to introduce a perturbation large enough to cause the laser to exceed its tracking range. When the pressure is removed the system resets itself to lock to optimum wavelength. It is the quick

and simple way to test whether the reset mechanism can withstand sudden perturbations.

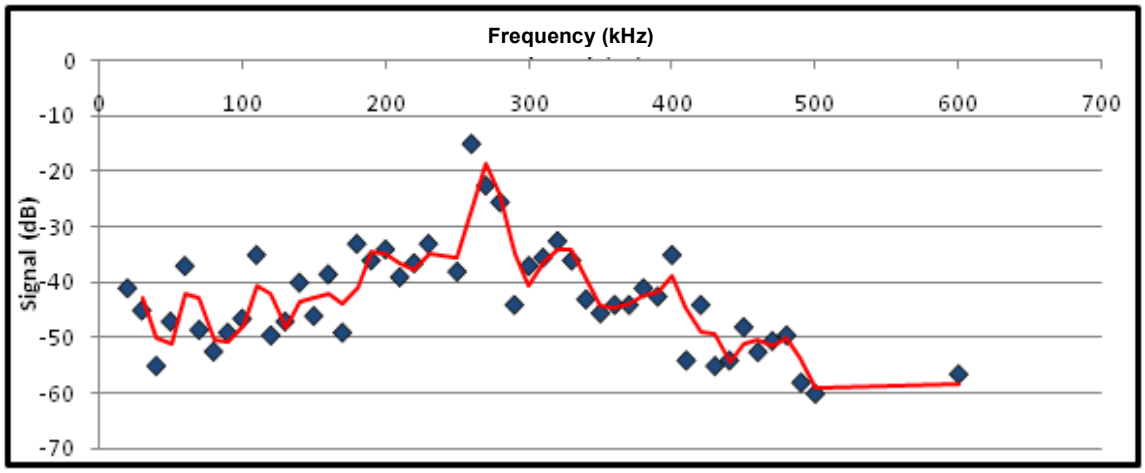

Figure 5.27 Typical Characteristic curve of the optical sensor (14mm Fabry-Perot)

The following figure 5.28 shows continuous signal response for a straight 14mm Fabry-Perot sensor which is connected to the interrogation system that uses a DFB laser and free running system with HP laser. The SNR of the sensor connected to the interrogation system was close to 60dB and the one to free running tunable laser was 45dB. Although, the noise level in the response from free running tunable laser system was very low. Even the burst signal response from the DFB laser system was having a better SNR. The initial burst response is denser than the free running laser response i.e. 14mm Fabry-Perot with DFB laser system with is more sensitive than the free running system as it is providing a better SNR data during the initialization of burst signal (say the developing of crack). Normally in burst signals the first part of the signal generally contains no signal and the end part of the signal will contain reflections, we shall consider a portion of the signal following the leading edge.

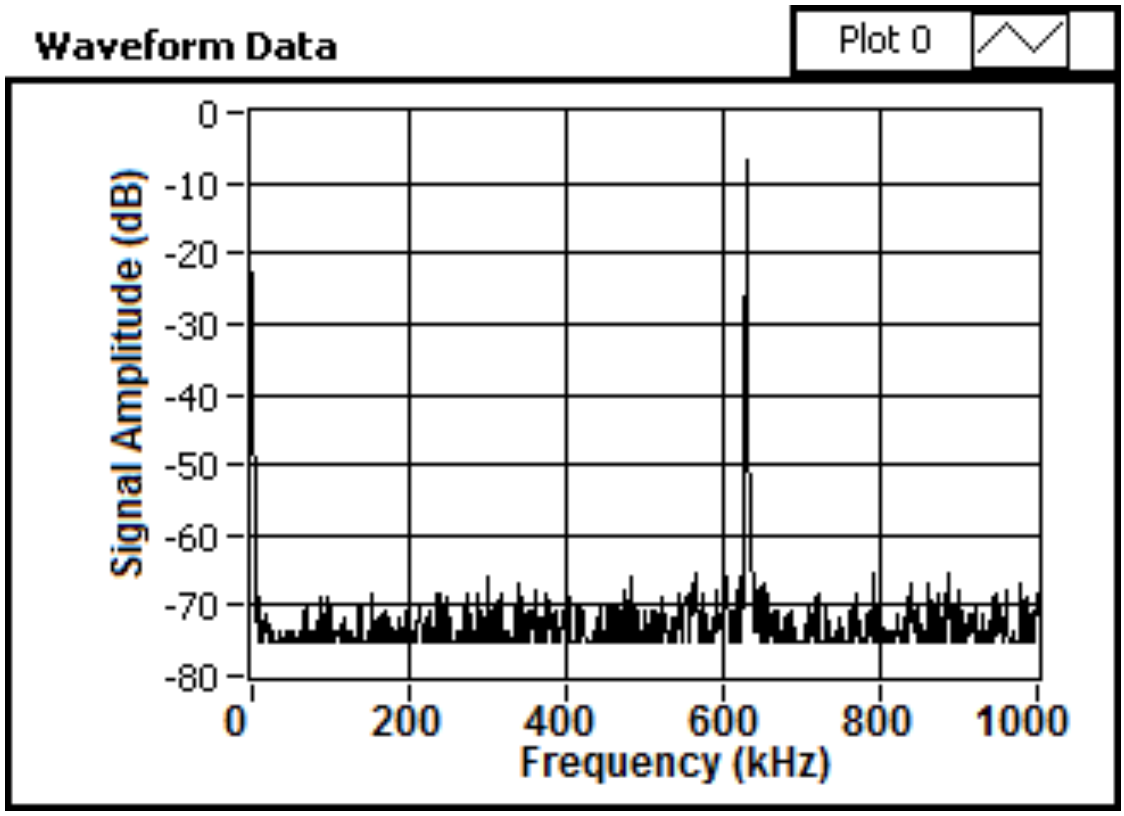
Waveform Data
Plot 0
Signal Amplitude (dB)
0
-10
-20
-30
-40
-50
-60
-70
-80
0
200
400
600
800
1000
Frequency (kHz)

5.28(a)

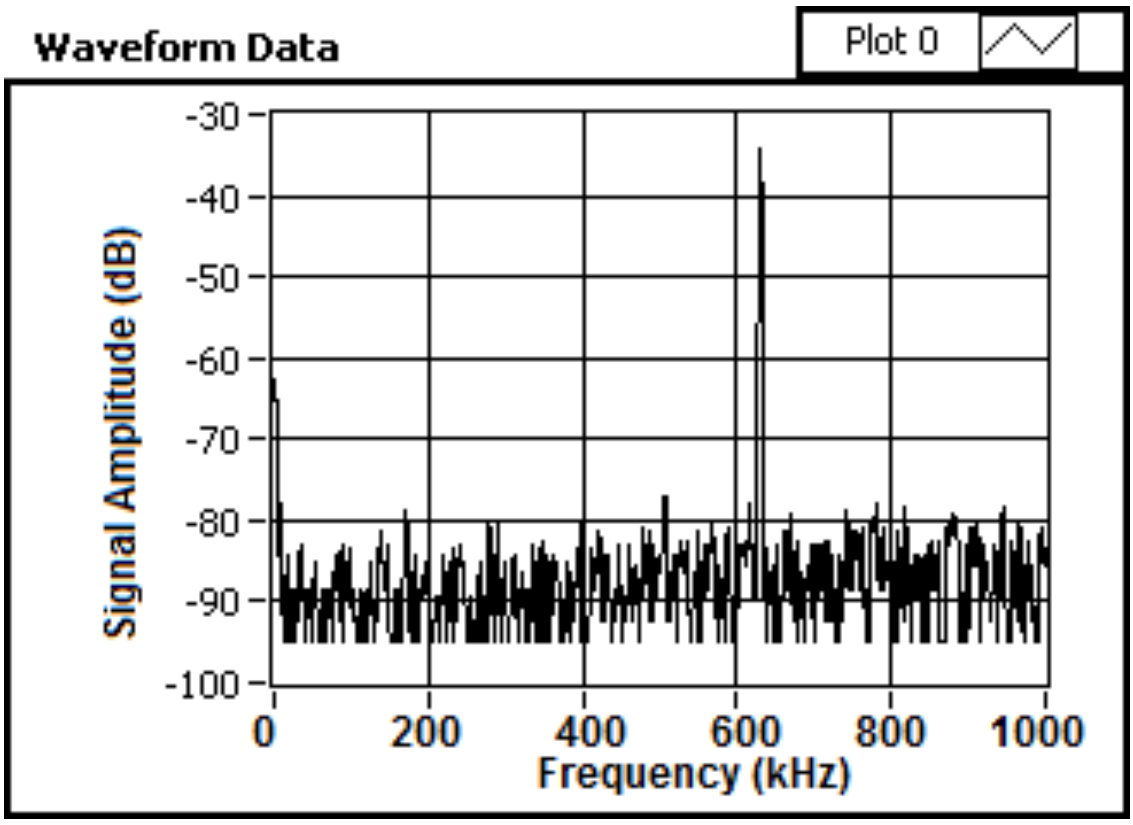
Waveform Data
Plot 0
Signal Amplitude (dB)
-30
-40
-50
-60
-70
-80
-90
-100
0
200
400
600
800
1000
Frequency (kHz)

5.28(b)

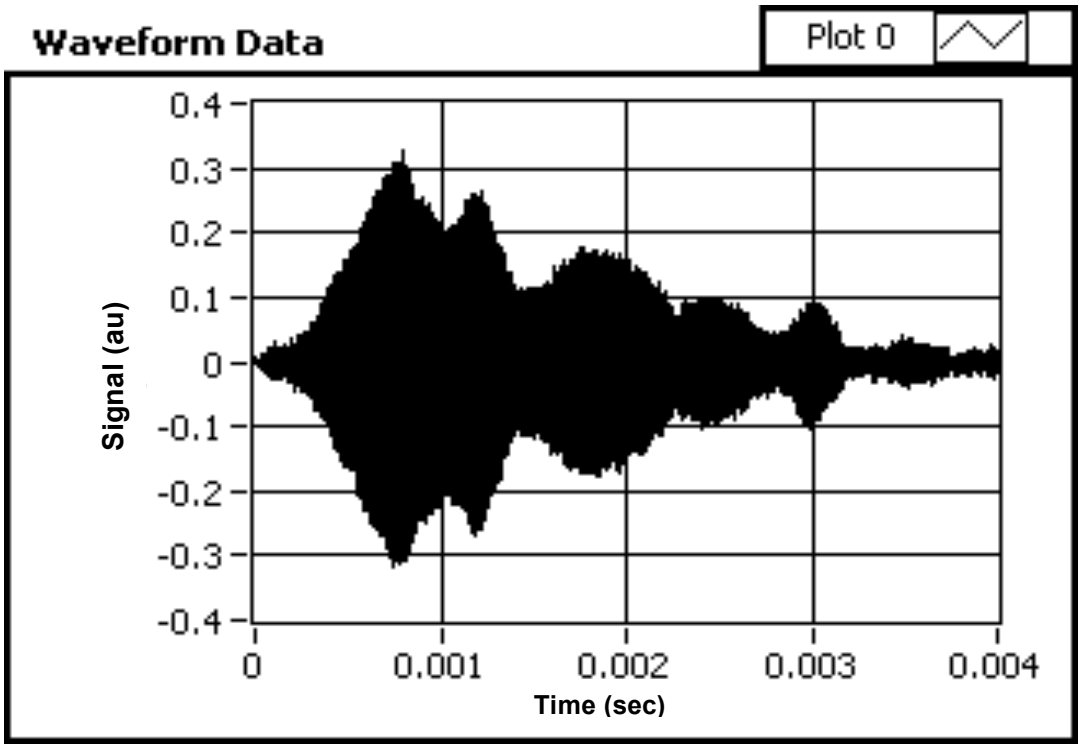

5.28(c)

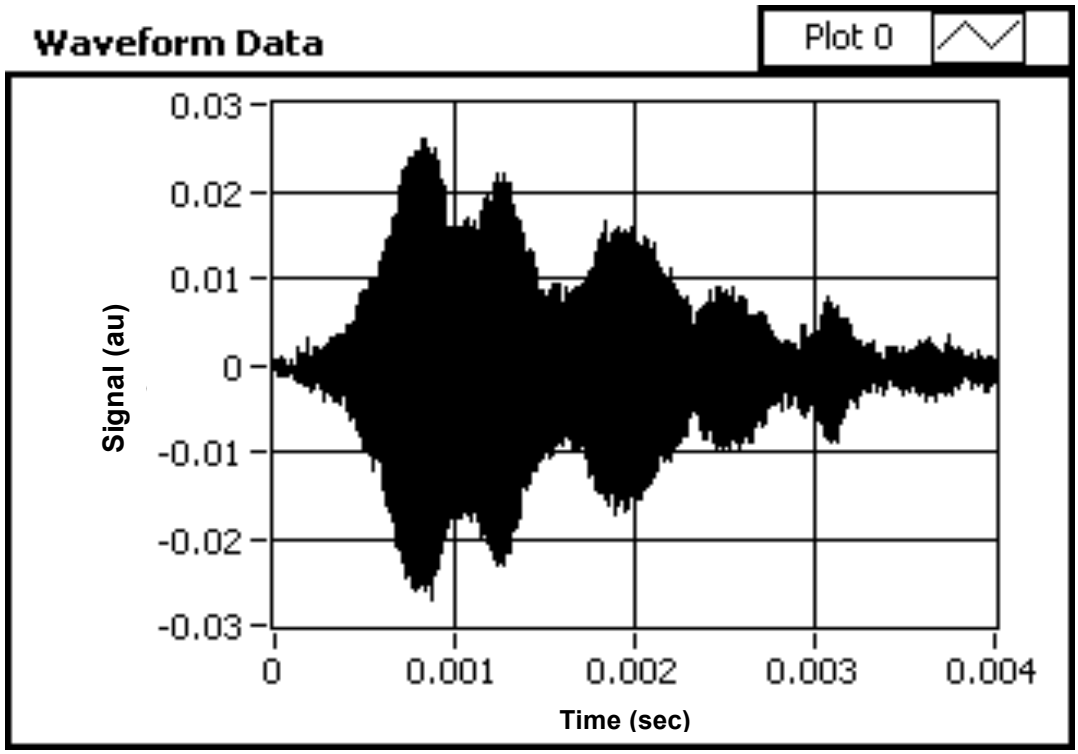

5.28(d)

Figure 5.28 Response of a 14mm FBG Fabry-Perot (a) Continuous wave response when Fabry-Perot is connected to LD system (b) Continuous wave response from a free running laser system (c) Burst signal response for Fabry-Perot connected to LD system (d) Burst signal response from the free running laser system

Figure 5.29 below shows the response of the Fabry-Perot sensor connected to the interrogation system when a signal with amplitude of 500mV was applied to the buzzer. The SNR improves (close to ~25dB) when the signal is passed through a high pass filter.

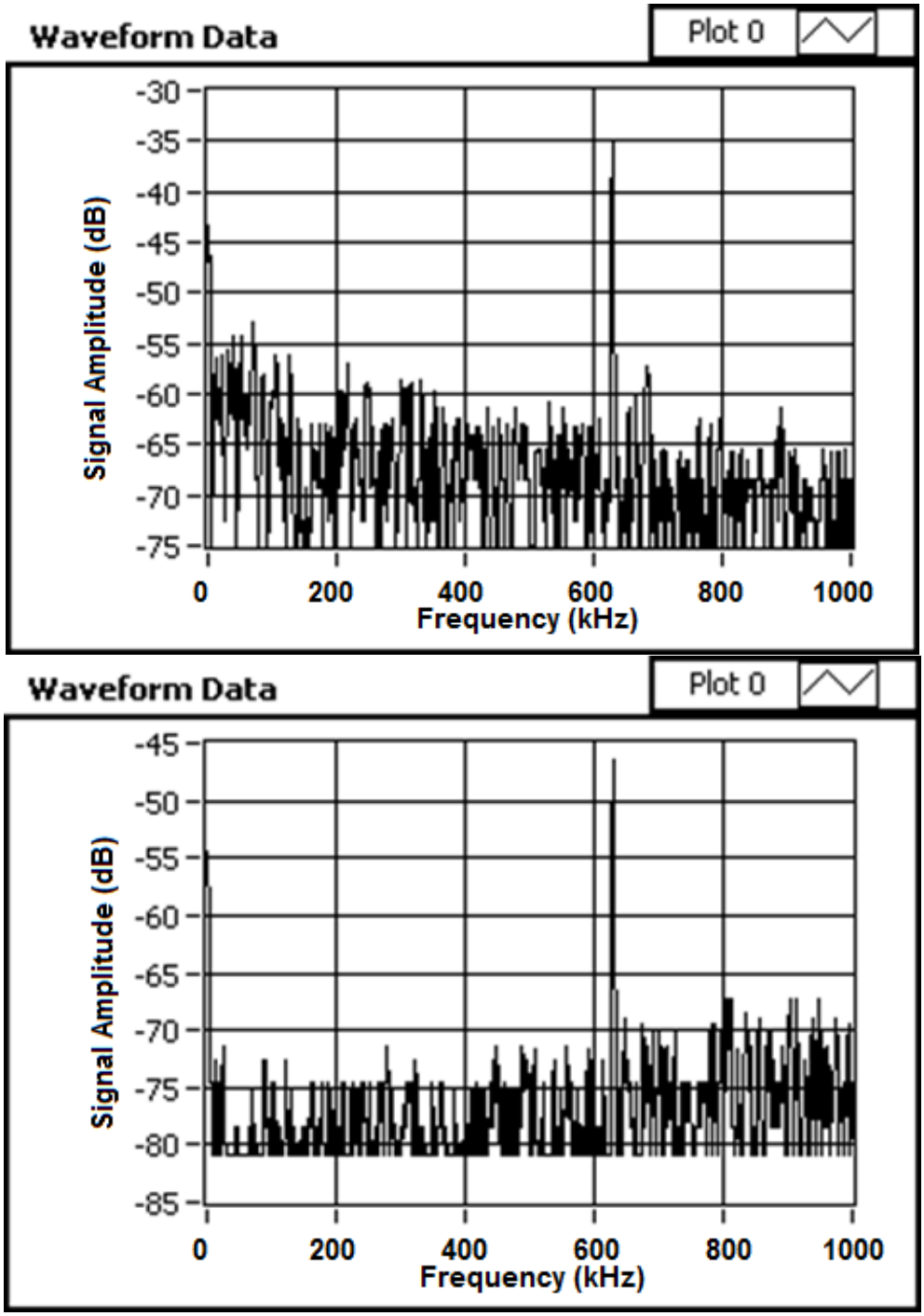

Figure 5.29 (a) Continuous wave response when signal amplitude was 500mV from the LD system (b) Continuous wave response with signal amplitude 500mV from the free running system

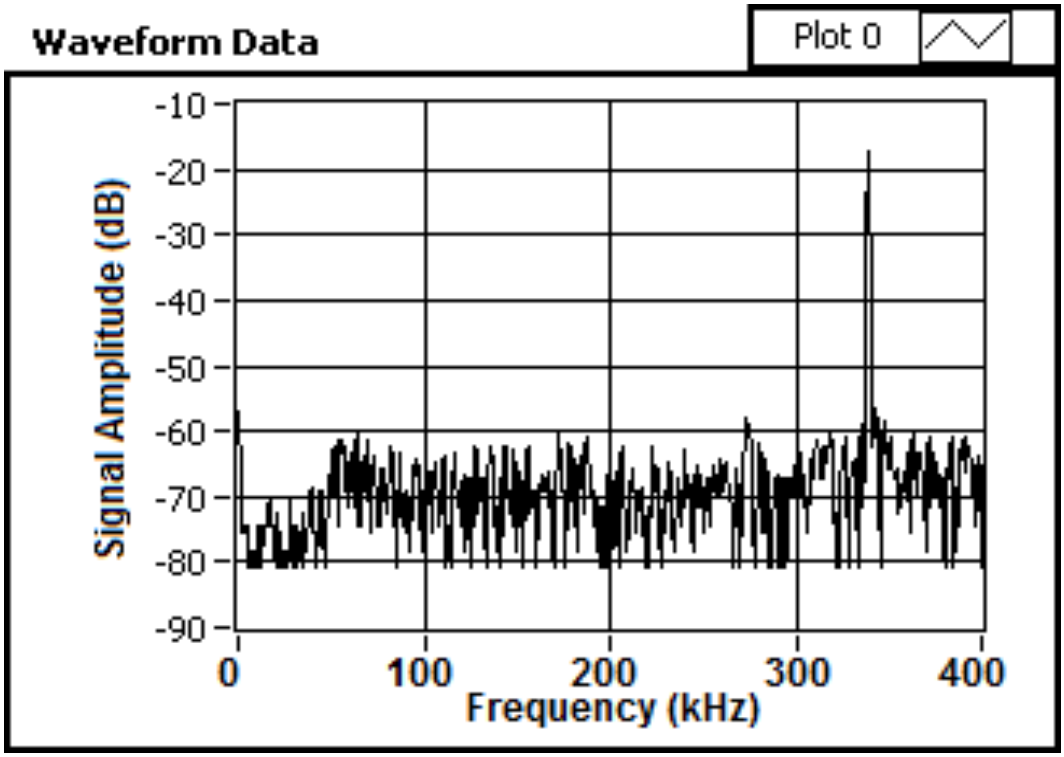
Waveform Data
Plot 0
Signal Amplitude (dB)
-10
-20
-30
-40
-50
-60
-70
-80
-90
0
100
200
300
400
Frequency (kHz)

5.30(a)

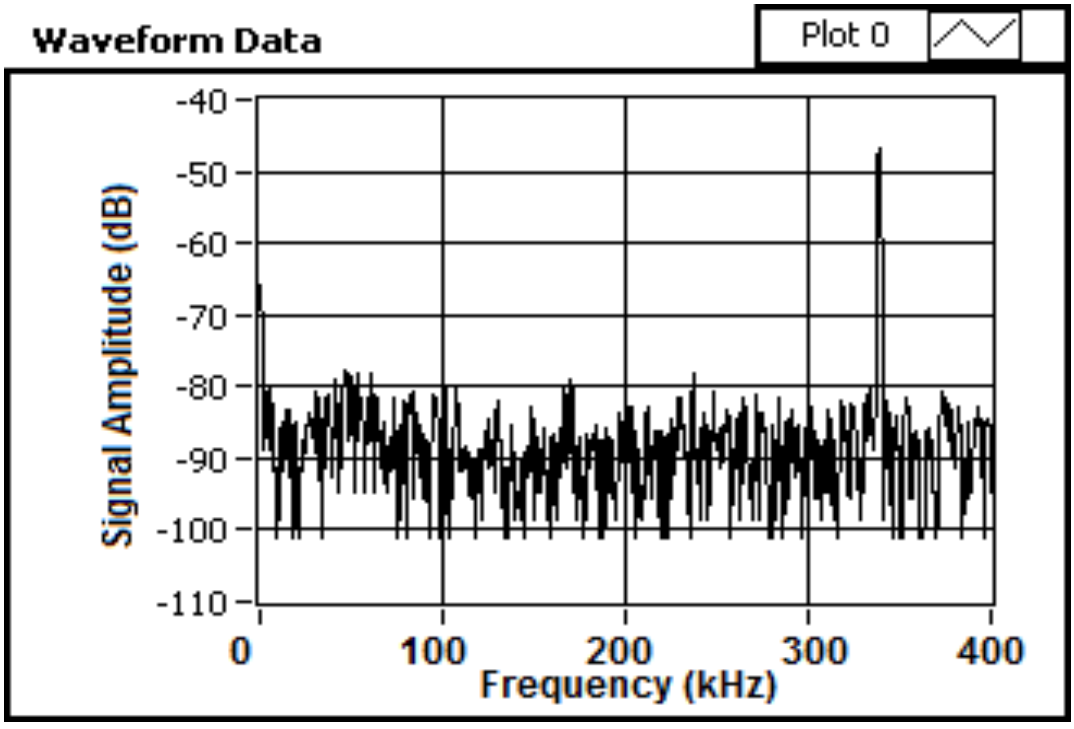
Waveform Data
Plot 0
Signal Amplitude (dB)
-40
-50
-60
-70
-80
-90
-100
-110
0
100
200
300
400
Frequency (kHz)

5.30(b)

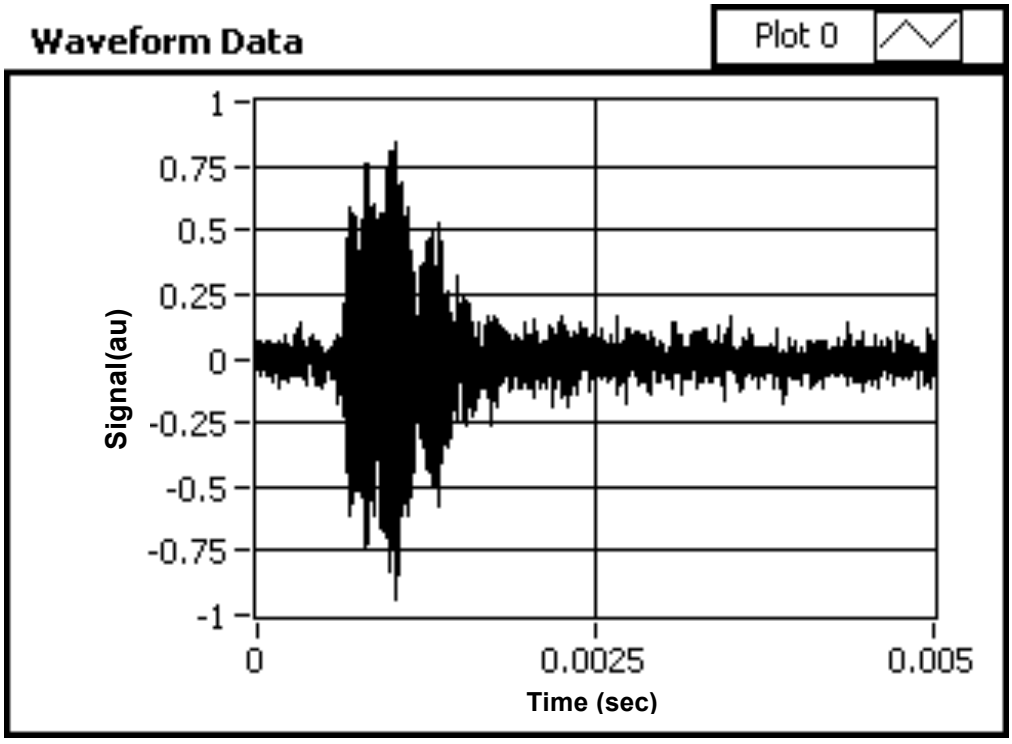

5.30 (c)

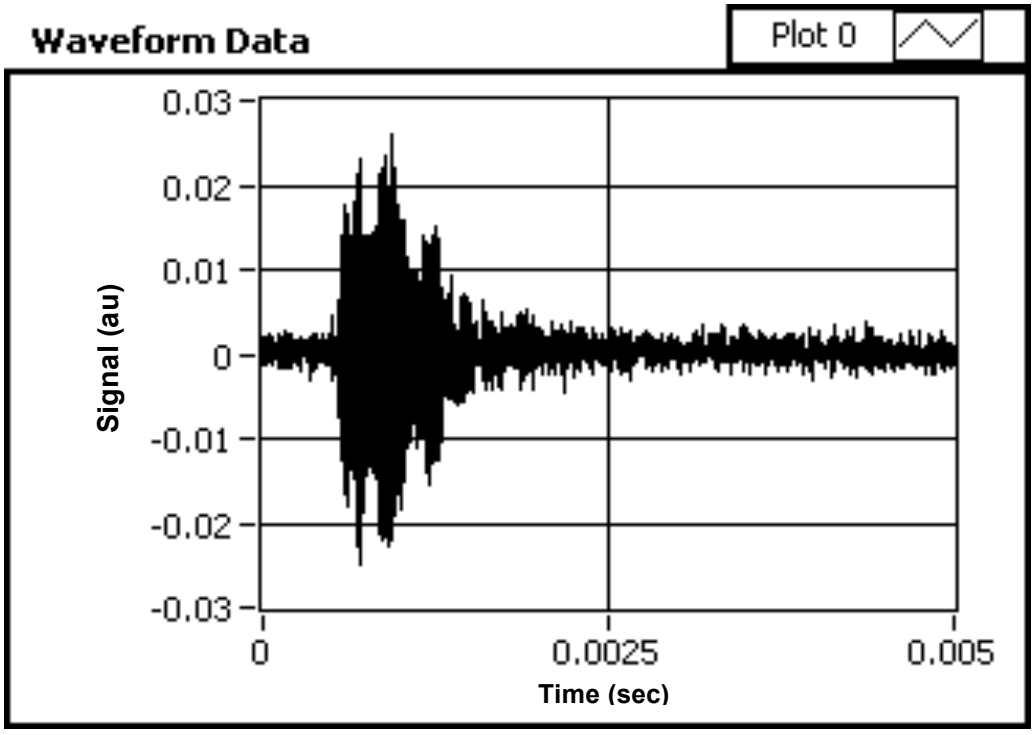

5.30 (d)

Figure 5.30 Response of a 25mm FBG Fabry-Perot (a) Continuous wave response when Fabry-Perot is connected to LD system (b) Continuous wave response from a free running laser system (c) Burst signal response for Fabry-Perot connected to LD system (d) Burst signal response from the free running laser system

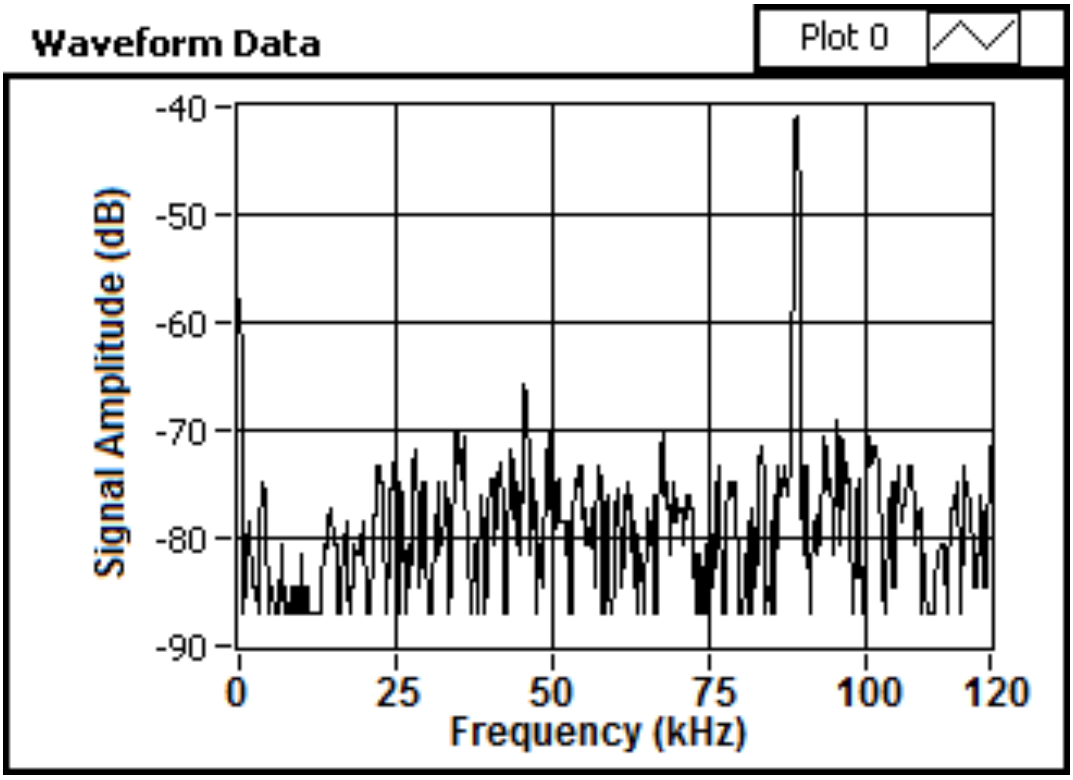

Figure 5.31 Continuous wave response when signal amplitude was 500mV from the LD system for a 25mm Fabry-Perot cavity

Figure 5.31 shows the continuous wave response of a 25 mm cavity. It is almost similar to a 14mm sensor. However, continuous wave response just shows the frequency of acoustic waves but burst signal actually provides more information about the damage and is close to real time scenario. Continuous wave response helps to estimate the performance of sensor at various frequencies and project the frequency response and the SNR of the sensor.

From Figure 5.8 $\Delta\lambda/\Delta I$ can be calculated and is equal to 0.00644444 nm/mA and $\Delta I/\Delta V$ is equal to 20mA/V (from the LD driver datasheet).

The sensitivity of the Fabry-Perot's can be determined from these data:

Sensor	Applied V (mV)	Sensor Output(V)	Modulation ΔI/ΔV (mA/V)	Δλ/ΔI (pm/mA)	V/pm
14mm	50	1.20	20	6	0.20
25mm	40	2.08	20	6	0.43
20cm Coiled	20	1.00	20	6	0.42
50cm BAE	10	2.24	20	6	1.87
50cm Patch	20	2.88	20	6	1.20
FBG	60	0.29	20	6	0.04
110cm	10	5.60	20	6	4.67

Table 5.2 Comparison of different sensors for sensitivity

It can be observed that the longest cavity sensor has the highest response and thus can be said to be most sensitive. Dr. Ian Read at BAE systems used a narrow linewidth laser in a free running system alongwith a 50 cm long cavity sensors for acoustic emission detection and found it to be very sensitive. The performance of sensor was good with an excellent signal to noise ratio as shown in figure 5.32.

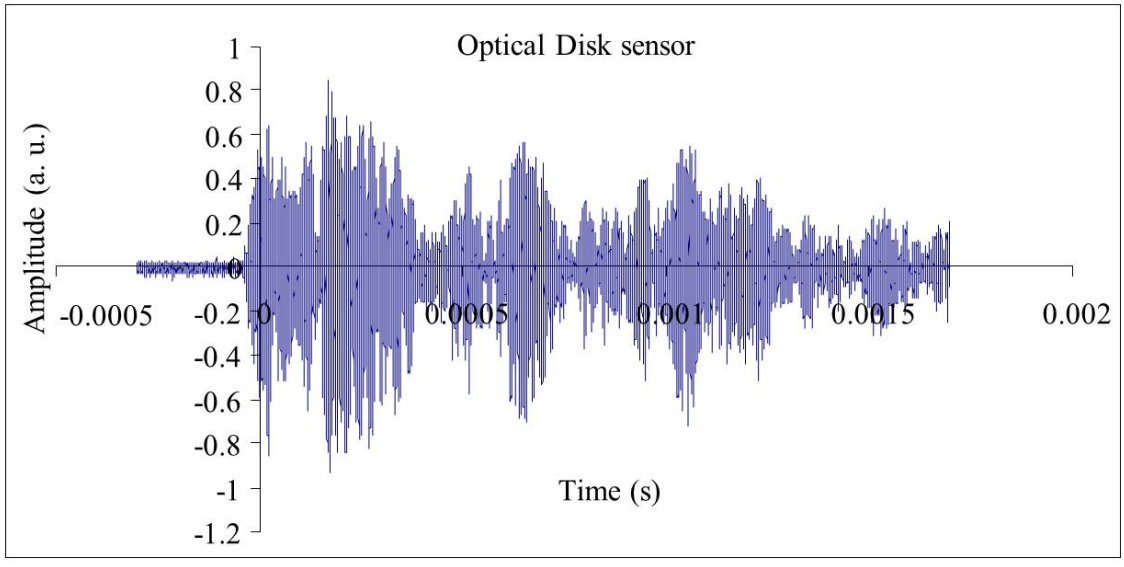

Figure 5.32 Response of an optical disk sensor (50 cm coiled long cavity sensor) Courtesy: Dr. Ian Read, BAE systems

Sensor	SNR
WDI	75dB
Straight Fabry-Perot Sensor	24dB
Cylinder	32dB
Flat Spiral	43dB

Table 5.3 SNR of different FBG Fabry-Perot sensors with WDI

Free running systems may not be suitable for such applications as the laser can miss important large acoustic events. It needs to be tuned to sensitive region of the Fabry-Perot for optimum functionality.

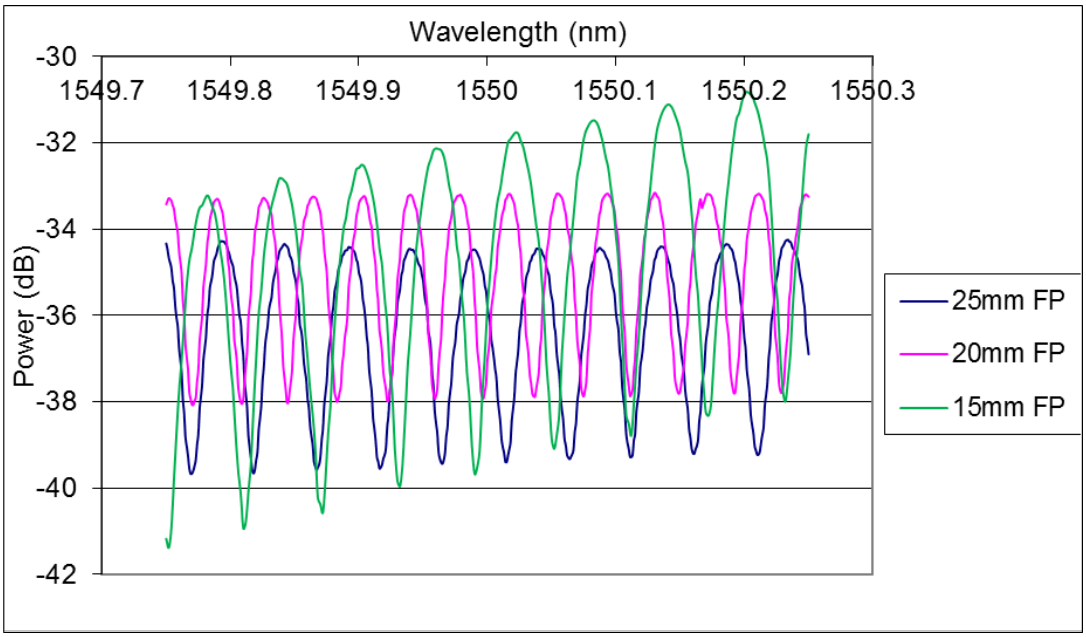

Figure 5.33 (a) FSR of 25 mm FBG Fabry-Perot is 40pm (b) FSR of 20 mm FBG Fabry-Perot is 50pm (c) FSR of 15 mm FBG Fabry-Perot is 60pm

However, with the interrogation system we can see that the best response was for 14mm, 25mm sensor. The signal level is good but the noise level is also very high in this sensor. In summary, from different tests it is evident that identifying a light source with narrow linewidth is very important. The reason

behind this is the coherence of the LD used. It may be seen that from figure 5.33 that as the cavity length increases the FSR of the Fabry-Perot decreases.

As for the long cavity FBG Fabry-Perots the FSR is small and the laser diode's linewidth is very broad, measured to be in range of MHz (both from datasheet of laser and measurements at lab). Narrow wavelength lasers can resolve higher acoustic emission. Linewidth of nearly six different lasers were measured by method proposed by Nguyen et.al. [4] and linewidth of each laser was found to be greater than 20MHz.

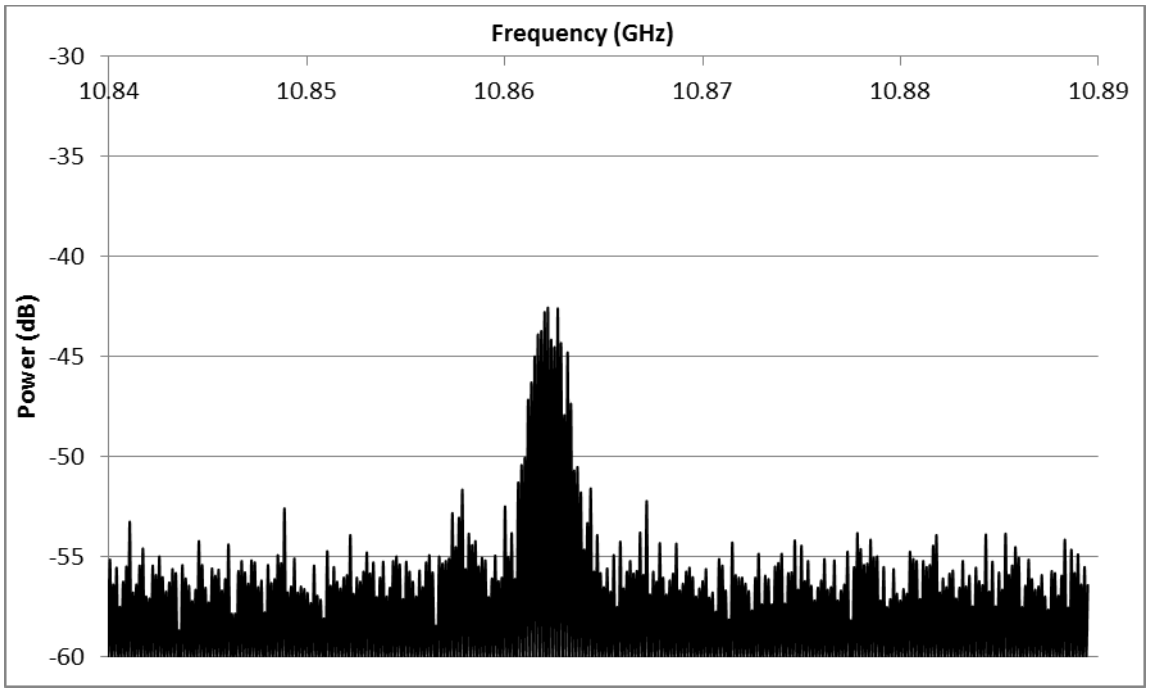

Figure 5.34 Linewidth measurement of the JDS Uniphase LD which is used as light source in the active feedback system

Thus the long cavity FBG Fabry-Perots were not resolved using these lasers and thus were not producing the desired results. Due to unavailability of narrow linewidth Lasers with modulation input in the laboratory the locking functionality cannot be used.

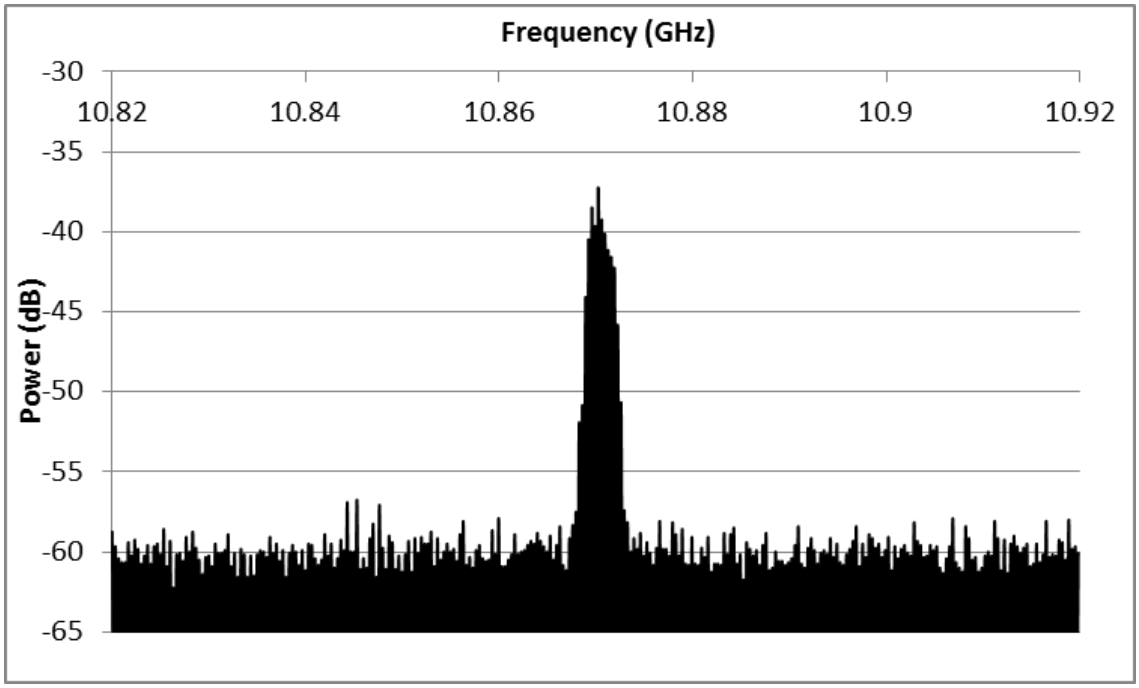

Figure 5.35 Linewidth measurement of HP laser (free running system) used in experiment

5.5 Chapter Conclusions

Novel fibre grating based Fabry-Perot sensors and an active feedback system is designed and good performance of the system is demonstrated. Any wavelength shift caused due to ultrasonic acoustic emission is intensity modulated and the servo electronics keeps the sensor working at optimized operational point. By using feedback electronics we can make sure the sensor always works at an optimised sensitivity and the reset mechanism maintains the sensor at optimum operation point if the fringe drifts out of the laser tracking range. This is a notable advantage over the free running systems. The response of an Fabry-Perot sensor has been shown for ultrasonic emission at different frequencies and it is experimentally demonstrated that the system has ability to detect high frequency wavelength change caused by acoustic perturbations up to 600kHz. But the optimisation of such system to interrogate different sensors is required. Long Fabry-Perot sensors were tested in coiled form. These sensors were tested in real time at Airbus premises. The test rigs were compressed to failure. Results show a

good performance of sensor. Further tests in lab show that flat spiral Fabry-Perot sensor shows a better response over straight Fabry-Perot and cylindrical Fabry-Perot sensor. However, it still needs to be enhanced to match the SNR of the WDI (piezo) sensor.

The linewidth of the laser is crucial for determining the maximum sensitivity of the optical sensor and so effort must be expended in this area to improve the results.

5.6 References

[1] Garth Nash,"Phase-Locked Loop Design Fundamentals," Motorola, Inc., Application Note AN-535.

[2] Zhang W., Sugden K., Pappu R. P., Webb D., and Bennion I., "Acoustic Emission Sensor Using Matched Fibre Bragg Gratings and Active Tracking Technique," in Mediterranean Photonics, Italy, pp. 351-353, 2008,.

[3] Hamstad G. J., "On the far-field structure of waves generated by a pencil lead break on a thin plate," Journal of Acoustic Emission, vol. 12, p. 157, 1994

[4] Nguyen Q-T., Besnard P., Bramerie L., Vaudel O., Girault G., Léguillon Y.," Simple Method to Measure Laser Linewidth Using Intensity Noise Spectrum Based on Rayleigh Backscattering Effect," Lasers and Electro-Optics 2009 and the European Quantum Electronics Conference. CLEO Europe - EQEC 2009, pp.1, 2009

6 Conclusion

This thesis presents the design and evaluation of various interrogation techniques that can be used for the detection of high and low frequency vibrations in various industrial applications. However, the main application area that has been discussed in this work was Aerospace. The option of using fibre optic based sensors has been explored widely and it had already been proven by several researchers prior to this work, that these can be used for sensing and damage detection. However, to be reliably deployed the sensors and the interrogator need to be small, solid state, easy to multiplex and relatively low cost. The development of a compact, low cost interrogation system that can be used with multiple optical fibre sensors that can match the signal to noise ratio of existing electrical counterparts was the main concern in the research.

Chapter 4 gives an insight into the various interrogation techniques that were developed during the course of the work. These were 'proof of concept' experiments.

Four novel fibre optic grating based experiments were carried out:

- Matched fibre grating technique with active tracking
- Fibre grating laser based sensor
- 3 by 3 coupler method with quadrature recombination technique
- Two laser method with a quadrature recombination technique

The matched pair grating system used two FBGs to measure acoustic emission sensing technique. In this system the wavelength change of the sensor is simply converted to intensity change making it compatible with existing PZT interrogation boxes. The principle of this sensor was based on measuring the

variation of the reflection from the fibre grating that is perturbed by acoustic emission. The problem with this sensor arrangement was the wavelength drifting of fibre grating caused by environmental temperature and strain fluctuation could move the grating out of range of the measurement grating and that can cause non-detection of important acoustic events. To overcome this a closed-loop circuit (active tracking technique) was designed to lock a reference grating to the sensor grating so that the reference grating always follows the sensor grating; in the output any low frequency components which usually is related to environmental perturbation is filtered out, and the change related to acoustic emission is recovered by photo detection.

By using active tracking technique we can ensure the sensor is always working at an optimised sensitivity without suffering the impact from environmental perturbations. The ability to measure high frequency wavelength changes caused by acoustic emission is demonstrated. Using this approach wavelength drifts (equivalent strain and/or ambient temperature drifts) up to 1 nm caused by environmental perturbation can be compensated. The good performance of the sensor has been demonstrated experimentally. It offers an important feature of being able to multiplex the grating sensors for damage detection in structural health monitoring.

The matched pair grating experiment proposes a sensitive and attractive option for damage detection of low frequencies but is unsuitable for the damage detection application in aircrafts as the dynamic range is much wider and the maximum detectable frequency from the experiment is 110 kHz. The sensor performance has been compared with the piezo sensor for the same acoustic emission.

A more viable option using a fibre grating based laser has been designed and fabricated. This fibre laser acts as acoustic sensor based on the same principle as the FBG acoustic sensors. Due to its lasing feature it provides a much narrower linewidth and higher output intensity than FBGs, thus provides higher sensitivity and signal-to-noise ratio. The maximum detectable frequency is 300 kHz from this technique.

To recover the wavelength information from wavelength encoded sensors, an optical fibre Mach-Zehnder interferometer can be used to give a simple and effective readout mechanism. An all optical configuration technique using Mach-Zehnder interferometer based on a 3 by 3 coupler was proposed where wavelength interrogation with frequency response up to 1MHz can be achieved. This system is capable of measuring both FBG and fibre laser sensors and is very cost effective. Generally by ramping the path difference of an interferometer low frequency drift of source wavelength (here FBG) can be monitored. For any signal with frequency close or higher than the ramping frequency, the change produced by the ramp change of the wavelength is difficult to recover.

A novel Quadrature Recombination Technique was proposed in this work and was investigated further. A modified Mach-Zehnder interferometer was employed and two quadrature optical outputs were recombined with a local carrier. The wavelength information is encoded in the phase of the local carrier and was recovered using a lock-in amplifier. The frequency of the local carrier can be set to meet the requirement for recovering acoustic emission.

But the output power ratio of 3×3 fibre coupler changes due to variable polarisation state in fibre and low coherence of optical source. Thus the phase

and wavelength relation is not satisfied. To overcome this we proposed a method to eliminate this by using two lasers and a single coupler. This method can also be used for high frequency detection.

However, using two lasers in practice is not a cost effective solution. If a practical application is considered, a large number of lasers would be required to be used in an aircraft for damage detection. It is a viable option but not necessarily cost effective. Also, both the lasers have to be tuned to maximum and minimum sensitive region manually to make sure that the sensor operates in quadrature. To overcome these issues work on a laser diode tracking system for interrogating high sensitivity fibre grating Fabry-Perot cavities has been carried out.

A laser diode whose wavelength is tuned by changing operating current is wavelength set to the operation point where the FBG Fabry-Perot cavity shows maximum wavelength shift against external perturbation. Any drift of the wavelength from the operation point is monitored by a photo detector and feedback to the laser diode driver through servo electronics. The output optical phase of the Fabry-Perot cavity is modulated by the cavity length change which in turn is modulated by the acoustic emission applied to the Fabry-Perot cavity. The responsivity of the sensor depends on both the cavity length and the coupling efficiency between the Fabry-Perot cavity and the structure to be monitored. Fabry-Perot cavities with different lengths (14mm, 25mm, 20cm, 30cm, 50cm and 100cm etc.) have been fabricated. The Fabry-Perot cavity has been deployed in both straight line (14mm and 25mm cavity length) and coiled form (30cm, 50cm and 100cm). For detection of high frequency acoustic emission, the coiled form will be considered. The others with long cavity lengths

made of Draka fibre which sustains large bending curvature, were tested in coiled form. The short cavity sensor (14mm) shows a better signal to noise ratio (close to 70dB) and was able to detect frequencies up to 600 kHz however, the upper cut off frequency was limited by a band pass filter. A long cavity sensor (50cm) shows a large signal level but has a large noise level also. It is easy to coil a large sensor for use in a commercial application.

However, this approach was limited by the amount that one can tune the laser. This was evident at the Airbus tests and to overcome the limit in wavelength tuning a resetting circuit has been designed. The principle of this resetting is to reset the LD wavelength to the initial value once the LD reaches its tracking limit. Since the reset time is in the order of ~10 ns there will be no important information lost.

The signal and noise performance of the optical Fabry-Perot cavity sensor is largely determined by the characteristics of the laser used. Currently laser tracking system is used to interrogate the phase information of the optical Fabry-Perot cavity in which DFB laser diode is wavelength tuned. The linewidth of the laser diode used not only defines the maximum Fabry-Perot cavity length, but also affects the noise performance at the desired frequency range. Different available DFB lasers and tunable lasers were investigated. The narrower linewidth lasers produced the better signal and noise performance which is evident from the results produced by the tests at BAE.

The work in this thesis indicates good progress against the requirements of the aerospace industry for optical acoustic emission sensors. The best optical sensor is the fibre laser scheme, the active tracking technique with the FBG Fabry-Perot and coiled Fabry-Perots. The active tracking experiment has

performed in the range of 60kHz – 600kHz and offered a good sensitivity. The coiled sensors with active tracking technique were also tested in real-time compression to failure tests at Airbus and has provided a good set of results although, the system was not matured to tackle with the tracking range problem which was later on taken care by introducing reset mechanism. A flat spiral Fabry-Perot sensor has shown a signal response of 43 dB which is better in comparison to a cylindrical or a flat Fabry-Perot sensor. It can be seen that a long Fabry-Perot cavity shows a better sensitivity close to 4.6 V/pm and since it can be coiled and formed into a compact sensor, it becomes obvious choice over other grating sensors.

The main issue to be considered going forward will be testing of multiple sensors with the tracking system and compactness of sensor. The operation of this tracking system is entirely dependent on the type of acoustic sensor that is being used. Further optimisation of the sensing system is required. However, the incumbent piezoelectric technology remains the target for the optical sensors to match. A more viable packaging solution must be designed to make sure that it can either be embedded in the structure or can be mounted on the structure reliably as done with the current technology.

The work in this thesis has proposed various practical solutions that can be realised commercially and can be a cost effective replacement to their electrical counterparts. This work will provide enough background for further research as it was carried out keeping in mind the commercial interest and potential it can generate.

Further work is being carried out at Aston using the principle of active tracking to develop a low cost patient breathing system. However, the electronics are modified and an AVR microprocessor based system has been designed.

Publications

W. Zhang, K. Sugden, R. P. Pappu, D. J. Webb, and I. Bennion, “Acoustic Emission Sensor Using Matched Fibre Bragg Gratings and Active Tracking Technique”, *Proc. of Mediterranean Photonics, Italy*, 2008.

Abstract: A novel acoustic emission sensor is proposed by using a pair of matched fibre Bragg gratings and an active tracking technique. The sensor output is intensity-modulated by the difference of the spectrum shifts between sensing grating and reference grating while the active tracking technique eliminates any low frequency spectrum shift between the matched fibre gratings and keeps the sensor always working at optimum operation point.

Raja P Pappu, Wei Zhang, Ian Bennion, Kate Sugden, “Acoustic Emission Detection Using Optical Fiber Based Fabry Perot Sensor And Quadrature Recombination Technique”, *Proc. of CLEO Europe, Munich, Germany*, 2009.

Abstract: A novel technique is proposed to monitor high frequency acoustic emission by Using Optical Fiber Bragg grating Based Fabry Perot cavity And Quadrature Recombination Technique.

Raja P Pappu, Wei Zhang, Ian Bennion, Kate Sugden, “Fiber Bragg Grating Fabry-Perot Resonator Based Acoustic Emission Sensor Using Active Feedback System”, *Proc. of CLEO US, Baltimore, USA*, 2009.

Abstract: We propose a novel optical fiber grating based Fabry-Perot acoustic emission sensor and active feedback system that eliminates low frequency spectrum shifts caused by environmental perturbations, ensuring the sensor always work at optimum operation point.

APPENDIX I

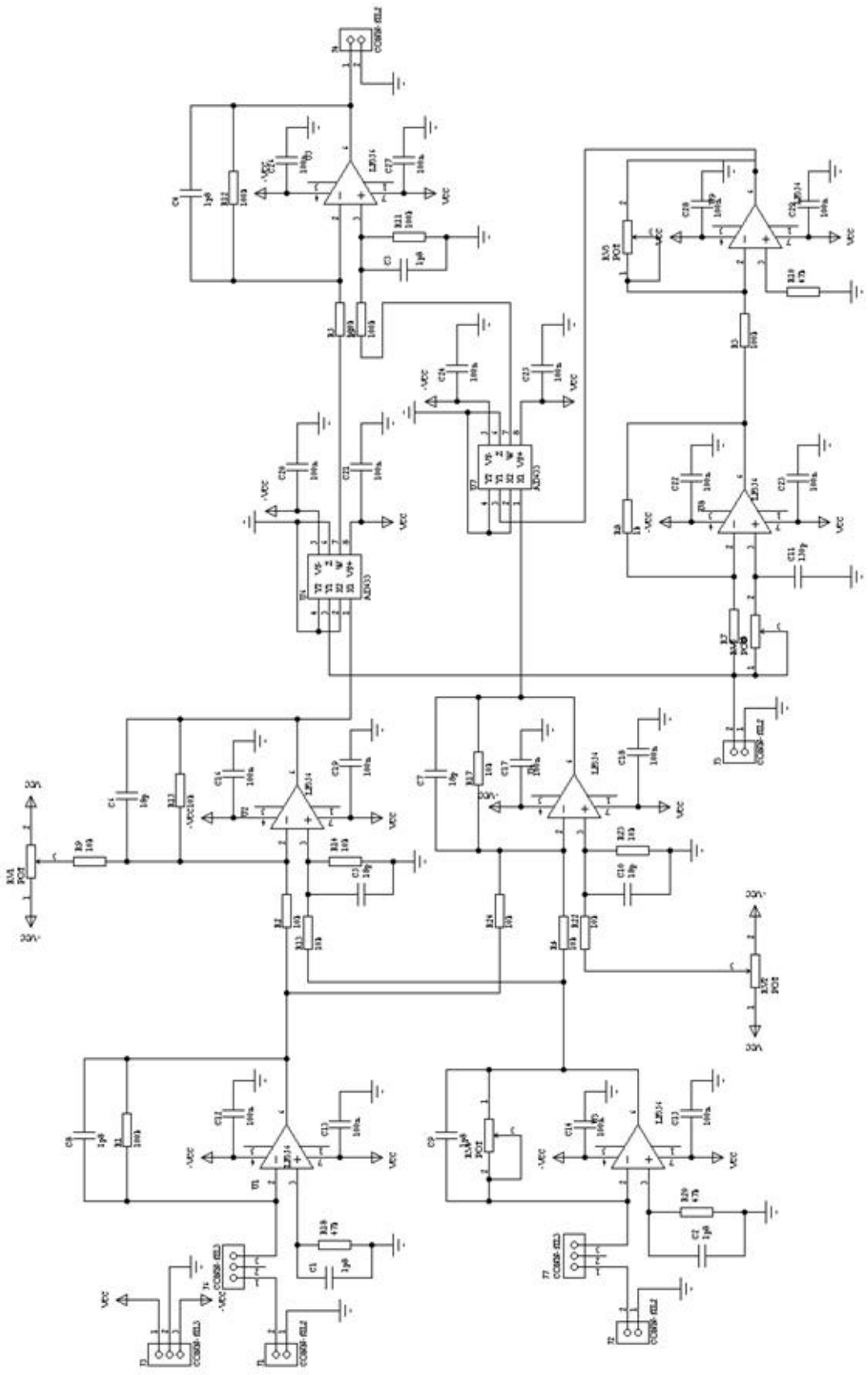

Figure 1 Quadrature Recombination electronic circuit design

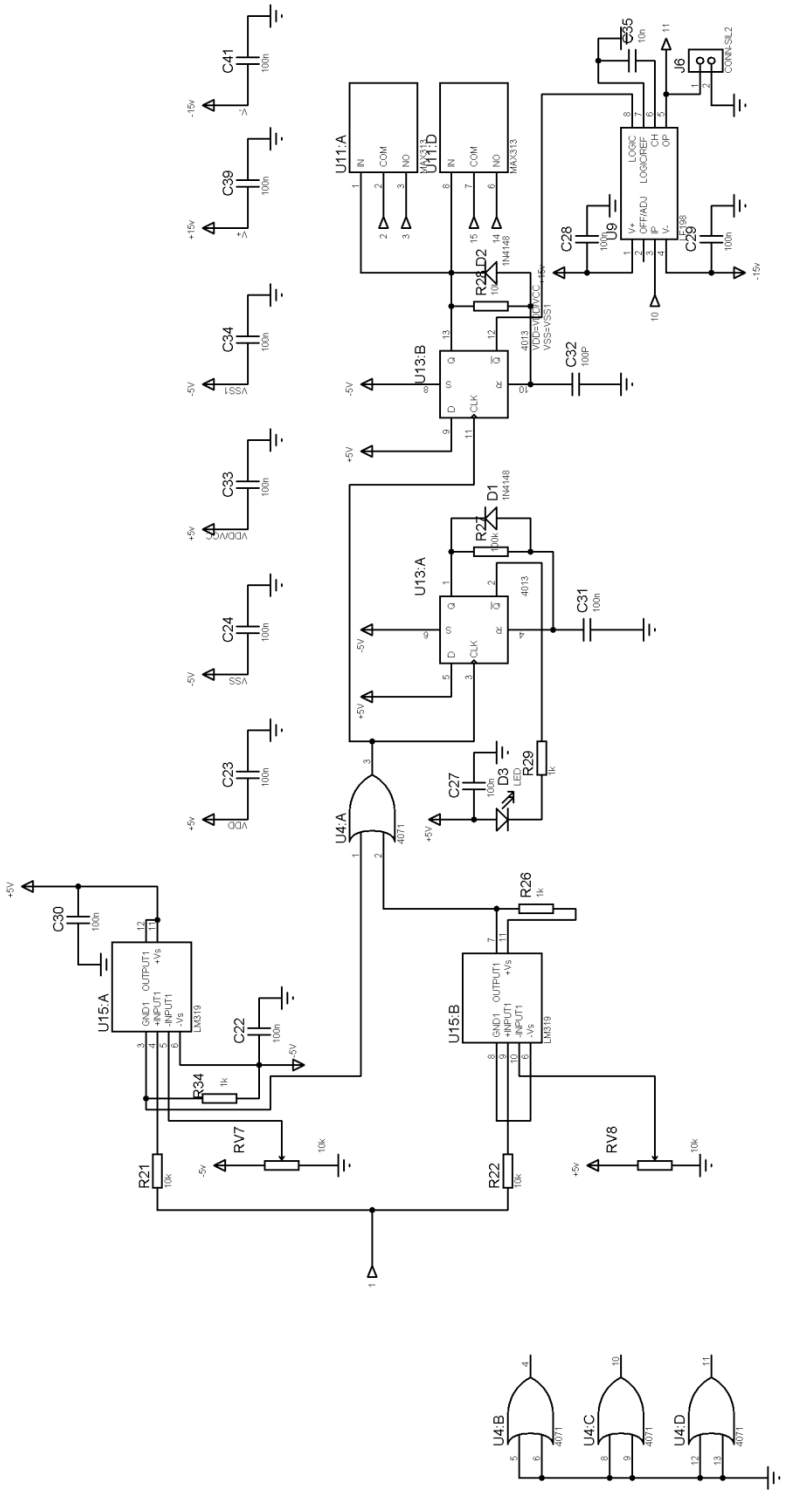

Figure 2 Reset Circuit design for the active feedback electronics

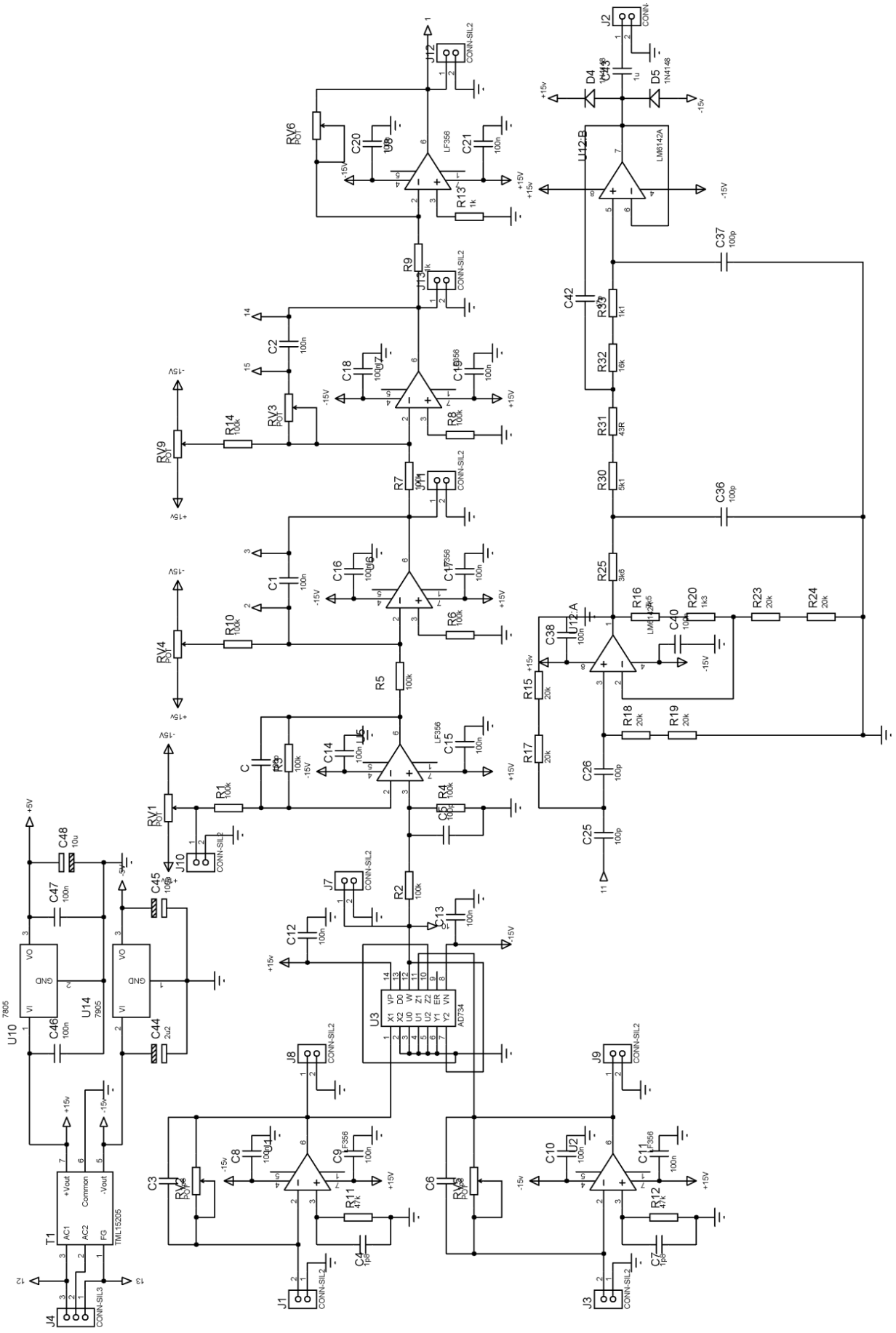

Figure 3 Active feedback technique electronic circuit design